Computational Investigation of the Tunability of HOMO- LUMO Levels and Band Gaps in Conducting Polymers

by

Saumya Rajinie Jayasundara

A Thesis Submitted to the Faculty of Graduate Studies of

The University of Manitoba

in partial fulfillment of the requirements of the degree of

MASTER OF SCIENCE

Department of Chemistry

University of Manitoba

Winnipeg, Canada

ABSTRACT

Conducting polymers have received a lot of attention in various fields due to their tunable properties. Density functional theory (DFT) calculations were carried out to investigate the tunable nature of band gaps and HOMO and LUMO levels of polythiophene (PTh) and polypyrrole (PPy) based conjugated polymers. A GGA functional (PBE) incorporating dispersion corrections was used with TZP or plane-wave basis sets and scalar ZORA or pseudopotentials for the relativistic effects. Molecular and periodic calculations were carried out. Two series of conjugated polymers were studied as S is replaced in PTh with O, Se, Te, and N is replaced in PPy with P, As, Sb, in the presence of Li and Cl atomic dopants. Li and Cl atoms facilitate n-type and p-type doping respectively. Narrowing band gaps or HOMO-LUMO gaps were obtained when going from O to Te in PTh analogs and P to Sb in PPy analogs. Further reduction in band gaps was observed upon doping especially in the series of PTh and analogs. The tuning of the HOMO-LUMO gap was also done by replacing the peripheral hydrogen in PTh by different electron-donating and electron-withdrawing groups. As electron-donating groups $-CH_3$, $-OCH_3$ and $-N(CH_3)_2$ were employed, and as electron-withdrawing groups -CHO, $-COOCH_3$, -CN and $-NO_2$ were used. Further, S replaced by Se in PTh (polyselenophene) and molecules containing alternating heteroatoms S-Se were also studied with these different peripheral groups. The addition of electron-donating groups results in increased HOMO and LUMO levels and the addition of electron-withdrawing groups results in decreased HOMO and LUMO levels. Planarization of the molecule was observed with electron-donating groups. By changing the heteroatom from S to Se more planarized structures were observed. The structures containing both S and Se as heteroatoms have intermediate properties. Due to the changes in both HOMO and LUMO levels, the values observed for the band gap did

not follow a specific trend. This study is useful in various device applications of conjugated polymers where HOMO-LUMO levels and band gaps are of concern.

ACKNOWLEDGEMENTS

This work would not have been possible without the guidance and aid of a large number of individuals.

First of all, I would like to express my deepest sincere gratitude to my supervisor Dr. Georg Schreckenbach, Department of Chemistry, University of Manitoba, Canada, who introduced me into the research field of Computational Chemistry and for his excellent guidance, caring, patience, and encouraging discussions throughout my work. And I also would like to express my gratitude to the advisory committee, Dr. Viktor Nemykin, Department of Chemistry, and Dr. Derek Oliver, Department of Electrical & Computer Engineering, for their feedback, sharing of knowledge, guidance and support.

I must also thank to the members of the computational chemistry research group during my work, Jeffery Perkins, Xiaobin Zhang, Gurpreet Kour, Payal Grover, Dr Yang Gao for a pleasant working environment and their helping hand in practical problems and Dr James Xidos and Dr Joshua Hollett for their suggestions during group discussions. My sincere thanks go to Dr. Grigory Shamov, for his invaluable technical support. I also thank Dr. T. Kaloni and Dr. M. Freund for their guidance and valuable discussions throughout the research.

I greatly acknowledge the support given by all the academic, administrative and supportive staff members of Department of Chemistry towards the fulfillment of my degree. The financial support from the Natural Sciences and Engineering Council of Canada (NSERC, Discovery Grant) and the University of Manitoba is also greatly acknowledged.

Especially I would like to thank my mother and my husband for their support and encouragement during my studies. Finally, my little daughter for being such a good girl.

Saumya R. Jayasundara

TABLE OF CONTENTS

LIST OF TABLES

LIST OF FIGURES

LIST OF ABBREVIATIONS

ADF	Amsterdam Density Functional
B3LYP	Becke, 3-parameter, Lee–Yang–Parr
B88	Becke 1988
CP	Conjugated Polymer
DFT	Density Functional Theory
ECP	Effective Core Potential
GGA	Generalized Gradient Approximation
GTO	Gaussian Type Orbitals
HF	Hartree-Fock method
HOMO	Highest Occupied Molecular Orbital
HT-HT	Head-Tail-Head-Tail
IR	Infrared Radiation
KS	Kohn-Sham
LDA	Local Density Approximation
LSD	Local Spin Density
LSDA	Local Spin-Density Approximation
LUMO	Lowest Unoccupied Molecular Orbital
LYP	Lee Yang and Parr
MO	Molecular Orbital
MP2	Møller-Plesset Perturbation Theory of the 2nd Order
P3DDT	Poly(3-dodecylthiophene)
P3HT	poly-3-hexylthiophene
PBE	Perdew, Burke, and Ernzerhof
PDOPT	poly(3-(2,5-dioctylphenyl)thiophene)
PES	Potential Energy Surface
PES	Potential Energy Surface
PLED	Polymer Light Emitting Diodes
PPy	Polypyrrole
PTh	Polythiophene

RFID	Radio Frequency Identification
RPA	Random Phase Approximation
SCF	Self Consistent Field
SD	Slater Determinant
SO	Spin-Orbit
SR	Scalar Relativistic
STO	Slater Type Orbitals
SWCNT	Single-Walled Carbon Nanotubes
TZP	Triple Zeta Polarized
V_{OC}	Open Circuit Voltage
W_{CB}	Conduction Band Width
W_{VB}	Valence Band Width
XC	Exchange Correlation
ZORA	Zeroth-Order Regular Approximation

Chapter 1 : INTRODUCTION

Computational chemistry applies theoretical ideas to solve chemical problems using computer programs where a mathematical method is developed, and the method is automated with computers. The modern development of powerful computers and software pave the way for sophisticated calculations. Computational chemistry helps to understand the chemistry behind the various processes, to improve such processes by making them efficient and productive, to introduce new processes. With quantum mechanics and thermodynamics, computational chemistry deals with electrons, atoms, molecules, and reactions. Computational chemistry is based on approximations and available methods vary from highly approximated to highly accurate. Highly accurate methods work only for small molecules, while they are computationally much more expensive with large molecules. Computational chemistry calculations are always a compromise between cost (time, storage, memory) and accuracy.[1]

During past decades, many studies were done on the development of the research field in computational chemistry. In 1998, Walter Kohn for Density Functional Theory (DFT) and John Pople for the development of computational methods in quantum chemistry won the Nobel Prize in Chemistry, which was a great milestone. Several empirical and quantum mechanics-based methods are available to use with computational calculations. Among them, DFT is a widely used quantum mechanics-based method which is having a good accuracy/cost ratio. DFT can handle molecules having more than 200 atoms. DFT generally performs well for geometries and energy calculations.[1,2]

Computational chemistry covers vast areas including biochemistry, biomedical, molecular sciences, drug design, polymer, and materials modeling etc. The calculations result in energies, structures, and properties of molecules which can be used to interpret the existing experimental

results and to make further predictions. Computers make handling of these data convenient even if they are hard to observe in real life.

1.1 POLYMERS

1.1.1 Conjugated polymers (CPs)

Conjugated systems are a specific class of molecules which has drawn much attention of the research community. The presence of alternating double bonds creates a conjugated system which results in electron delocalization. The electron density is not fixed to one location, instead, it is spread among multiple atoms. In general, more extensively conjugated systems make more stable molecules. This increased stability is known as delocalization energy. Molecules having delocalized π-system of electrons are promising candidates in advanced functional materials. Easy synthesis and tunable structure are among the notable features of these materials. Their applications spread over various branches of devices including memory devices, solar cells, batteries, light-emitting diodes, biosensors, etc.[3]

1.1.2 Conductivity of polymers and doping

The conventional polymers were considered as materials having significant resistance to electrical conductivity until the discovery of conducting polymers several decades ago by Shirakawa et al.[4] The tunability of electrical conductivity, the flexibility of the material, lighter weight, and resistance to corrosion are amongst the attractive properties of conducting polymers which merge the good properties of metals and conventional polymers.[3,5]

The conductivity of polymer arises through several features; mainly the conjugated backbone chain of the polymer which creates delocalized π electrons by overlapping π orbitals. This results

in interesting optical and electronic properties. The tunability of the electrical conductivity can be achieved via doping. The conductivity of the polymers can be raised up to conductivities of metals by p-doping, where the polymer is oxidized and has a positive charge, or n-doping, where the polymer is reduced and has a negative charge. *Tsukamoto et al.* presented a conductivity of more than 10^4 S cm^{-1} when doping polyacetylene with iodine; this is close to the room temperature conductivity of lead (4.8×10^4 S cm^{-1}).[5,6] The electron neutrality of the polymer is maintained by counterions. In the case of p-doping (oxidation), it is a counter-anion, and in the case of n-doping (reduction), it is a counter-cation. Un-doped conjugated polymers act as semiconductors or insulators. This switching between metal and insulator results in a vast area of applications.[5]

Doping is achieved either via the addition of electrons or removal of electrons. The novel structure obtained after the doping leads to the formation of novel charge carriers in the polymer. The trans-polyacetylene polymer which has a degenerate ground state forms solitons as charge carriers while polymers like polythiophene and polypyrrole form polarons and bipolarons as charge carriers. The polaron P^+ is formed after the oxidation of the polymer and the polaron P^- is formed after the reduction of the polymer. Polarons produce two new energy levels in the band gap. At higher polaron concentration, the formation of bipolarons can be achieved and a bipolaron is considered as two coupled P^+ or P^-. Polarons or bipolarons are delocalized over the polymer and facilitate the electrical conductivity.[5,7,8] Figure 1.1 shows a schematic diagram of p-type and n-type doping of polythiophene. The difference between the structure of polaron and bipolaron is also shown.

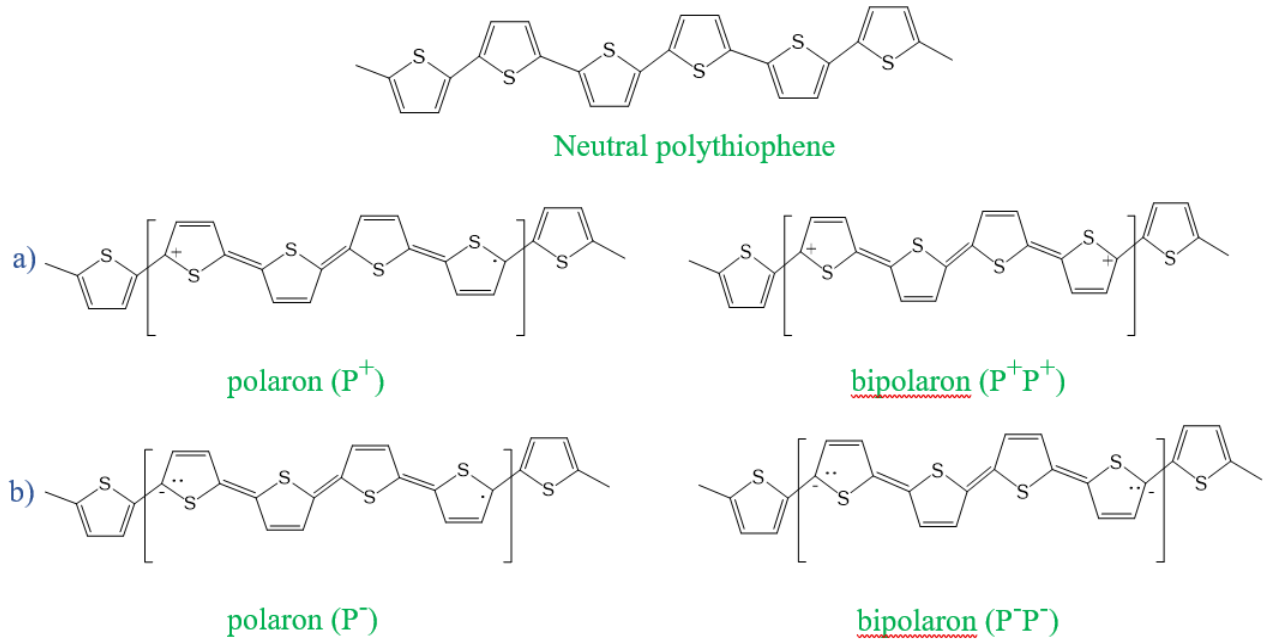

Figure 1.1: a) p-type doping and b) n-type doping of polythiophene[8]

Doped CPs are also reported as promising candidates for high-performance memory devices. In the device structure, undoped metal oxide and a doped CP makes a junction. In the presence of a large field, cations relocate into the metal oxide-forming an n-doped metal oxide and p-doped CP.[9]

1.1.3 HOMO- LUMO levels and band gaps

The HOMO (highest occupied molecular orbital) – LUMO (lowest unoccupied molecular orbital) gap or the band gap is one of the unique properties of a molecule which can be used to make predictions about capabilities of the molecule. For instance, the HOMO - LUMO gap decreases when increasing the conjugation in a conjugated polymer. The low band gap enhances light absorption at visible and near IR region and carrier mobility and favors the photo-generated

electron-hole pair separation in photovoltaic cells.[10] In polymer light-emitting diodes (PLEDs) the band gap of the incorporated conjugated polymer determines the emitting color.[11]

The absolute levels of HOMO and LUMO are also important. A low HOMO is needed in the conjugated polymer to obtain an increased open-circuit voltage of the solar cell. When a conjugated system acts as a donor, a high LUMO level (compared to the acceptor) is needed for efficient charge transfer. On the other hand, when a conjugated system acts as the acceptor it is necessary to have a low LUMO level compared to the donor.[12]

Therefore, the study of the tunability of the HOMO-LUMO energy gap and the energy levels in conjugated polymers is important to fulfill different performance requirements.

1.2 ORGANIZATION OF THE THESIS

This thesis is purely based on theoretical calculations which were used to study the turnability of the HOMO-LUMO gap and levels in conjugated polymers. DFT calculations were carried out with various conjugated polymers and results will be discussed in subsequent chapters.

Chapter 2 contains the details of the theory behind computational calculations performed throughout this thesis work.

Chapter 3 presents the tunability of HOMO-LUMO levels and band gaps in polythiophene and polypyrrole based conjugated polymers by doping. Li and Cl atoms were used as dopants. The series of conjugated polymers incorporated in this study are, S replaced by O, Se and Te in polythiophene and N replaced by P, As and Sb in polypyrrole. The chapter describes the structural and electronic properties of these materials, the changes in HOMO-LUMO levels and band gaps before and after the doping.

Chapter 4 presents the tunability of HOMO- LUMO levels and band gaps in polythiophene-based conducting polymers by introducing different peripheral groups. The replacement of peripheral hydrogen in polythiophene with different electron-donating and electron-withdrawing groups results in changes in the structural and electronic properties of these materials.

Chapter 5 presents the conclusions of this work and a brief outlook.

References

(1) Cramer, C. J. *Essentials of Computational Chemistry: Theories and Models*; John Wiley & Sons, 2013.

(2) Jones, R. O. Density Functional Theory: Its Origins, Rise to Prominence, and Future. *Rev. Mod. Phys.* **2015**, *87*, 897–923.

(3) Bureš, F. Fundamental Aspects of Property Tuning in Push–Pull Molecules. *RSC Adv.* **2014**, *4* (102), 58826–58851.

(4) Chiang, C. K.; Fincher, C. R.; Park, Y. W.; Heeger, A. J.; Shirakawa, H.; Louis, E. J.; Gau, S. C.; MacDiarmid, A. G. Electrical Conductivity in Doped Polyacetylene. *Phys. Rev. Lett.* **1977**, *39* (17), 1098–1101.

(5) Li, Y. Conducting Polymers. In *Organic Optoelectronic Materials*; Li, Y., Ed.; Springer International Publishing: Cham, 2015; pp 23–50.

(6) Tsukamoto, J. Recent Advances in Highly Conductive Polyacetylene. *Adv. Phys.* **1992**, *41* (6), 509–546.

(7) Bredas, J. L.; Street, G. B. Polarons, Bipolarons, and Solitons in Conducting Polymers. *Acc. Chem. Res.* **1985**, *18* (10), 309–315.

(8) Le, T.-H.; Kim, Y.; Yoon, H.; Le, T.-H.; Kim, Y.; Yoon, H. Electrical and Electrochemical Properties of Conducting Polymers. *Polymers* **2017**, *9* (4), 150.

(9) Kumar, M. R.; Rahman, G. M. A.; Thomson, D. J.; Freund, M. S. Controlling Volatility in Solid-State, Redox-Based Memory Devices Using Heterojunction Barriers to Ion Transport. *Chem. Commun.* **2012**, *48* (75), 9409–9411.

(10) Ma, X.; Lv, Y.; Xu, J.; Liu, Y.; Zhang, R.; Zhu, Y. A Strategy of Enhancing the Photoactivity of G-C3N4 via Doping of Nonmetal Elements: A First-Principles Study. *J. Phys. Chem. C* **2012**, *116* (44), 23485–23493.

(11) Deng, X.-Y. *Light-Emitting Devices with Conjugated Polymers*; 2011; Vol. 12.

(12) Kim, B.-G.; Ma, X.; Chen, C.; Ie, Y.; Coir, E. W.; Hashemi, H.; Aso, Y.; Green, P. F.; Kieffer, J.; Kim, J. Energy Level Modulation of HOMO, LUMO, and Band-Gap in Conjugated Polymers for Organic Photovoltaic Applications. *Adv. Funct. Mater.* **2013**, *23* (4), 439–445.

Chapter 2：THEORY

This chapter describes the fundamental theories and computational tools used during this thesis work. Theories are based on quantum chemistry and these theories are used in computational tools to understand, predict and reproduce the experimental chemistry.

2.1 INTRODUCTION TO QUANTUM CHEMISTRY

The following brief introduction about quantum chemistry is mainly based on Dronskowski & Hoffmann[1] and Cramer.[2]

2.1.1 The Schrödinger equation

The Schrödinger equation which was introduced by Erwin Schrödinger in 1926 is considered as the foundation of quantum chemistry. Any physical system that is composed of nuclei and electrons can be entirely described by solving the (molecular) Schrödinger equation. The time-independent form of the Schrödinger equation is given in equation 2.1.

$$H\Psi=E\Psi \tag{2.1}$$

E is the energy eigenvalue which can be obtained by applying the Hamiltonian operator (H) on the wave function Ψ. H is the sum of kinetic (T) and potential energy (V) operators. In general, a system contains many particles and the Hamiltonian is described as follows (Eq. 2.2). The first two parts represent the kinetic energies of electrons and nuclei, respectively. The third term describes the Coulomb attraction between electrons and the nuclei which are r_{ik} apart from each other. The fourth term is the potential energy from electrostatic repulsion between electrons and

the fifth term is the potential energy from electrostatic repulsion between the nuclei separated by r_{kl}. The conditions $i<j$ and $k<l$ are used to exclude the double-counting of these effects.

$$H = -\sum_i \frac{\hbar}{2m_e}\nabla_i^2 - \sum_k \frac{\hbar}{2m_k}\nabla_k^2 - \sum_i \sum_k \frac{e^2 Z_k}{r_{ik}} + \sum_{i<j} \frac{e^2}{r_{ij}} + \sum_{k<l} \frac{e^2 Z_k Z_l}{r_{kl}} \tag{2.2}$$

Where; i and j stand for electrons and k and l stand for nuclei

m_e = mass of the electron — m_k = mass of nucleus k

$\hbar$ = Planck's constant divided by 2π — Z = atomic number

e = electron charge — $\boldsymbol{\nabla}^2$ = Laplacian operator

r_{ab} = distance between particle a and b

In Cartesian coordinates, the Laplacian is,

$$\nabla_i^2 = \frac{\partial^2}{\partial x_i^2} + \frac{\partial^2}{\partial y_i^2} + \frac{\partial^2}{\partial z_i^2} \tag{2.3}$$

Simply; $H = T_e + T_n + V_{en} + V_{ee} + V_{nn}$ (2.4)

Where e and n represent electron and nucleus.

Most of the constants in equation (2.2) can be made equal to 1 and the resulting unit system is called Hartree atomic units. 1 Hartree equals 27.2114eV or 2 Rydbergs.

2.1.2 The Born-Oppenheimer approximation

According to equation (2.2), H depends on the position of both electrons and nuclei. The Born-Oppenheimer approximation states that since electrons move very much faster than the heavier nuclei ($m_e << m_k$), it can be considered that the electrons are moving in a field of fixed nuclear potential. Therefore, the kinetic energy term for the nucleus disappears from equation 2.2. Further, the fifth term of equation 2.2, the nuclear-nuclear potential energy term, will be a constant for a

given geometry. With the Born-Oppenheimer approximation and considering Hartree units, the final form of the equation (2.2) will be as follows (2.5).

$$H_{el} = -\sum_i \frac{1}{2}\nabla_i^2 - \sum_i \sum_k \frac{Z_k}{r_{ik}} + \sum_{i<j} \frac{1}{r_{ij}} \tag{2.5}$$

Then the (electronic) Schrödinger equation is,

$$(H_{el} + V_N)\Psi_{el}(q_i; q_k) = E_{el}\Psi_{el}(q_i; q_k) \tag{2.6}$$

V_N is the nuclear-nuclear potential energy (repulsion), q_i, are electronic coordinates which are independent variables, and q_k, nuclear coordinates which are parameters. The eigenvalue of the electronic Schrödinger equation is called the electronic energy. When the electronic energy is found without considering V_N, it is called pure electronic energy and then one could add V_N and get the E_{el}.

The Born-Oppenheimer approximation leads to the concept of potential energy surface (PES). The E_{el} over all possible nuclear coordinates is called PES.

2.1.3 The variational method

Within the Born-Oppenheimer approximation, the need is to find the electronic distribution which is having the minimum $E_{el.}$ The variational method is one way of finding approximate solutions to quantum-mechanical problems. Basically, in the variational method, one could guess a trial wave function for a problem and then some of the parameters in the wave function can be adjusted so that the energy of the trial wave function is minimized. According to the variational principle, the energy of a model wave function Φ cannot be lower than the exact ground state energy E_o (equation 2.7). This provides a way to obtain an approximate solution to the Schrödinger equation.

$$E_{el} = \frac{\int \Phi * H\Phi d\tau}{\int \Phi * \Phi d\tau} = \frac{|\langle\Phi|H|\Phi\rangle|}{\langle\Phi|\Phi\rangle} \geq E_o \tag{2.7}$$

2.1.4 Antisymmetric many-body representation

The many-body wave function is derived from the solutions of one-electron systems (hydrogen-like). The simple ansatz for the many-body wave function Ψ_{HP} (Hartree ansatz), is presented as a product of one-particle wave functions (ψ).

$$\Psi_{HP}(r_1, r_2, \ldots\ldots r_N) = \psi_1(r_1)\,\psi_2(r_2)\,\ldots\ldots\ldots\,\psi_N(r_N) \tag{2.8}$$

However, Ψ_{HP} fails the Pauli exclusion principle (antisymmetric test). The Pauli exclusion principle states that fermions (particles with half-integer spin) cannot occupy the same quantum state within the quantum system simultaneously. The wave function must be antisymmetric as per equation 2.9.

$$P_{ik}\,\Psi(x_1, \ldots., x_i, \ldots., x_k, \ldots.) = \Psi(x_1, \ldots., x_k, \ldots., x_i, \ldots.) = -\Psi(x_1, \ldots., x_i, \ldots., x_k, \ldots.) \tag{2.9}$$

P_{ik} = permutation operator

The electronic wave function changes sign when the (generalized) coordinates of two electrons are exchanged.

A fourth quantum number is used to describe a particle and its wave function, which is called the spin number. The term spin-orbitals, denoted by $\chi(x)$, is presented with some spatial orbital $\psi(r)$ and the spin functions $\alpha(\omega)$ or $\beta(\omega)$.

$$\chi(x) = \begin{cases} \psi(r)\alpha(\omega) \\ \boldsymbol{or} \\ \psi(r)\beta(\omega) \end{cases} \tag{2.10}$$

A modified ansatz for the N-electron wave function which fulfills the antisymmetry requirement can be constructed as in equation 2.11.

Where, SD = Slater determinant

$$\Psi_{SD}(x_1, \ldots., x_N) = \frac{1}{\sqrt{N!}} \begin{vmatrix} X_1(x_1) & \chi_2(x_1) & \cdots & \chi_N(x_1) \\ \chi_1(x_2) & \chi_2(x_2) & \cdots & \chi_N(x_2) \\ \vdots & \vdots & \ddots & \vdots \\ \chi_1(x_N) & \chi_2(x_N) & \cdots & \chi_N(x_N) \end{vmatrix} \equiv |\Psi(x_1, \ldots\ldots, x_N)\rangle \equiv |\chi_1\chi_2 \ldots\ldots\ldots \chi_N\rangle \quad (2.11)$$

2.1.5 Basis sets

The term basis set refers to a set of one-particle functions which are used to build molecular orbitals. These can be composed of atomic orbitals, which are linear combinations of atomic eigenfunctions, or plane waves, which can be found in calculations having periodic boundary conditions. A mathematically complete basis set is in general infinite, and approximations make the basis set finite. In modern quantum chemistry, there are two types of atomic orbitals available namely Gaussian-type orbitals (GTO) and Slater-type orbitals (STO), Figure 2.1.

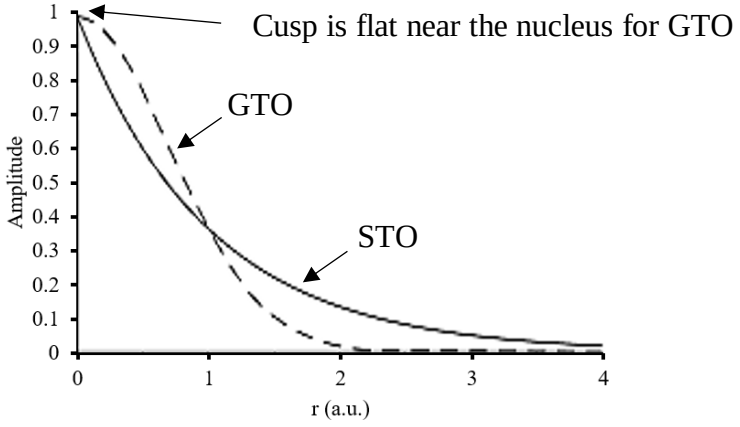

Figure 2.1: Comparison of Gaussian-type orbitals (GTO) and Slater-type orbitals (STO)

STOs were introduced by Slater in 1930. The general form of an STO is given in equation 2.12. N is the normalization factor and the Y_l^m are the spherical harmonics. The distance of the electron from the nucleus is given by *r*. ζ is a constant related to the effective charge of the nucleus which can be estimated by the method introduced by Slater. The principal quantum number is denoted as *n*, (*n*=1, 2, …) and *l* and *m* are angular momentum quantum numbers. r, θ, φ are the spherical coordinates.

$$\varphi(r, \theta, \varphi; \zeta, n, l, m) = Nr^{n-1}e^{-\zeta r}Y_l^m(\theta, \varphi) \tag{2.12}$$

STOs correctly describe the cusp at the nucleus and then decay exponentially with the distance from the nucleus. Many integrals resulting from the use of STOs need to be calculated numerically, and this makes calculations very time-consuming. For the reduction of computational cost, a new type of orbitals (basis functions) called GTOs were introduced by S.F. Boys (1950). GTOs are having a much faster evaluation of integrals. Even though GTOs save computational cost, GTOs do not match with the shape of an atomic orbital well. GTOs give a wrong cusp which is flat near the nucleus, Figure 2.1.

The general form of a GTO is given in equation 2.13.

$$\varphi(x, y, z; \alpha, i, j, k) = Nx^i y^j z^k e^{-\alpha(x^2+y^2+z^2)} \tag{2.13}$$

N is a normalization factor. The exponent α controls the width of the Gaussian functions. The terms *i*, *j*, *k* are non-zero integers. The main difference between STO and GTO is in the variable *r*, where it is squared in GTO, that is e^{-r} becomes e^{-r2}.

2.1.6 Hartree-Fock method

The Hartree-Fock method (HF) was introduced by Hartree and Fock soon after the origin of quantum mechanics. HF iteratively finds a set of molecular orbitals (MOs) that minimizes the

energy of the wave function using equation 2.11. The energy minimization is carried out with the variational principle (equation 2.7). According to the HF method, each electron does not experience other individual electrons, but a mean-field from their charges. Finally, the HF method reduces an N-electron problem to N one-electron problems. Then we have a one-electron Fock operator (Hamiltonian).

$$f_i = -\frac{1}{2}\nabla_i^2 - \sum_{k}^{nuclei} \frac{Z_k}{r_{ik}} + V^{HF} \tag{2.14}$$

The first 2 terms of equation 2.14 depend on the electronic variable *i* and the fixed nuclei.

V^{HF} is the Hartree-Fack potential which involves the electron-electron interactions in an average potential.

$$V^{HF} = \sum_{j}^{N} J_j\,(i) - K_j(i) \tag{2.15}$$

The J_j and K_j operators compute the J_{ji} and K_{ji} integrals. They are Coulomb and exchange operators respectively.

$$J_j(i) = \int \left|\chi_j(j)\right|^2 r_{ij}^{-1} dr_j \tag{2.16}$$

$$K_j(i)\chi_i(i) = \int \left[\chi_j^*\,(j) r_{ij}^{-1} \chi_i(j)\right] \chi_j(i) dr_j \tag{2.17}$$

$J_j(i)$ is the electrostatic repulsion between electron *i* and *j*; $K_j\chi_i$ arises due to the antisymmetry of Ψ.

Using the Fock operator, the HF equations (2.18) can be constructed.

$$f(i)\chi_i(i) = \varepsilon_i \chi_i(i) \tag{2.18}$$

ε_i is the energy of the i^{th} orbital. Together with a basis set, the HF equations can be written in a matrix from which is known as the Roothan-Hall equations (2.19).

$$FC=\varepsilon SC \tag{2.19}$$

F, the Fock matrix contains the elements $F_{\mu\upsilon} = \langle\chi_\mu|f|\chi_\upsilon\rangle$; S, the overlap matrix, has the elements $S_{\mu\upsilon} = \langle\chi_\mu|\chi_\upsilon\rangle$; and C contains all basis set coefficients. The iterative calculation is used to find C such that the norm of the diagonal eigenvalue matrix ε is minimized. This iterative calculation is called Self- Consistent Field (SCF) method.

For an N-electron system, the HF ground state energy is given by the equation (2.20).

$$E_{HF} = \sum_{i}^{N} \varepsilon_i - \frac{1}{2}\sum_{ij}^{N}\left(J_{ij} - K_{ij}\right) + V_{nn} \tag{2.20}$$

(ε_i is a diagonal element of F: $\varepsilon_i = \langle\chi_i|f(i)|\chi_i\rangle$)

$J_{ij} and\ K_{ij}$ are two-electron integrals. The summation runs over all i's and j's and contains self-interactions. However, these are canceled out because $J_{ii} = K_{ii}$.

The HF energy is always larger than the exact ground state energy. This difference is called correlation energy. In the HF method, the antisymmetric many-electron wave function is approximated by a single Slater determinant. This does not consider Coulomb correlation which results in a higher HF energy compared to the ground state energy.

2.1.7 Density Functional Theory (DFT)

DFT is a widely used method these days since it is accurate and computationally efficient compared to the HF method. The Thomas-Fermi model and Slater's X_a exchange functional provide the idea of using the electron density rather than the wavefunction. The Hamiltonian depends on the position of the nuclei, atomic number and the number of electrons. If we have the electron density (ρ), when it is integrated overall space, we can get the number of electrons (N).

$$\text{Number of electrons (N)} = \int \rho(r) dr \tag{2.21}$$

Modern DFT is based on the Hohenberg-Kohn theorems, published in 1964. The Hohenberg-Kohn theorems prove that the one-electron density uniquely determines the Hamiltonian of a system. There are two Hohenberg-Kohn theorems. The first states (existence theorem) that the non-degenerate ground-state electron density ($E_{el}[\rho]$) determines the external potential.

$$E_{el}[\rho] = \int \rho(r) V_{eN} dr + F_{HK}[\rho] \tag{2.22}$$

$$F_{HK}[\rho] = T[\rho] + V_{ee}[\rho] \tag{2.23}$$

F_{HK} = Hohenberg-Kohn functional

V_{eN} =The external potential applied by the fixed nuclei

T = Kinetic energy operator

V_{ee} = Interaction operator (electron-electron)

The second theorem says that the ground state energy can be obtained variationally (variational theorem).

$$E[\rho] = \int \rho(r) V_{ext} dr + T[\rho] + V_{ee}[\rho] \geq E_0 \tag{2.24}$$

V_{ext}= An external potential, such as V_{eN} of equation 2.22

Kohn-Sham SCF methodology

In 1965 Kohn-Sham SCF methodology was introduced where a fictitious non-interacting electron system is used to find the ground state density. The fictitious system has exactly the same density as the real system. The energy functional can be split up into different contributions according to equation (2.25), for further analysis.

$$E[\rho(r)] = T_{ni}[\rho(r)] + V_{ne}[\rho(r)] + V_{ee}[\rho(r)] + \Delta T[\rho(r)] + \Delta V_{ee}[\rho(r)] \tag{2.25}$$

T_{ni} =kinetic energy of the non-interacting electrons

V_{ne}= nuclear-electron interaction

V_{ee} = electron-electron interaction

ΔT and ΔV_{ee}=correction to the kinetic energy from interacting nature of the electrons and electron-electron repulsion energy

The orbital expression of the density is given in equation 2.26

$$E[\rho(r)] = \sum_{i}^{N} \mathbb{I}\left(\left\langle \chi_i \left| -\frac{1}{2}\nabla_i^2 \right| \chi_i \right\rangle - \mathbb{I}\left\langle \chi_i \left| \sum_{k}^{nuclei} \frac{Z_k}{|r_i - r_k|} \right| \chi_i \right\rangle\right)$$

$$+ \sum_{i}^{N} \left\langle \chi_i \left| \frac{1}{2} \int \frac{\rho(r')}{|r_i - r'|} dr' \right| \chi_i \right\rangle + E_{XC}[\rho(r)] \qquad (2.26)$$

The density for a Slater determinantal wave function is given as in equation 2.27.

$$\rho = \sum_{i=1}^{N} \langle \chi_i | \chi_i \rangle \qquad (2.27)$$

In equation 2.26, E_{XC} is called the exchange-correlation energy and it contains the unknowns, corrections ΔT and ΔV_{ee} given in equation 2.25. E_{XC} contains the correction for the classical self-interaction energy (correction for unphysical Coulombic self-repulsion) which comes under ΔV_{ee}. The Hamiltonian, yielding the Kohn-Sham (KS) orbitals, is given by equation (2.28)

$$h_i^{KS} = -\frac{1}{2}\nabla_i^2 - \sum_{k}^{nuclei} \frac{Z_k}{|r_i - r_k|} + \int \frac{\rho(r')}{|r_i - r'|}\, dr' + V_{XC} \qquad (2.28)$$

The ground state density is found by an iterative method (SCF) similar to the HF method, starting with an initial guess of the KS orbitals. The exact XC potential, V_{XC}, which is known as the functional derivative of E_{XC} with respect to ρ, is needed to find the correct density.

$$V_{XC} = \frac{\delta E_{XC}}{\delta \rho} \tag{2.29}$$

Exchange-correlational functional

Exchange and correlation make atoms stick together and form molecules. In DFT, the term V_{XC} which depends on E_{XC}, is completely unknown. Hence, various approximations have been made to describe exchange and correlation in DFT.

1) The local density approximation (LDA) is the simplest approximation to E_{XC}. It considers electron density as a single value at each position. E_{XC} depends only on that local density *ρ(r)*.

$$E_{xc}^{LDA}[\rho] = \int \rho(r)\varepsilon_{xc}(\rho)dr \tag{2.30}$$

$\varepsilon_{xc} =$ exchange correlation energy per particle

2) Generalized Gradient Approximation- GGA

In GGA, E_{XC} depends on the density at a point and also the density gradient at that point.

$$E_{xc}^{GGA}[\rho(r)] = E_{xc}^{LDA}[\rho(r)] + \Delta E_{xc}\left[\frac{|\nabla\rho(r)|}{\rho^{\frac{4}{3}}(r)}\right] \tag{2.31}$$

3) Meta-GGA

In GGA, the density gradient is considered and a logical further development beyond GGA is the inclusion of the second derivative of the density. Such functionals are called meta-GGAs. A meta-

GGA depends on $\nabla^2 \rho(r)$ which is the Laplacian of the density or τ(r) which is called the kinetic energy density.

$$\tau(r) = \sum_{i}^{occupied} \frac{1}{2}|\nabla\psi_i(r)|^2 \qquad (2.32)$$

Ψ_i = self consistently determined Kohn-Sham orbitals.

4) Hybrid functional

Hybridization of DFT with HF exchange creates hybrid functionals.

$$E_{xc} = (1-a)E_{xc}^{DFT} + aE_x^{HF} \qquad (2.33)$$

B3LYP is one of the most popular hybrid functionals. It contains B88 and HF exchange.

(equation 2.34)

$$E_{XC}^{B3LYP} = (1-0.20)E_X^{LSDA} + 0.20E_X^{HF} + 0.72\Delta E_X^{B88} + (1-0.81)E_C^{LSDA} + 0.81E_C^{LYP} \qquad (2.34)$$

LYP - Lee Yang and Parr correlation functional

LSDA- local spin-density approximation

5) Double Hybrid functional

Unoccupied KS orbitals are incorporated in the calculation (hybrid DFT + MP2)

$$E_{XC} = (1-a_X)E_X^{DFT} + a_X E_X^{HF} + (1-a_C)E_X^{DFT} + a_C E_X^{PT2} \qquad (2.35)$$

PT2 is the MP2 contribution

E.g. B2PLYP; a_X =0.53 and a_C=0.27

Perdew's Jacob's Ladder[3] scheme for DFT (given in figure 2.2) presents the different approximations in DFT which connect the Hartree world and heaven of chemical accuracy.

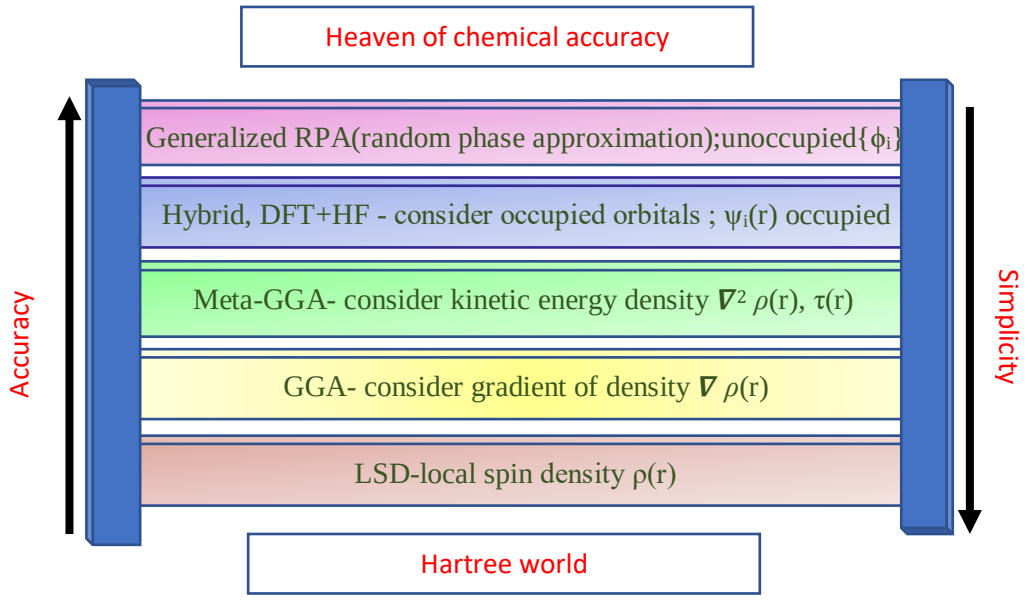

Figure 2.2: Perdew's Jacob's Ladder[3]

2.1.8 Relativistic effects [4,5]

Relativistic effects arise when the speed of electrons comes close to the speed of light. These relativistic effects strongly influence the properties of heavy metals. According to Einstein's theory of special relativity, the mass of a moving object changes with its velocity (equation 2.36).

$$m_{moving} = \frac{m_0}{\sqrt{1-\left(\frac{v}{c}\right)^2}} \tag{2.36}$$

m_{moving} is the mass when moving, m_0 is the mass at zero velocity, c is the speed of light. When the velocity of the object, v, is small, $\frac{m_{moving}}{m_0} \sim 1$. However, when v is significantly large, $\frac{m_{moving}}{m_0}$ is not equal to 1. According to the Bohr model, the electron obeys the following equations (equations 2.37-39).

$$v = \left(\frac{2\pi e^2}{\mathrm{nh}}\right)\mathrm{Z} \tag{2.37}$$

$$E = -\left(\frac{2\pi^2 e^4}{n^2 h^2}\right) mZ^2 \tag{2.38}$$

$$r = \frac{Ze^2}{mv^2} \tag{2.39}$$

Z, n, e, r and *h* are the atomic number, the principal quantum number, the electron charge, orbital radius, and Planck's constant, respectively. The velocity calculated from equation 2.37 can be substituted into equation 2.36 and the ratio $\frac{m_{moving}}{m_0}$ can be found. According to equation 2.38, the energy change resulting when m_o is replaced by m_{moving} increases with *Z*. As shown in equation 2.39 *r* is inversely proportional to mass, therefore, the orbital radius decreases with increasing mass.

The Dirac equation best describes the relativistic effects on the electronic structure. The four-component relativistic quantum chemical methods, the Dirac Hamiltonian is given as equation 2.40.

$$H = c\,\alpha.p + c^2\beta + V \tag{2.40}$$

The 4 x 4 Dirac matrices can be written in terms of 2 x 2 submatrices

$$\beta = \begin{pmatrix} I & 0 \\ 0 & -I \end{pmatrix} \quad \alpha = \begin{pmatrix} 0 & \sigma \\ \sigma & 0 \end{pmatrix}$$

$$\sigma = (\sigma_x, \sigma_y, \sigma_z)$$

$$\sigma_x = \begin{pmatrix} 0 & 1 \\ 1 & 0 \end{pmatrix} \sigma_y = \begin{pmatrix} 0 & -i \\ i & 0 \end{pmatrix} \sigma_z = \begin{pmatrix} 1 & 0 \\ 0 & -1 \end{pmatrix} \tag{2.41}$$

c = speed of light

p = momentum operator

V = external potential

σ = vector of the 2 x 2 Pauli spin matrices

I = two-dimensional identity matrix

The Zeroth-Order Regular Approximation (ZORA) is a two-component approximation to the Dirac equation. The regular approximation expands the full four-component relativistic Hamiltonian with respect to a potential-dependent perturbation parameter. The zeroth order of this expansion already leads to a relativistic energy correction. ZORA contains spin-orbit (SO) and scalar relativistic (SR) corrections (equation 2.42 and 2.43).

$$H^z\varphi^z = \left(V + \sigma.p\frac{c^2}{2c^2 - V}\sigma.p\right)\varphi^z = (H^z_{SR} + H^z_{SO})\varphi^z \tag{2.42}$$

$$H^z_{SR}\varphi^z_{SR} = \left(V + p\frac{c^2}{2c^2 - V}p\right)\varphi^z_{SR} \tag{2.43}$$

The potential *V* comprises the nuclear field and the electron Coulomb and exchange-correlation potentials. Upon neglecting the coupling of spin and orbital angular momentum, the equation for scalar ZORA (equation 2.43) is obtained.

With the consideration of the relativistic energy corrections, calculations become challenging and the effective core potential (ECP) approach is an alternative relativistic approach which can be used to overcome this. Significant reduction in computational cost is achieved by replacing the inner shell electrons with a suitable parameterized effective potential (or a pseudopotential – will discuss in detail in section 2.2.5) and this can also contain relativistic effects. The reliable ECPs separate core and valence shells according to the main quantum number, e.g.,3s and 3p for Ti and 4s, 4p, 4d, 5s and 5p for Ce is included in the valence shell[6].

2.1.9 Geometry optimization and frequency analysis

The geometry optimization in computational chemistry is the process of finding an arrangement in space of a given collection of atoms which is a stationary point on the potential energy surface (PES) and net inter-atomic forces on each atom are zero. This is usually the first step in the

calculation and the optimized structure can be used for further studies or making predictions. During the calculation, we are looking for zero gradients. However, not all zero gradient points are having minimum energy. The zero gradient points can be maxima, minima and saddle points in the PES.

To differentiate the zero gradient points, the second derivatives of the PES are generated with respect to the geometry (equation 2.44). This is called a Hessian matrix ($H_{ij}^{(k)}$). Diagonalization of a Hessian matrix gives eigenvalues and eigenvectors. Eigenvalues are proportional to the square of vibrational frequencies. A negative eigenvalue means, one of its square roots is an imaginary number (imaginary frequency) and this corresponds to the negative curvature of the corresponding normal coordinate. That is, geometry at this coordinate is passing through an energy maximum. In other words, the Hessian matrix can be used to identify the local shape (curvature) of the PES. Maxima or saddle points (maximum in one direction and minima in other directions) are having one or more imaginary frequencies. A minimum is only having real frequencies.

$$H_{ij}^{(k)} = \left.\frac{\partial^2 U}{\partial q_i \partial q_j}\right|_{q=q^{(k)}} \tag{2.44}$$

i and *j* = Cartesian coordinates

U = energy

q = n-dimensional coordinate vector

2.1.10 Charge analysis [7]

Partial atomic charges are important when interpreting results and there are various models for quantifying the atomic charges. Partial charges do not have a strict quantum mechanical definition and different model can provide different numbers for atomic charges. The Mulliken population analysis is the oldest and best-known model for finding the atomic charges.

The Mulliken population analysis uses the basis functions, in terms of which the molecular wave function is expressed. If the coefficients of the basis functions in the molecular orbital are $C_{\mu i}$ for the μ'th basis function in the i'th molecular orbital and n_i is the orbital population,

$$D_{\mu\nu} = \sum_i n_i C_{\mu i} C_{\nu i} \tag{2.45}$$

$$P_{\mu\nu} = D_{\mu\nu} S_{\mu\nu} \tag{2.46}$$

D = density matrix

P = population matrix

S = overlap matrix

$$Q_\mu = D_{\mu\mu} S_{\mu\mu} + \sum_{\nu(\neq\mu)} \frac{1}{2}\left(D_{\mu\nu} S_{\mu\nu} + D_{\nu\mu} S_{\nu\mu}\right) \tag{2.47}$$

The diagonal elements $D_{\mu\mu} S_{\mu\mu}$ represent the net Mulliken population that basis function acquires in the molecule. The gross Mulliken population Q_μ is obtained by assigning half of each total overlap population $(D_{\mu\nu} S_{\mu\nu} + D_{\nu\mu} S_{\nu\mu})$ to this basis function (and the other half to the corresponding other basis function).

The gross atomic population is the sum of Q_μ over all the orbitals μ belonging to atom A.

$$Q_A = Z_A - \sum_{\mu\in A} Q_\mu \tag{2.48}$$

Q_A = charge of atom A

Z_A = atomic number of atom A

2.2 BAND STRUCTURE DIAGRAMS

This section is mainly based on Hoffmann[8] and Dronskowski & Hoffmann.[1]

The electronic band structure diagrams can be used to classify the material as a metal (conductor), semiconductor or insulator. The magnitude of the Brillouin can be obtained for certain materials and the band gap can be classified as direct or indirect by examining the band structure diagram.

2.2.1 Bloch's theorem

Bloch's theorem uses the translational symmetry to generate a wave function which can be applied to crystals. This contains crystal orbitals or so-called electronic bands (crystal orbitals that are very close together form a band).

$$V(r + T) = V(r) \tag{2.49}$$

V(r) = potential determined by the crystal lattice

T= translation vector of the lattice (lattice vector)

This theorem assumes a perfect crystal which neglects impurities, defects (missing atoms) in a real crystal. The Bloch's theorem for a given wave function $\psi(k,r)$ which fulfills the Schrödinger equation, can be express as in equation 2.49. It uses the quantum number *k* as an index to differentiate the various solutions. The extended wave function for the crystal which is a function of a lattice vector is given on the left-hand side of the equation 2.49.

$$\psi(k,r+T) = e^{ikT}\psi(k,r) \tag{2.50}$$

We have to know the $\psi(k,r)$ at the point *r* inside the crystallographic unit cell. Then we can find it for the entire crystal *r*+*T*. Because of *k*, the wave function generated is symmetry-adapted to an infinite system. The *k*, the quantum number is having restrictions on the value it can adopt.

2.2.2 Reciprocal space and k-value

Reciprocal space is introduced to simplify infinite systems such as crystals. In the real space a vector R can be given as equation 2.51. where a_1, a_2, a_3 are basic vectors.

$$R = n_1a_1, n_2a_2, n_3a_3 = a \tag{2.51}$$

In the reciprocal lattice, we have the vector K constructed from reciprocal basic vectors.

$$K = m_1g_1, m_2g_2, m_3g_3 = g \tag{2.52}$$

The real space and reciprocal space vectors are connected as follows,

$e^{iKR} = 1$

The quantum number *k* comes with a small area which is called the Brillouin zone. The *k* provides energy and crystal momentum ρ of free electrons.

$E = k^2$, $\rho = k$ (these values are having Rydberg units)

The band structure diagram describes the energy range of an electron within a crystal. Therefore, to generate the band structure diagram $E(\psi(k,r))$ must be calculated. This can be considered as a diagram equivalent to a molecular orbital diagram. The term $\psi(k,r)$ is known as crystal orbital, and for a given *k* value, there may be many one-electron wave functions, as molecules are having several molecular orbitals.

With the help of periodic boundary conditions, the values for *k* can be obtained. In the one-dimensional situation, there is a crystal of length *L* repeating *N* times (N is the number of unit cells) with lattice parameter *a* (like a string). If the two ends of the string are fastened so as to make a circle, then the Bloch's theorem would look like the equation 2.53 for any *k* value.

$$\psi(k,0) \equiv \psi(k,L) = e^{ikL}\psi(k,0) \tag{2.53}$$

To make equation 2.53 valid to all k, make $kL = 2\pi$

$$-\frac{\pi}{a} \leq k \leq \frac{\pi}{a} \quad \text{or } 0 \leq |k| \leq \frac{\pi}{a} \tag{2.54}$$

Just as the left and right ends are fastened in the one-dimensional case, it is possible to fasten left/right, top/down, back/front faces of the three-dimensional case. Even though it is hard to imagine the resulting structure, it is mathematically acceptable. To plot the band structure diagram

of the three-dimensional case, it follows the conventional method of plotting the band structure along a one-dimensional path that passes through points of symmetry.

2.2.3 Brillouin zone

In the reciprocal space, a zone which satisfies the condition in equation 2.54 is called the Brillouin zone. It is considered as the unit cell in reciprocal space. According to Bloch's theorem, any number of *k* points can be considered within this unit cell or Brillouin zone.

When performing calculations, the irreducible Brillouin zone is introduced for further simplification. It is an irreducible wedge of reciprocal space which can be used to obtain the whole Brillouin zone by applying all symmetry operations.

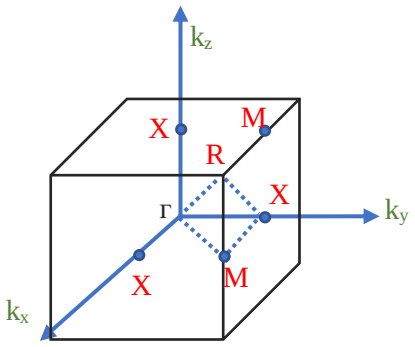

Figure 2.3: Brillouin zone for cubic space group

(The diagram is adapted from Dronskowski & Hoffmann,[1] p.67)

In the Brillouin zone, Γ is the center of the zone. The other points are fractions of reciprocal vectors, that is multiples of 2π/a. This convention is similar to any space group. Figure 2.3 represents a cubic space group and the X, M, R points can be defined as below.

X = $(\frac{1}{2}, 0, 0)$ or $(0, \frac{1}{2}, 0)$ or $(0, 0, \frac{1}{2})$

M = $(\frac{1}{2}, \frac{1}{2}, 0)$ or $(0, \frac{1}{2}, \frac{1}{2})$

R = $(\frac{1}{2}, \frac{1}{2}, \frac{1}{2})$

2.2.4 Band structure of a one-dimensional system

A chain of equally spaced hydrogen atoms (Scheme 2.1) can be considered as a one-dimensional system. The position of the H atoms in the chain is given in terms of the translational vector *T*. If the interatomic distance is *a*, *T*=*n a*

----H----H----H----H----H----H----H----H----H---- Scheme 2.1

H atoms are having single 1s atomic orbitals, ϕ_s. $\psi(k)$ goes over all atomic orbitals and can be written as equation 2.55.

$$\psi(k) = \sum_{n=1}^{N} e^{ikna}\phi_n \quad with \;\; 0 \leq |k| \leq \frac{\pi}{a} \tag{2.55}$$

At the center of the zone (Γ), with *k*=0, e^{ikna}=1. Therefore, the crystal orbital at the center of the zone can be given as equation 2.56.

$$\psi(0) = \sum_{n=1}^{N} \phi_n \;\; = \phi_1 + \; \phi_2 + \phi_3 + \phi_4 \ldots, \tag{2.56}$$

For the zone edge, X, the crystal orbital can be given as equation 2.57. The constituting atomic orbitals are having alternating -/+ signs.

$$\psi\left(\frac{\pi}{a}\right) = \sum_{n=1}^{N} e^{i\pi n}\phi_n \;\; = -\phi_1 + \; \phi_2 - \phi_3 + \phi_4 \ldots, \tag{2.57}$$

Between the center of the zone (Γ) and the zone edge (X), $k = \frac{\pi}{2a}$. The corresponding energies of the crystal can be calculated using equation 2.58.

$$E(k) = \frac{\langle \psi(k) | H | \psi(k) \rangle}{\langle \psi(k) | \psi(k) \rangle} \tag{2.58}$$

Since the H atom chain is having one atomic orbital per unit cell, we can get only a single band.

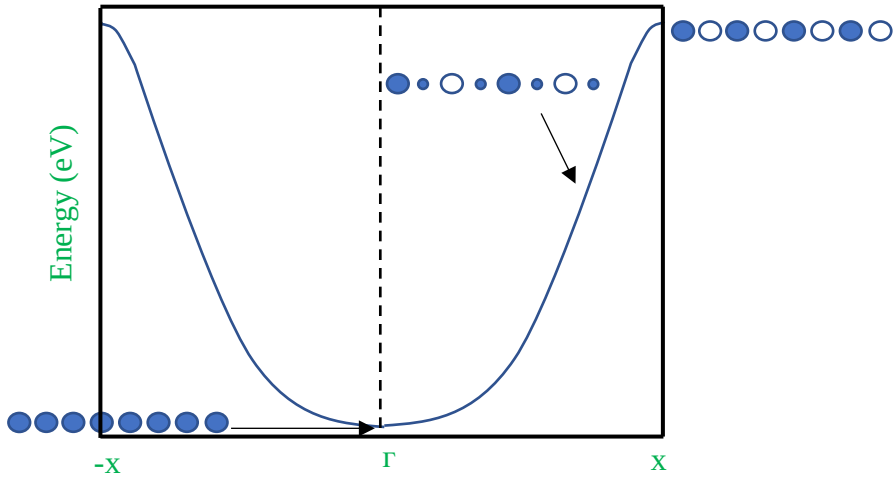

Figure 2.4: Band structure diagram for the 1D chain of H given in scheme 2.1

(The diagram is adapted from Dronskowski & Hoffmann[1], p.70)

As given in figure 2.4, the in-phase bonding combination of all atomic orbitals are at *k*=0 (Γ) is giving the lowest energy. At $k = \frac{\pi}{a}$, that is at X, is the highest energy point where all the atomic orbitals are out of phase. At X the interactions are antibonding. At the middle, $k = \frac{\pi}{2a}$, orbitals are nonbonding and having medium energy. The right side of the graph represents the energy values at -*k*. Overall the band is going uphill from *k*=0 to π /a. On the other hand, if the material under consideration has sigma interactions of p orbitals, a downhill trend will result. An example is given by a chain of nitrogen atoms which is analogous to scheme 2.1.

Consider an H chain having two different interatomic distances (scheme 2.2) which creates a unit cell containing 2 H atoms. The band structure diagram will have two bands due to the two atomic orbitals. The value of *a* in scheme 2.2 is greater than in scheme 2.1 and that reduces the size of the Brillouin zone ($0 \leq |k| \leq \frac{\pi}{a}$).

----H---H------H---H------H---H------H---H------ **Scheme 2.2**

a

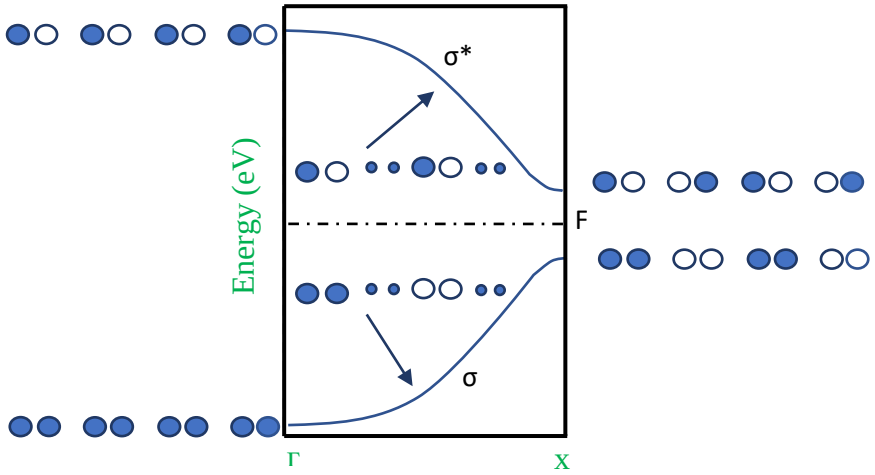

Figure 2.5: Band structure diagram for the 1D chain of H (two different interatomic distances) given in scheme 2.2

(The diagram is adapted from Dronskowski & Hoffmann,[1] p.75)

The lower-lying band (valence band) looks like an *s* band and curves uphill. The upper lying band (conduction band) is pointing downhill. The interactions between the H_2 molecules have the following features as given in table 2.1.

Table 2.1: Inter- and intramolecular interactions between molecules[9] with reference to scheme 2.2

The value of *k*	In the conduction band (σ*)		In the valence band (σ)	
	intramolecular	intermolecular	intramolecular	intermolecular
0 (at Γ point)	σ*	σ*	σ	σ
π /2a (at the middle point)	σ*	nonbonding	σ	nonbonding
π /a (at X point)	σ*	σ	σ	σ*
	Form Γ to X; σ* ⟶ σ The band is having a downhill		Form Γ to X; σ ⟶ σ* The band is having an uphill	

Since the unit cell has 2 electrons, the valence band is full, and the conduction band is empty. Hence, the minimum energy difference between these 2 bands is the HOMO-LUMO gap of the material. If the bottom of the conduction band and the top of the valance bands lie just one above the other, the band gap is said to be a direct band gap. Line *F* represents the Fermi level, and in this example, it lies midway between the two bands. The Fermi level is a hypothetical energy level where the probability of finding an electron is 50% at finite temperature. When the Fermi level cuts a band, one can expect conductivity in the material, and if not, that material is either a semiconductor or an insulator. When we are generating a band structure diagram for any other material, we might get many bands. The number of bands is equal to the number of atomic orbitals in the unit cell. Depending on the degree of intermolecular overlap it will result in wide or narrow bands. With a large intermolecular overlap, electrons are more delocalized and result in a wide band. With a weak intermolecular overlap, electrons are more localized and result in a narrow band.

2.2.5 Band structure calculations

Plane waves are considered as the most suitable basis functions for band structure calculations. Plane waves (e^{ikr}) act as symmetry adopted wave functions to a crystal's boundary conditions and a plane wave is unbiased by the position of the atoms. The crystal wavefunction $\psi_n\,(k,\, r)$ is expressed as a linear combination of various exponential functions.

$$\psi_n(k,r) = \sum_K c_n\,(k,K)e^{i(k+K)r} = e^{ikr}\sum_K c_n\,(k,K)e^{iKr} \qquad (2.59)$$

K = reciprocal lattice vector (given in equation 2.52)

c_n= mixing coefficient (can be found analytically or numerically)

In practice, to control the size of the basis set, a plane wave cut off energy condition is applied to equation 2.59. Then only the plane waves having kinetic energy that is smaller than the given cut-off value will be considered for the calculation. Higher cut-off energy increases accuracy.

$E_{cut} > \frac{(k+K)^2}{2}$ (kinetic energy of plane wave)

$\psi_n\,(k,\, r)$ show rapid oscillations closer to the nuclei. Then it becomes a smooth function when going away from the nucleus as shown in figure 2.6. These oscillations reflect the atomic nature at the core region, and if we neglect the core region, $\psi_n\,(k,\, r)$ stay as a simple plane wave (figure 2.6).

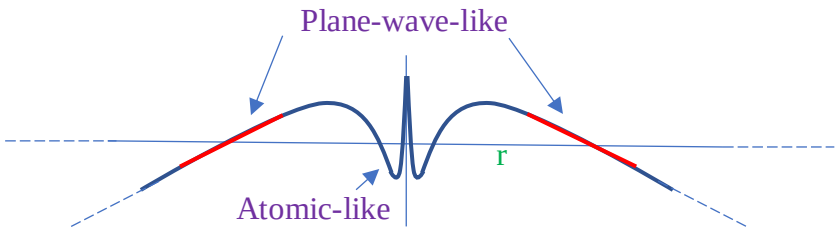

Figure 2.6: Schematic diagram for atomic orbital's atomic and plane wave nature

(The diagram is adapted from Dronskowski & Hoffmann[1], p.136)

The pseudopotential approach, which was first introduced by Hellmann [10], is used to overcome the effect of oscillations where the strong ion-electron potential is replaced by a much weaker pseudopotential. According to Pauli's principle, valence electrons have a low probability of entering the core region and there is a strong repulsion between the core and valence electrons. At the same time, valance electrons experience Coulomb attraction by the nucleus. These opposite effects cancel each other and only a weak pseudopotential will remain. In other words, as core electrons are screening the nucleus from the valence electrons, the valence electrons are experiencing only this pseudopotential which is much smoother than nuclear electron coulomb potential. Today pseudopotentials are categorized as either semi-local or nonlocal. So that, s, p, d, f levels see the pseudopotentials in different ways. In the semi-local category, each orbital feels its own correct pseudopotential. In the non-local category individual levels are treated entirely in a different way.

In the solid-state calculations, nonlocal but norm-conserving pseudopotentials are used which hold the same charge density in the atom's inner part. The valence electrons do not notice when the charge distribution is replaced by a smoother one inside the atom's inner part as long as its charge density is constant.

When we can use a smaller plane-wave cut off energy with a given pseudopotential, the pseudopotential is considered as a soft pseudopotential. The elements like alkali metals and transition metals are having a large plane wave cut off energy. Ultra-soft pseudopotentials are introduced to overcome this which do not follow the norm-conservation. Ultra-soft pseudopotentials were first introduced by Vanderbilt (1990) by relaxing the norm-conservation constraint (by removing the charge associated with the core region). More effort is needed for the

generation of ultra-soft pseudopotentials, but they can have low plane wave cut off energy in the calculation.

Practically, a finite number of k point are used for the calculation (numerical integration over the Brillouin zone). A higher number of *k* points makes the calculation more accurate than a lower number of *k* points. A small unit cell in real space is having a large Brillouin zone, which needs a higher number of *k* points to get better results. Larger unit cells are having small Brillouin zones and a few *k* points will be enough to get accurate results.

2.3 COMPUTATIONAL DETAILS

The Amsterdam Density Functional (ADF) software package[11–13] was used to perform DFT calculations. ADF uses STOs as basis functions. STOs correctly describe the cusp at the nucleus and then decay exponentially with the distance from the nucleus. ADF is popular in industrial and academic research especially because ADF excels in spectroscopy, transition metal, and heavy elements problems.

Molecular calculations were performed, specifically, geometry optimizations followed by frequency calculations[14–16] for gas-phase structure. The absence of imaginary frequencies confirms that the geometry is a local minimum. For the relativistic effects, ZORA is used. [17,18] Relativistic effects cannot be neglected especially when we have heavy atoms.[19,20]

For the calculations performed in this thesis, dispersion corrected Density Functional Theory (DFT-D) was incorporated to improve the accuracy of the energy.[21] The GGA in the form of the Perdew, Burke, and Ernzerhof (GGA PBE) functional[22] and TZP (triple zeta polarized) basis sets were applied, and [23] and a high numerical integration parameter 7 was used to achieve convergence in the systems.

GGA PBE provides reasonable results when compared to available experimental results in similar systems. However, in GGA PBE the electron density and its gradient are one-electron functions and these cannot give dispersion interactions.[24] Weak, long-range dynamic correlations between fluctuating charge distributions are described as dispersion interactions. The standard DFT fails to describe these non-covalent interactions present in conducting polymers. The DFT-D approach provides a solution to these non-covalent interactions while adding very little cost to the calculations.[24,25,26] In triple zeta basis sets, three basis functions are used for each atomic orbital. The polarization functions add flexibility to the basis set. Practically, most properties converge at TZP.

Band structure diagrams were generated for the systems under study by performing periodic calculations. The Quantum-Espresso software package[27] was used for the calculations with the DFT-D approach, GGA PBE and plane-wave basis set. Ultra-soft pseudopotentials were incorporated to have efficient calculations. Monkhorst-Pack k-mesh[28] was used for sampling the Brillouin zone. Monkhorst-Pack method distributes the k points homogeneously in the Brillouin zone. Self-consistent calculations followed by band structure calculations were carried out with a relaxed structure.

References

(1) Dronskowski, R.; Hoffmann, R. *Computational Chemistry of Solid State Materials: A Guide for Materials Scientists, Chemists, Physicists and Others*, 1 edition.; Wiley-VCH: Weinheim, 2006.

(2) Cramer, C. J. *Essentials of Computational Chemistry: Theories and Models*; John Wiley & Sons, 2013.

(3) Perdew, J. P.; Ruzsinszky, A.; Tao, J.; Staroverov, V. N.; Scuseria, G. E.; Csonka, G. I. Prescription for the Design and Selection of Density Functional Approximations: More Constraint Satisfaction with Fewer Fits. *J. Chem. Phys.* **2005**, *123* (6), 062201.

(4) Filatov, M.; Cremer, D. On the Physical Meaning of the ZORA Hamiltonian. *Mol. Phys.* **2003**, *101* (14), 2295–2302.

(5) Thayer, J. S. Relativistic Effects and the Chemistry of the Heavier Main Group Elements. In *Relativistic Methods for Chemists*; Barysz, M., Ishikawa, Y., Eds.; Springer Netherlands: Dordrecht, 2010; pp 63–97.

(6) *Modern Methods and Algorithms of Quantum Chemistry: Winterschool, 21 - 25 February 2000, Forschungszentrum Jülich, Germany. ... Proceedings*, 2. ed.; Grotendorst, J., Ed.; NIC series.

(7) Fonseca Guerra, C.; Handgraaf, J.-W.; Baerends, E. J.; Bickelhaupt, F. M. Voronoi Deformation Density (VDD) Charges: Assessment of the Mulliken, Bader, Hirshfeld, Weinhold, and VDD Methods for Charge Analysis. *J. Comput. Chem.* **2004**, *25* (2), 189–210.

(8) Hoffmann, R. *Solids and Surfaces: A Chemist's View of Bonding in Extended Structures*; VCH Publishers: New York, NY, 1988.

(9) Https://Authorzilla.Com/AJBrN/Microsoft-Powerpoint-Bandstr1-Lect17.Html Accessed 2018-10-02.

(10) Schwerdtfeger, P. The Pseudopotential Approximation in Electronic Structure Theory. *ChemPhysChem* **2011**, *12* (17), 3143–3155.

(11) Baerends, E. J.; Ziegler, T.; Atkins, A. J.; et al. *ADF2017, SCM, Theoretical Chemistry, Vrije Universiteit, Amsterdam, The Netherlands, Https://Www.Scm.Com*.

(12) te Velde, G.; Bickelhaupt, F. M.; Baerends, E. J.; Fonseca Guerra, C.; van Gisbergen, S. J. A.; Snijders, J. G.; Ziegler, T. Chemistry with ADF. *J. Comput. Chem.* **2001**, *22* (9), 931–967.

(13) Fonseca Guerra, C.; Snijders, J. G.; te Velde, G.; Baerends, E. J. Towards an Order-N DFT Method. *Theor. Chem. Acc.* **1998**, *99* (6), 391–403.

(14) Bérces, A.; Dickson, R. M.; Fan, L.; Jacobsen, H.; Swerhone, D.; Ziegler, T. An Implementation of the Coupled Perturbed Kohn-Sham Equations: Perturbation Due to Nuclear Displacements. *Comput. Phys. Commun.* **1997**, *100* (3), 247–262.

(15) Jacobsen, H.; Bérces, A.; Swerhone, D. P.; Ziegler, T. Analytic Second Derivatives of Molecular Energies: A Density Functional Implementation. *Comput. Phys. Commun.* **1997**, *100* (3), 263–276.

(16) Wolff, S. K. Analytical Second Derivatives in the Amsterdam Density Functional Package. *Int. J. Quantum Chem.* **2005**, *104* (5), 645–659.

(17) van Lenthe, E.; Baerends, E. J.; Snijders, J. G. Relativistic Regular Two-component Hamiltonians. *J. Chem. Phys.* **1993**, *99* (6), 4597–4610.

(18) van Lenthe, E.; Baerends, E. J.; Snijders, J. G. Relativistic Total Energy Using Regular Approximations. *J. Chem. Phys.* **1994**, *101* (11), 9783–9792.

(19) Kaloni, T. P.; Schreckenbach, G.; Freund, M. S. Band Gap Modulation in Polythiophene and Polypyrrole-Based Systems. *Sci. Rep.* **2016**, *6* (1), 36554.

(20) Autschbach, J. Perspective: Relativistic Effects. *J. Chem. Phys.* **2012**, *136* (15), 150902.

(21) Grimme, S. Semiempirical GGA-Type Density Functional Constructed with a Long-Range Dispersion Correction. *J. Comput. Chem.* **2006**, *27* (15), 1787–1799.

(22) Perdew, J. P.; Burke, K.; Ernzerhof, M. Generalized Gradient Approximation Made Simple. *Phys. Rev. Lett.* **1996**, *77* (18), 3865–3868.

(23) van Lenthe, E.; Baerends, E. J. Optimized Slater-Type Basis Sets for the Elements 1–118. *J. Comput. Chem.* **2003**, *24* (9), 1142–1156.

(24) Chen, X. P.; Jiang, J. K.; Liang, Q. H.; Yang, N.; Ye, H. Y.; Cai, M.; Shen, L.; Yang, D. G.; Ren, T. L. First-Principles Study of the Effect of Functional Groups on Polyaniline Backbone. *Sci. Rep.* **2015**, *5*, 16907.

(25) Ehrlich, S.; Moellmann, J.; Grimme, S. Dispersion-Corrected Density Functional Theory for Aromatic Interactions in Complex Systems. *Acc. Chem. Res.* **2013**, *46* (4), 916–926.

(26) Grimme, S. Density Functional Theory with London Dispersion Corrections. *Wiley Interdiscip. Rev. Comput. Mol. Sci.* **2011**, *1* (2), 211–228.

(27) Giannozzi, P.; Baroni, S.; Bonini, N.; Calandra, M.; Car, R.; Cavazzoni, C.; Davide Ceresoli; Chiarotti, G. L.; Cococcioni, M.; Dabo, I.; et al. QUANTUM ESPRESSO: A Modular and Open-Source Software Project for Quantum Simulations of Materials. *J. Phys. Condens. Matter* **2009**, *21* (39), 395502.

(28) Monkhorst, H. J.; Pack, J. D. Special Points for Brillouin-Zone Integrations. *Phys. Rev. B* **1976**, *13* (12), 5188–5192.

Chapter 3 : RESULTS AND DISCUSSION - PROJECT I

The study discussed in this chapter has been submitted to the Journal of Physical Chemistry C. Authors: Jayasundara, W.J.M.J.Saumya R.; Schreckenbach, Georg; submitted on 20 June 2019.

Tunability of HOMO- LUMO Levels and Band Gaps in Polythiophene and Polypyrrole Based Conducting Polymers by Doping

3.1 INTRODUCTION

3.1.1 Research objective

The objective of this research is to study the tunability of the band gap and HOMO-LUMO energy levels of several conducting polymers by doping with Cl and Li. Ultimately, this research presents new conducting polymers for potential applications.

3.1.2 Introduction

Polypyrrole (PPy) and polythiophene (PTh) can be considered as two widely studied conjugated polymers having five-membered heteroaromatic rings as monomers.[1–4] Polyselenophene and polytellurophene (S replaced by Se/Te in PTh) are two lesser-known, higher period analogs of PTh which have recently drawn the attention of the research community.[5,6] PTh, Polyselenophene and polytellurophene are having various applications, for instance, in photovoltaics,[7,8] thin-film transistors,[9] biosensors,[10,11] batteries,[12,13] and memory devices.[14] Polyfuran (S replaced by O in PTh) is a lower period analog of PTh which is less stable compared to PTh.[15,16] Successful applications can also be found with polyfuran in photovoltaics[17] and as humidity sensors (the conductivity of polyfuran is sensitive to humidity).[18] In the case of PPy, replacement of N with P and As has been reported as higher period analogs of PPy.[2] PPy is having a large band gap

compared to PTh. The larger band gap results in PPy having lower conductivity than PTh. PPy is also having many applications, for instance, in batteries,[19,20] thin-film transistors,[21] biosensors, [22,23] and memory devices.[24]

The literature provides examples for theoretical studies of structural and electronic properties of PPy and PTh derivatives with doping.[3,25–29] Doping of PTh with Cl_3^- as the dopant has been studied for oligomeric models containing up to 25 monomers.[3,27,29] The doping and dedoping processes of PPy have been reported.[25] Doping of α-tetrathiophene derivatives has been studied with SCN^-, Cl^-, Br^-, NO_3^- , ClO_3^- , ClO_4^- as dopants.[26] PTh has been investigated with Cl and Li atoms as dopants.[28] PPy has been investigated with Li and F atomic dopants.[30–32] To the best of our knowledge, no reports can be found for the above mentioned PPy and PTh analogs with doping atoms. Thus, the current chapter provides a computational study of structural and electronic property changes of PPy and its analogs (N replaced by P, As, Sb in PPy) and PTh and its analogs (S replaced by O, Se, Te in PTh) in the presence of Li and Cl atoms as dopants (Figure 3.1). The dopant atoms are explicitly included into the model of the polymer and are not covalently bound to the polymer. With the use of atomic dopants, it is straightforward to confirm the successful doping by analyzing the change in charge of each dopant.[28,33]

In conjugated polymers, a reduction in the band gap can be observed when increasing the number of monomers.[25,28] Kaloni et. al. reports a study based on polythiophene chains with increasing numbers of monomer units (2, 4, 6, 8) that shows a decrease in the HOMO-LUMO gap when going from 2 to 8 monomers. Moreover, chains having 6 and 8 monomer units have similar values for the HOMO-LUMO gaps showing that the chains are getting similar electronically. Therefore, it is possible to assume convergence of physical properties at that level towards those of the polymer. It was concluded that polymer chains having 6 monomers units (hexamers) are suitable for

modeling such systems.[28] One dopant atom per six monomers was used which is also a reasonable model.[3,28,34]

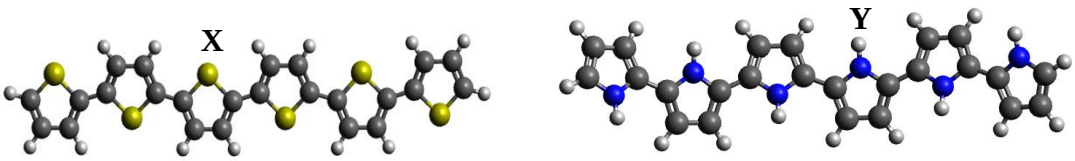

(a) **(b)**

Figure 3.1: Structure of a) polythiophene b) polypyrrole, (X = S/O/Se/Te and Y = N/P/As/Sb to get the corresponding analogs)

The entire study is based on DFT calculations. Molecular and periodic calculations are used to extract HOMO-LUMO energy levels and gaps. Calculations were performed with oligomers having six repeating units (hexamers).[28] In the periodic calculations, plane wave cut-off energy of 70 Ry and Monkhorst-Pack 12 x 1 x1 k-mesh were used with the supercell consisted of six monomers.

3.2 POLYTHIOPHENE AND ITS ANALOGS

3.2.1 Molecular calculations

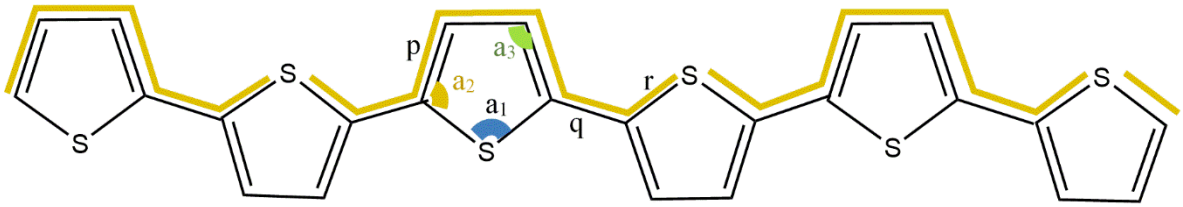

Figure 3.2: Schematic diagram of PTh; S was replaced by O, Se, Te to get the analogs. The values correspond to bond lengths (p, q, r) and angles (a_1, a_2, a_3) are provided in Table 3.1. The orange line represents the specific bond path used in Figure 3.5.

For the molecular calculations, oligomer chains containing 6 monomers (hexamers) were used. Figure 3.2 shows a schematic diagram of PTh; the heteroatom S was replaced by O, Se and Te to get the analogs. Optimized geometries, HOMOs and LUMOs are given in Figure 3.3. Key geometry parameters such as bond lengths and angles of the optimized structures are given in Table 1. Only slight variations were observed in C-C and C=C bond lengths. An increase in bond lengths was observed for the C-X bond lengths when the heteroatom is changed from O to Te due to the increasing size of the atom along with the series, from 1.38 Å to 2.13 Å. Regarding bond angles, the C-X-C angle decreases when going from O to Te (106.5˚ to 82.0˚). All of these parameters are consistent with computational and experimental values reported elsewhere.[1–3,35–38]

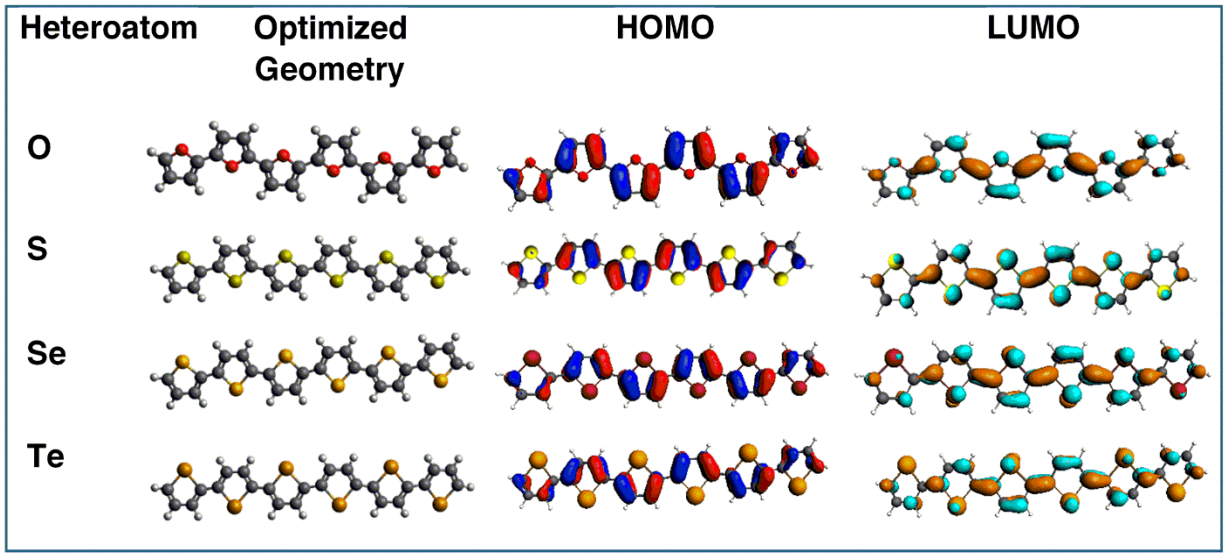

Figure 3.3: Optimized geometries, HOMO and LUMO of PTh and analogs before doping

Table 3.1: Bond lengths (in Å) and bond angles (in °) of PTh and analogs before doping, Molecular calculations (see Figure 3.2). The experimental values [35–38] are given in brackets for the monomer.

Heteroatom (X)	p(C=C)	q(C-C)	r(C-X)	a_1(C-X-C)	a_2(X-C-C)	a_3(C-C-C)
O	1.38 (1.36)	1.43	1.38 (1.36)	106.5 (106.55)	110.0 (110.7)	106.7 (106.5)
S	1.39 (1.37)	1.43	1.75 (1.71)	92.3 (92)	110.0 (111)	113.8 (112)
Se	1.39 (1.37)	1.43	1.90 (1.86)	87.7 (87.72)	109.6 (111.22)	116.5 (114.92)
Te	1.39 (1.37)	1.42	2.13 (2.05)	82.0 (82.53)	109.3 (110.81)	120.0 (117.93)

We have studied thiophene oligomers with one dopant atom per chain. After doping, Li is sitting on top of the polymer chain while Cl is moving away from the polymer chain (Figure 3.4). (About 10 different Initial geometries were considered for the calculation and all ended up showing Li on the top of the polymer and Cl is moving away from the polymer). Similar geometries were observed for the other polymers. The distance between the dopant and atoms in the 3rd monomer ring was measured. For PTh, Li–C distances are in the range of 2.2 -2.4 Å, and in the case of Cl, they are in the range of 2.6 - 4.2 Å, Table 3.2. Cl and Li act as counterions upon doping. The charge transfer process between the polymer chain and the counterions can be analyzed using Mulliken population analysis (Table 3.3). According to the Mulliken population analysis, in PTh, the Cl atom gains -0.45 charge while the Li atom gains 0.50 positive charge. That is, Cl becomes

partially negatively charged, and thus is repelled by the electron-rich monomer ring. In the case of Li doping, the Li atom becomes partially positively charged, leading to attraction by the electron-rich monomer ring.[28] Further, from the results of the Mulliken population analysis, it is clear that the Cl atom has been reduced while the polymer chain has been oxidized. In other words, this is p-type doping of the polymer chain. In the case of Li, the dopant atom has been oxidized while the polymer chain has been reduced. This is n-type doping of the polymer chain.

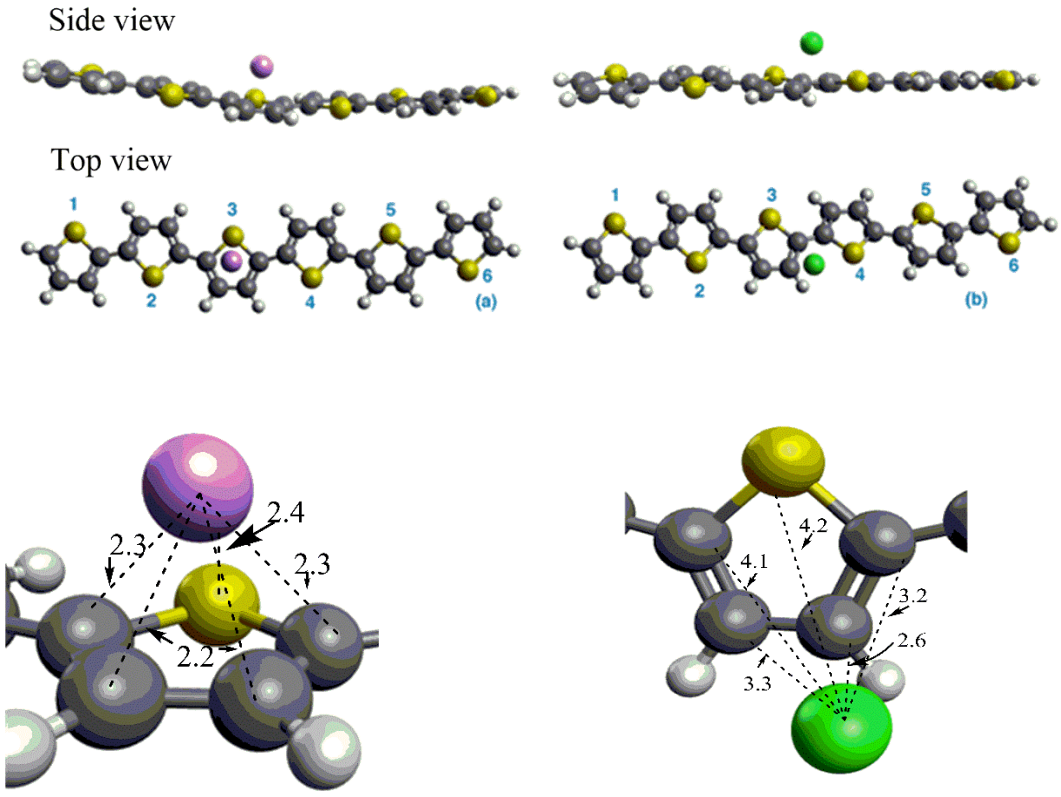

Figure 3.4: Top and side view of optimized geometries (a) PTh doped with Li (b) PTh doped with Cl in molecular calculations. Distance (in Å) to the dopant from atoms in 3rd ring is also shown.

Table 3.2: Distance (in Å) to the dopant (Cl/Li) from atoms in 3rd ring as marked in Figure 3.4

Heteroatom	Distance to the dopant	
	Li	Cl
O	2.1-2.2	2.7-4.0
S	2.2-2.4	2.6-4.2
Se	2.2-2.6	2.7-4.5
Te	2.2-2.8	2.1-4.3

Table 3.3: Mulliken charge of the counterion (e^-)

Heteroatom	Mulliken charge	
	Cl	Li
O	-0.48	0.60
S	-0.45	0.50
Se	-0.49	0.51
Te	-0.26	0.48

The doping process introduces changes in the geometry of the molecules. Changes in bond lengths and bond angles are prominent. In the undoped state, conjugated polymers show mostly aromatic structures, whereas with doping, partially quinoid geometries are expected.[29] The comparative bond length changes along the oligomer chain are shown in Figure 3.5. The corresponding bond path is marked in Figure 3.2, the orange line running along the top of the polymer chain. The bond length changes upon doping are not prominent at two ends of the chain. The counterion is placed in the middle region of the polymer chain and the bond length alternation is partly localized at the

counterion. Changes in bond angles were also observed in the polymer chain. For instance, the C-S-C angle in the 3rd thiophene ring has decreased by 0.8° with Cl dopant and by 0.7° with Li dopant.

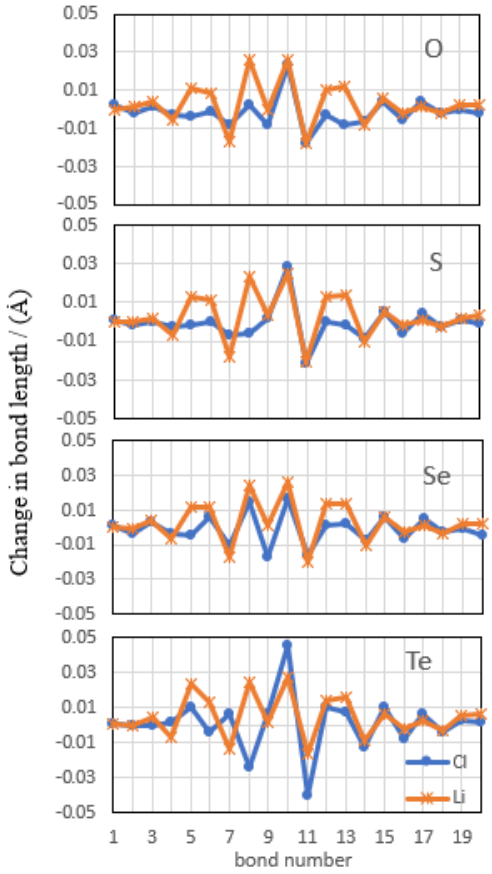

Figure 3.5: The comparative bond length changes along the polymer chain with reference to Figure 3.2, the y-axis represents the difference in bond length before and after doping

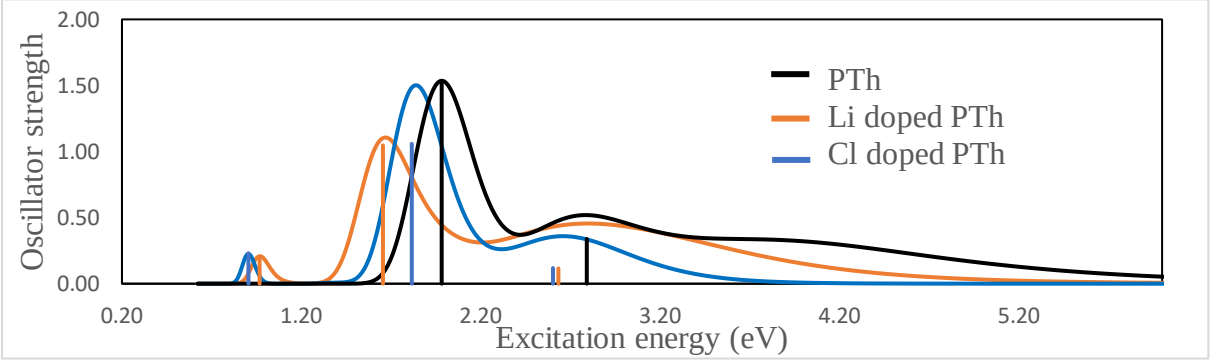

Figure 3.6: UV-vis spectra of PTh (black), Li doped PTh (brown) and Cl doped PTh (blue)

The successful doping was further confirmed by the TD-DFT results. The calculated UV-vis spectra for PTh, Cl/Li doped PTh are given in Figure 3.6. Subband absorptions should be observed after the successful doping due to the formation of a polaron band (in-gap band).[25,39,40] In the present study, the absorption maximum of PTh is at 1.98 eV (625nm) and upon doping it shows a redshift. The excitation occurring from the valence band to the lower polaron band is characterized by the peaks observed at 0.91 eV (1370 nm) in Cl doped PTh and 0.97 eV (1282 nm) in Li doped PTh.[25] The Cl doped polymers containing O, Se, Te heteroatoms show infrared absorptions at 1.17 eV,0.87 eV, 1.02 eV (1064 nm, 1423 nm, 1217 nm) respectively, corresponding to the excitation from the valence band to the lower polaron band. In the case of Li doped polymers, these longer wavelength absorptions were observed at 1.06 eV, 0.93 eV, 0.88 eV (1167 nm, 1327 nm, 1411 nm) respectively.

The HOMO and LUMO energies before and after doping and their corresponding band gaps (E_{gap}) are given in Table 3.4. The band gap values obtained for undoped PTh and analogs are consistent with previous theoretical studies.[2] Experimental values are also shown and they are following a similar trend. The band gap decreases when going from O to Te. As is clearly shown in Figure 3.7, before doping, the HOMO levels of all the polymers show only a slight variation while the LUMO level is decreasing when going form O to Te. Previous reports show that, in PTh, the HOMO level does not have significant contributions by the heteroatom S.[2,41,42] This is also clearly indicated in Figure 3.3. There are no contributions from the heteroatom to the HOMO. All the other polymers show a similar trend. On the other hand, there is a considerable heteroatom contribution to the LUMO. The lower ionization potentials of Se and Te move the LUMO level further down compared to S in PTh, and this results in a decreased band gap when going from S to Se to Te.

Further, low LUMO energies are important to obtain higher n-type properties. Hence, when going from S to Se to Te, the material becomes a promising candidate for n-doping.[43,44]

Figure 3.7 shows the HOMO and LUMO levels of undoped and doped polymers. As shown in Table 3.4, a significant reduction in the HOMO-LUMO energy gap can be seen after the Li and Cl doping. The reduction is higher in the presence of Li dopant as compared to Cl dopant. As Li stays closer to the polymer after doping (Figure 3.4), it is providing effective doping to the polymer. Mulliken charges (Table 3.3) also show higher charge gain by Li atom compared to Cl. Both HOMO and LUMO levels are affected by the doping. Both HOMO and LUMO levels are having a contribution from the counterion, Figure 3.8. Further, this contribution is localized at the counterion. In the case of Li dopant, the contribution is higher at the central rings and it is decreasing when going to both ends of the polymer chain. But in the case of Cl dopant, this uniform behavior is not prominent.

Table 3.4: Calculated HOMO – LUMO gap (E_{gap}) (eV) in PTh and analogs from Molecular calculations. Experimental band gaps (E_{gap} Exp. - in eV) are also given.

Hetero-atom	without dopant				doping with Cl			doping with Li		
	HOMO	LUMO	E_{gap}	E_{gap} Exp.[1]	HOMO	LUMO	E_{gap}	HOMO	LUMO	E_{gap}
O	-4.39	-2.62	1.77	2.35	-4.60	-3.02	1.58	-2.84	-2.06	0.78
S	-4.56	-3.01	1.55	2.05	-4.68	-3.30	1.38	-3.25	-2.48	0.77
Se	-4.57	-3.16	1.41	2.00	-4.71	-3.45	1.26	-3.40	-2.62	0.78
Te	-4.52	-3.37	1.15	1.40	-4.31	-3.32	0.99	-3.60	-2.83	0.77

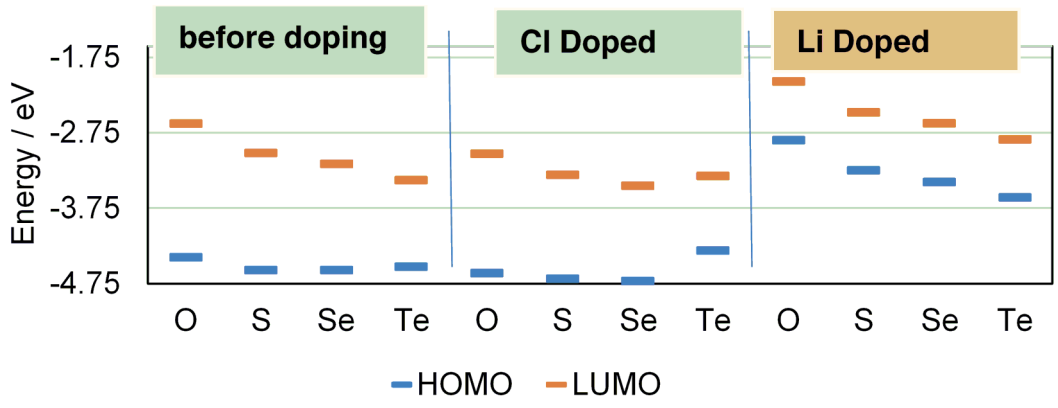

Figure 3.7: HOMO and LUMO levels of PTh and analogs before and after doping

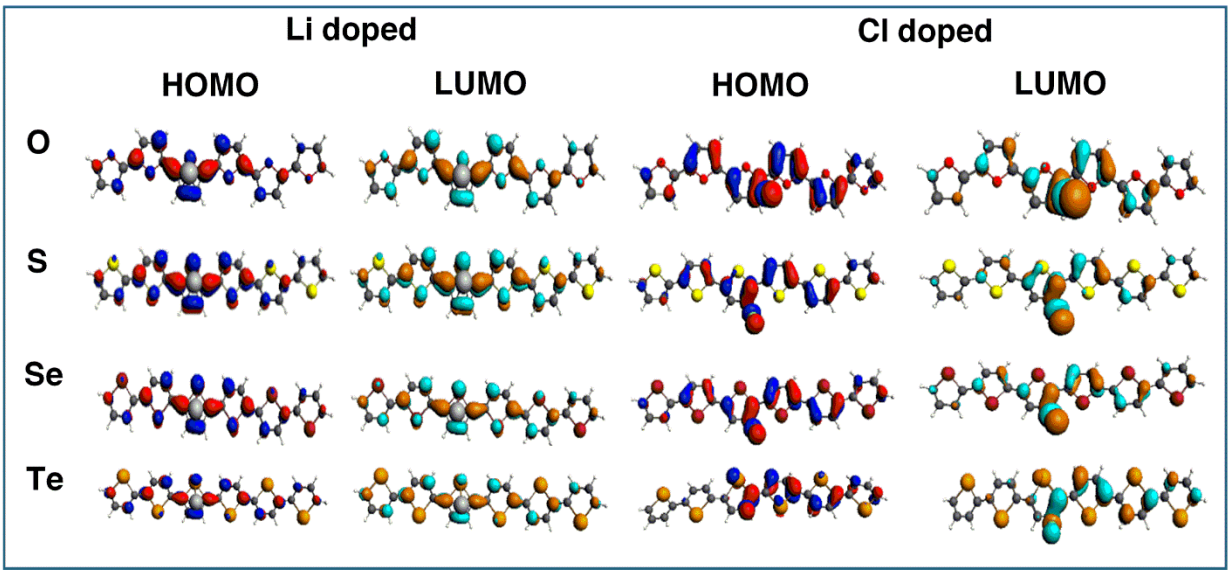

Figure 3.8: HOMO and LUMO of PTh and analogs after doping

3.2.2 Periodic calculations

Molecular calculations on oligomer structures are common, however, they do not provide access to band structures of the periodic geometry. In molecular calculations, the structure is free to move in all three directions while in periodic calculations it is fixed in one direction, due to the periodic boundary conditions. As a consequence, differences in geometry parameters and HOMO-LUMO gaps were observed when comparing periodic calculations with molecular calculations. However, the values more or less follow the same trends. Crystalline structures are used when designing electronic devices using these materials and a periodic model is somewhat closer to that situation. Molecular calculations are also important since their results can be closer to experimental results especially regarding geometries.[2,45] From the periodic calculations, the band structure of the material as a function of electron momentum is obtained.

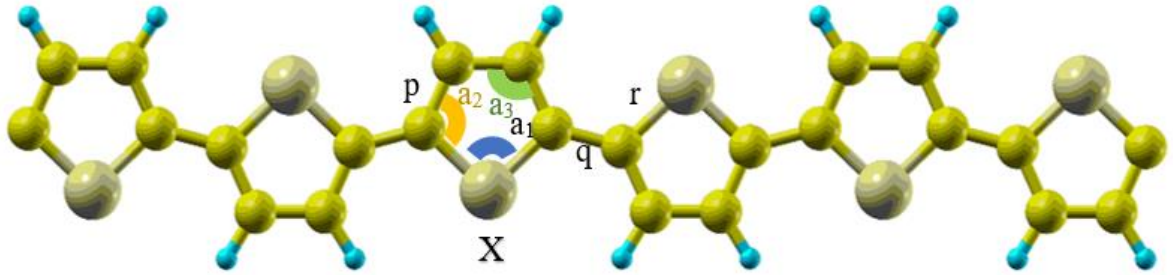

Figure 3.9: The optimized structure of periodic PTh : S was replaced by O, Se, Te to get the analogs. The values correspond to bond lengths (p, q, r) and angles (a_1, a_2, a_3) are given in Table 3.5.

Figure 3.9 shows the optimized structure of PTh from the periodic calculations. The supercell contains 24 carbon (C), 6 sulfur (S) and 12 hydrogen (H) atoms. S was replaced by O, Se and Te to get corresponding analogs. The bond distances and angles of optimized structures are given in Table 3.5. Similar trends can be seen when compared with the molecular calculations, for instance,

an increase in C-X bond distance and a decrease in C-X-C bond angle when the heteroatom X is going from O to Te.

The aromaticity of the heterocycles of these polymers increases when going from O to S but it decreases when going from S to Te.[46,47] On the other hand, when the aromaticity of the polymer chain decreases, the quinoid resonance structure plays a major role. The diffuse lone pairs of large atoms like Se and Te can contribute to the conductivity of the polymer. That is, the interchain charge transfer process can be achieved through the heteroatoms.[6] The bridging bond or the bond between monomers is marked as 'q' in Figure 3.9. According to Table 3.5, the corresponding bond distance for q(C-C) is decreasing when going from S to Te (1.46 Å to 1.41 Å). The decreased bridging bond length proves increased quinoid resonance when going from S to Te.[46] The decreasing trend in bridging bond length when going from S to Te is more prominent in the periodic calculations than in the molecular calculations (Table 3.1). In the molecular calculations, it is only decreasing from 1.43 Å to 1.42 Å when going from S to Te. When comparing O and S containing structures, the bridging bond lengths are the same.

Table 3.5: Bond lengths (in Å) and bond angles (in °) of PTh and analogs before doping with reference to Figure 3.9-Periodic calculations

Heteroatom (X)	p(C=C)	q(C-C)	r(C-X)	a_1(C-X-C)	a_2(X-C-C)	a_3(C-C-C)
O	1.38	1.46	1.40	107.8	108.2	107.9
S	1.39	1.46	1.76	94.3	107.9	114.9
Se	1.39	1.42	1.91	87.3	110.1	116.3
Te	1.39	1.41	2.11	81.9	109.5	119.5

Table 3.6: Conduction bandwidth (W_{CB}), valence bandwidth (W_{VB}), HOMO-LUMO gap (E_{gap}) of PTh and analogs (in eV) form periodic calculations. Experimental band gaps (E_{gap} Exp. - in eV) are also given.

Heteroatom	W_{CB}	W_{VB}	E_{gap}	E_{gap} Exp.[1]
O	0.34	0.41	1.31	2.35
S	0.34	0.39	1.17	2.05
Se	0.38	0.41	0.82	2.00
Te	0.41	0.41	0.60	1.40

Calculated values for the conduction bandwidth (W_{CB}), valence bandwidth (W_{VB}) and HOMO-LUMO gap (E_{gap}) of PTh and analogs are given in Table 3.6. The W_{VB} is the energy difference between the first band just below the Fermi level at Γ to the M point. Correspondingly, the W_{CB} is the energy difference between the first band just above the Fermi level at Γ to the M point.[2]

A slight increase in W_{CB} is observed when going from O to Te. Increased conduction bandwidth is a sign that the material is a promising candidate for n-doping.[2,48] W_{VB} is somewhat constant when going from O to Te. The HOMO-LUMO gap is decreasing when going form O to Te, following a similar pattern observed in the molecular calculations. Molecular calculations result in higher values for the HOMO-LUMO gap when compared to the periodic calculations due to the reasons mentioned above.

The computed electronic band structures, before and after doping, are given in Figure 3.10. The corresponding HOMO-LUMO gaps (band gaps) are summarized in Table 3.7 for Li and Cl doped polymers. It is clear from the band structure diagrams that all the polymers have a direct band gap at the Γ point. With a direct band gap, the polymer can exhibit photoelectronic properties.[49]

According to Figure 3.10, Li doping has caused the band gap to shift below the Fermi level while Cl doping has caused the band gap to shift above the Fermi level. This shift is also summarized in Table 3.7. In the case of Li doping, the dopant atom donates electron charge to the polymer facilitating n-type doping, and as a result of that, the Fermi level is raised. On the other hand, Cl gains electron charge from the polymer while facilitating p-type doping. Thus, Cl moves the Fermi level down from the undoped state. With this shift in Fermi level, metallic conductivities can be expected from these doped polymers.[28,50,51]

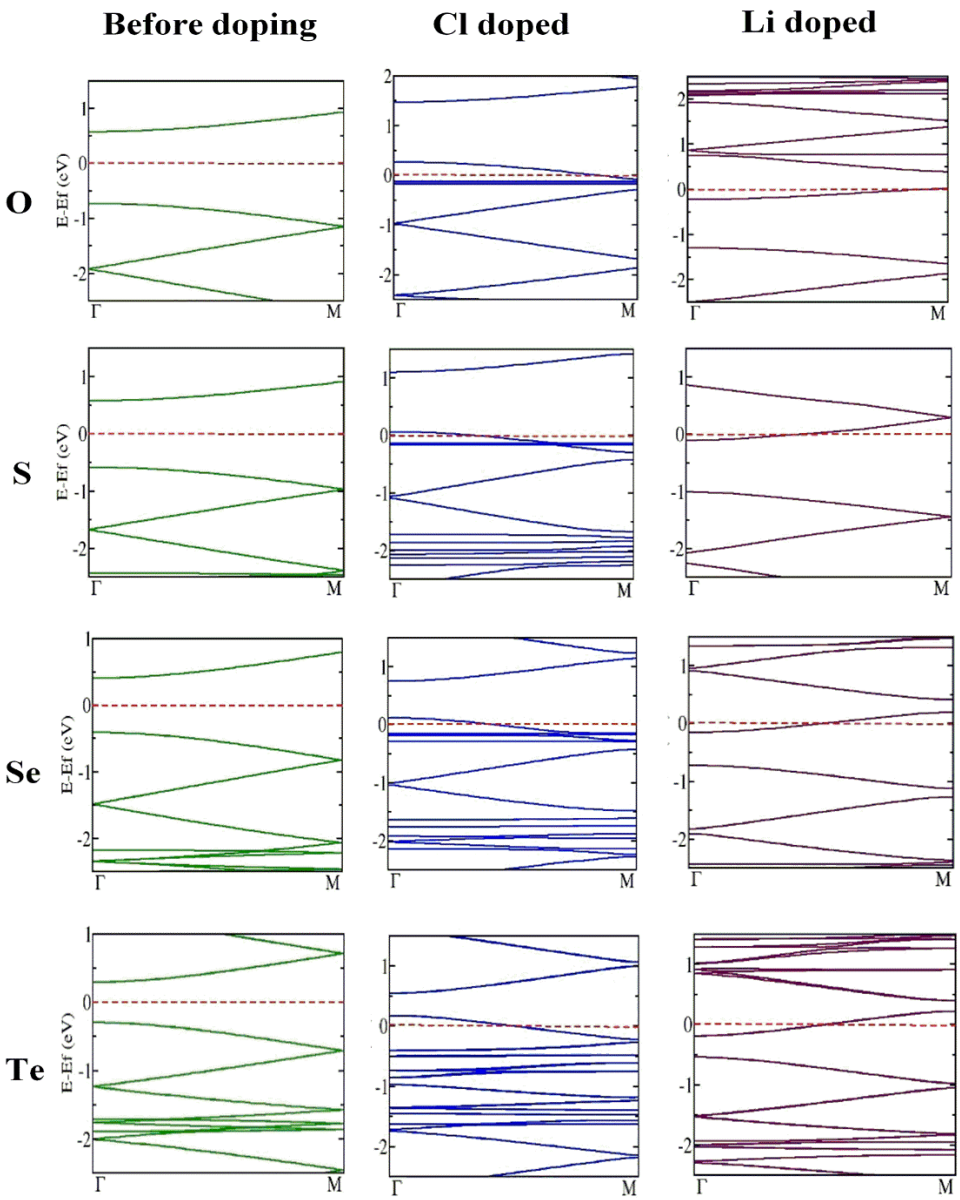

Figure 3.10: Electronic band structures of PTh and analogs before and after doping

Table 3.7: Shift in Fermi level, Energy gap (E_{gap}) of PTh and analogs; after doping with Cl and Li (in eV) form periodic calculations

Heteroatom	Cl doped		Li doped	
	E_{gap}	Shift in Fermi level[a]	E_{gap}	Shift in Fermi level[a]
O	1.20	-1.43	1.07	0.87
S	1.05	-1.03	0.90	0.70
Se	0.63	-0.86	0.57	0.54
Te	0.36	-0.66	0.36	0.41

[a]Shift in Fermi level =Fermi level at doped state - Fermi level at undoped state

PTh and analogs can be considered as low band gap semiconductors. Overall, further reduction in band gap was achieved successfully with Li and Cl doping. The lone pairs of large atoms like Se and Te contribute to the conductivity of the polymer by interchain charge transferring process.[6] Therefore, higher conductivities can be obtained from the Se and Te containing polymers, and further enhancement in conductivity can be obtained by introducing doping.

3.3 POLYPYRROLE AND ITS ANALOGS

3.3.1 Molecular calculations

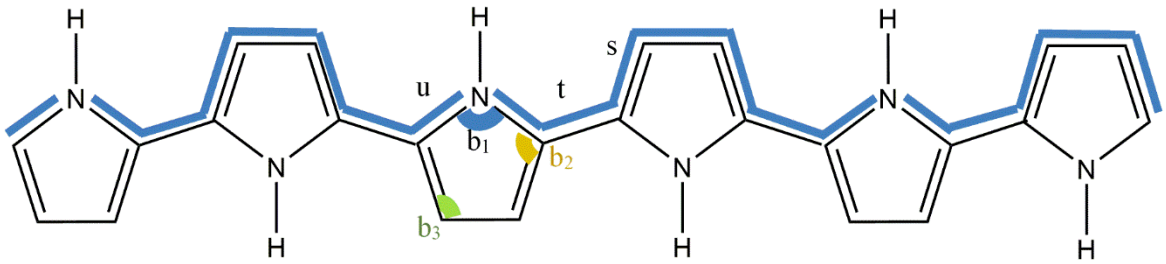

Figure 3.11: Schematic diagram of PPy; N was replaced by P, As, Sb to get the analogs. The values correspond to bond lengths (s, t, u) and angles (b_1, b_2, b_3) are provided in Table 3.1. The blue line represents the specific bond path used in Figure 3.5.

Figure 3.11 shows a schematic diagram of PPy, the heteroatom N was replaced by P, As and Sb to get the analogs. The geometry parameters for the optimized structures of PPy and analogs are provided in Table 3.8. Optimized geometries, HOMOs and LUMOs are shown in Figure 3.12. An increase in bond length was observed for C-Y bonds when the heteroatom is going from N to Sb due to the increasing atomic size. Likewise, the C-Y-C angle decreases when going from N to Sb. A similar trend could be observed in PTh and its analogs as well, see above. The decrease in the bridging bond length (t) proves increased quinoid resonance character when going from N to Sb. The geometry parameters given in Table 1 for PPy and analogs are matching with the available literature values.[2,52]

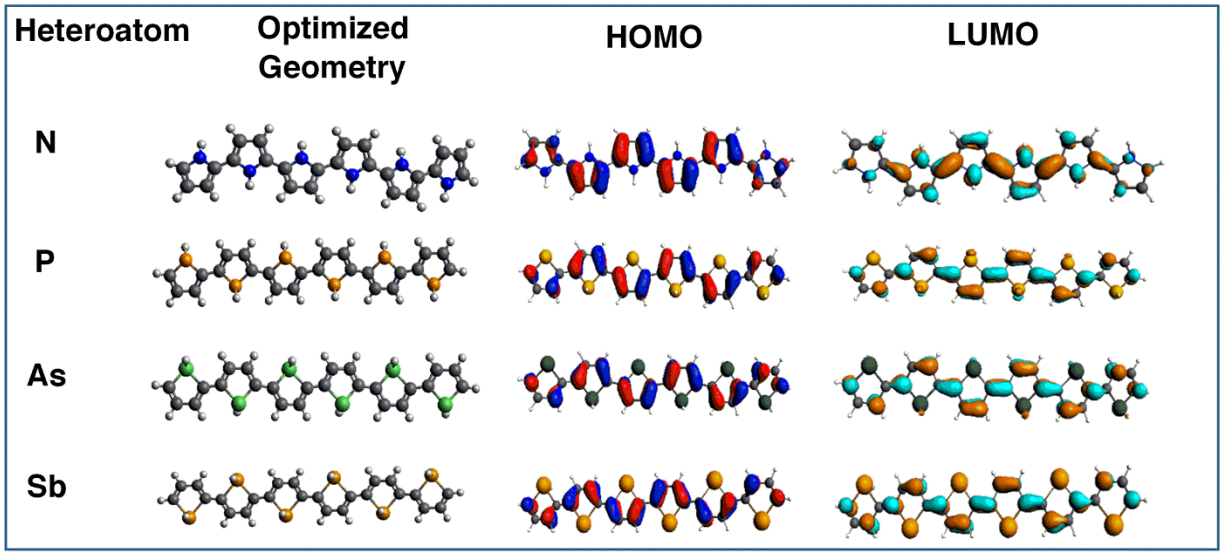

Figure 3.12: Optimized geometries, HOMO and LUMO of PPy and analogs before doping

Table 3.8: Bond lengths (in Å) and bond angles (in °) of PPy and analogs before doping with reference to Figure 3.11- Molecular calculations. Experimental values[52] are given in brackets for the monomer.

Heteroatom (Y)	s(C=C)	t(C-C)	u(C-Y)	b1(C-Y-C)	b2(Y-C-C)	b3(C-C-C)
N	1.39 (1.38)	1.44	1.38 (1.37)	110.7 (109.8)	107.9 (107.7)	106.7 (104.7)
P	1.39	1.42	1.84	90.5	115.8	108.7
As	1.39	1.41	2.00	85.8	118.0	108.8
Sb	1.39	1.40	2.21	80.4	121.1	108.6

As observed in PTh and its analogs, after the doping, Li is sitting on top of the polymer chain while Cl is moving away from the polymer chain. The distance between Li and the C atoms in the 3rd

pyrrole ring is in the range of 2.1 - 2.3 Å. However, in the case of Cl, it is in the range of 3.4 – 5.7 Å. In Cl doped PPy, the Cl atom is located further away from the polymer chain compared to the position of the Cl in PPy analogs (1.9 - 4.2 Å). The optimized PPy has a planar structure whereas in PPy analogs, the P-H, As-H, Sb-H bonds are facing out of the plane. Therefore, N-H is pointing directly at the Cl dopant and pushing the Cl atoms far away from the polymer chain compared to the Cl in PPy analogs (Table 3.9). Mulliken population analysis was performed (Table 3.10), and again, Cl introduces p- type doping. In PPy, Cl gained -0.65 charge while Li introduces n- type doping by gaining a positive charge of 0.26. By looking at the charge gain it is clear that PPy is a promising material for p-type doping. However, the PPy analogs can be considered as promising candidates for n-type doping because the absolute charge gain is higher in Li as compared to Cl. When going from P, As to Sb, the charge gained by Li is 0.49, 0.55, 0.42 and by Cl it is -0.18, -0.20, -0.12 respectively.

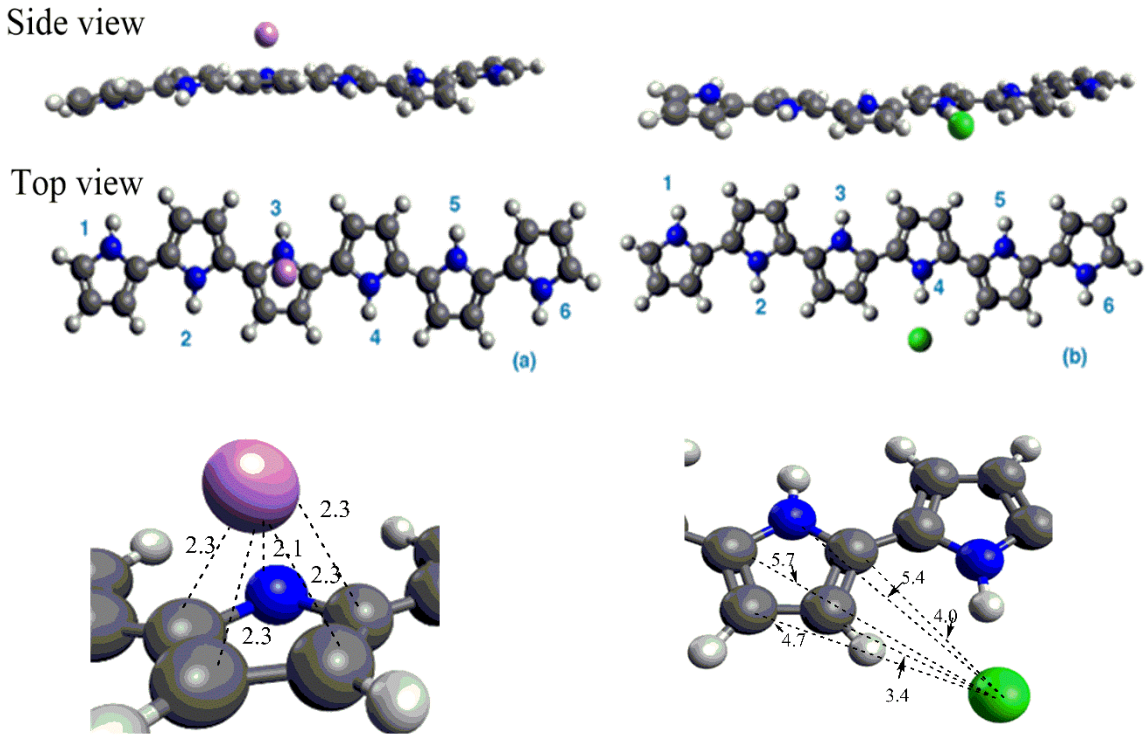

Figure 3.13: Top and side view of optimized geometries (a) PPy doped with Li (b) PPy doped with Cl in molecular calculations. Distance (in Å) to the dopant from atoms in 3rd ring is also shown.

Table 3.9: Distance (in Å) to the dopant (Cl/Li) from atoms in the 3rd ring as marked in Figure 3.13

Heteroatom	Distance to the dopant	
	Li	Cl
N	2.1-2.3	3.4-5.7
P	2.2-2.6	1.9-4.1
As	2.2-2.7	1.9-3.8
Sb	2.2-2.9	2.0-4.3

Changes in bond lengths and bond angles were observed with doping, confirming that the structure is going from aromatic to quinoid. The comparative bond length changes along the polymer chain are given in Figure 3.14. The corresponding bonds are marked in Figure 3.11, as the blue line running along the top of the polymer chain. As observed with PTh and analogs, this bond length change after doping is not prominent at the two ends of the chain. Bond length alternation is partly localized at the counterion.

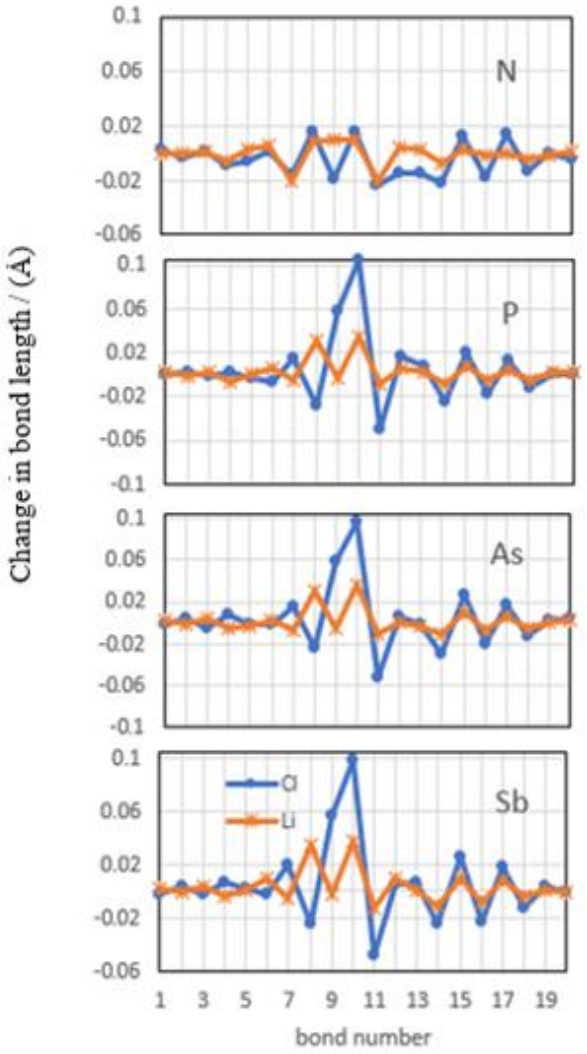

Figure 3.14: The comparative bond length changes along the polymer chain with reference to Figure 3.11, the y axis represents the difference in bond length before and after doping

Table 3.10: Mulliken charge of the counterion (e^-)

Heteroatom	Mulliken charge	
	Cl	Li
N	-0.65	0.26
P	-0.18	0.49
As	-0.20	0.55
Sb	-0.12	0.42

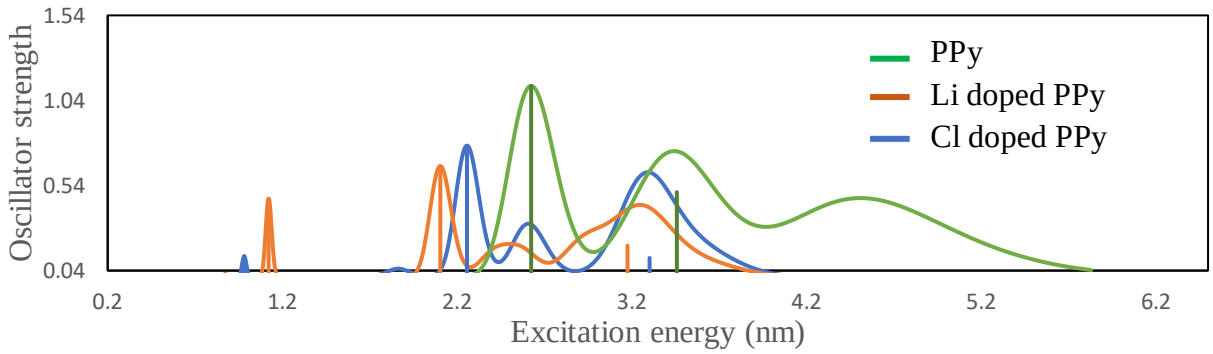

Figure 3.15: UV-vis spectra of PPy (green), Cl doped PPy (blue) and Li doped PPy (brown)

The calculated UV-vis spectra for PPy and Cl/ Li doped PPy are given in Figure 3.15. The absorption maximum of PPy is at 2.63 eV (472nm) and upon doping it shows a redshift. The excitation occurring from the valence band to the lower polaron band is characterized by the peaks observed at 1.12 eV (1105 nm) in Cl doped PPy and 0.98 eV (1263 nm) in Li doped PPy. The Cl doped polymers containing P, As, Sb heteroatoms show longer wavelength absorptions at 1.04 eV,

1.01 eV, 1.01 eV (1197 nm, 1229 nm, 1230 nm) respectively, corresponding to the excitation from the valence band to the lower polaron band. In the case of Li doped polymers, longer wavelength absorptions were observed at 1.26 eV, 1.24 eV, 0.71 eV (987 nm, 996 nm, 1743 nm), respectively. The HOMO and LUMO levels before and after doping and their corresponding band gaps (E_{gap}) are given in Table 3.11. The band gap values obtained before the doping of PPy and analogs are consistent with previous reports.[2] A significant decrease in band gap can be seen when going from N to Sb. The E_{gap} obtained for PPy is 2.29 eV and when the heteroatom N is replaced by the P, As, Sb, the E_{gap} values are 0.88eV, 0.81eV, 0.74eV respectively. When comparing HOMO and LUMO levels (Figure 3.16), the polymers containing P, As, Sb maintains consistency while PPy is showing a considerable difference. The structural variation discussed above in PPy compared to the others is the likely reason behind these results. The HOMO and LUMO levels of PPy are at -3.96 eV and -1.67 eV respectively. The HOMO level of polymers containing P, As, Sb is at about -4.4 eV and the LUMO level is going from -3.58 eV to -3.62 eV to -3.70 eV for the series P, As, Sb. The PPy analogs confirm that the HOMO level does not have contributions from the heteroatom. Overall, narrow band gap polymers have been obtained by the replacement of the heteroatom (N) in PPy with P, As and Sb.

HOMO and LUMO levels of Li and Cl doped polymers are also shown in Figure 3.16. In PPy, doping reduces the band gap. The same effect was observed for PTh and analogs. With Cl dopant, the HOMO-LUMO gap of PPy is reduced to 2.07 eV, and with Li dopant, an even narrower band gap of 1.94 eV has been obtained. Slight increases in band gap can be observed upon doping of the PPy analogs. Overall, for the PPy analogs, doping is having a rather small effect. Figure 3.17 shows HOMO and LUMO contributions upon doping. With the addition of a dopant both HOMO and LUMO levels are changing; the changed proportions are not that uniform to show a clear trend

in the band gaps as band gaps vary in a small range ~0.1 eV. As observed in PTh here also this contribution is localized at the counterion (Figure 3.17). In the case of Li dopant, the contribution is larger at the central rings and it is decreasing when going to the ends of the polymer chain. But in the case of Cl dopant, the behavior is less uniform.

Table 3.11: Calculated HOMO – LUMO gap (E_{gap} – in eV) in polypyrrole and N replaced by P, As after and before doping from Molecular calculations. The experimental band gap (E_{gap} Exp. - in eV) is also given for PPy.

Hetero-atom	without dopant				doping with Cl			doping with Li		
	HOMO	LUMO	E_{gap}	E_{gap} Exp.[1]	HOMO	LUMO	E_{gap}	HOMO	LUMO	E_{gap}
N	-3.96	-1.67	2.29	2.85	-4.26	-2.19	2.07	-3.96	-2.02	1.94
P	-4.46	-3.58	0.88		-4.32	-3.31	1.01	-3.78	-2.93	0.85
As	-4.43	-3.62	0.81		-4.34	-3.41	0.93	-3.83	-2.97	0.86
Sb	-4.44	-3.70	0.74		-4.41	-3.43	0.98	-3.92	-3.03	0.89

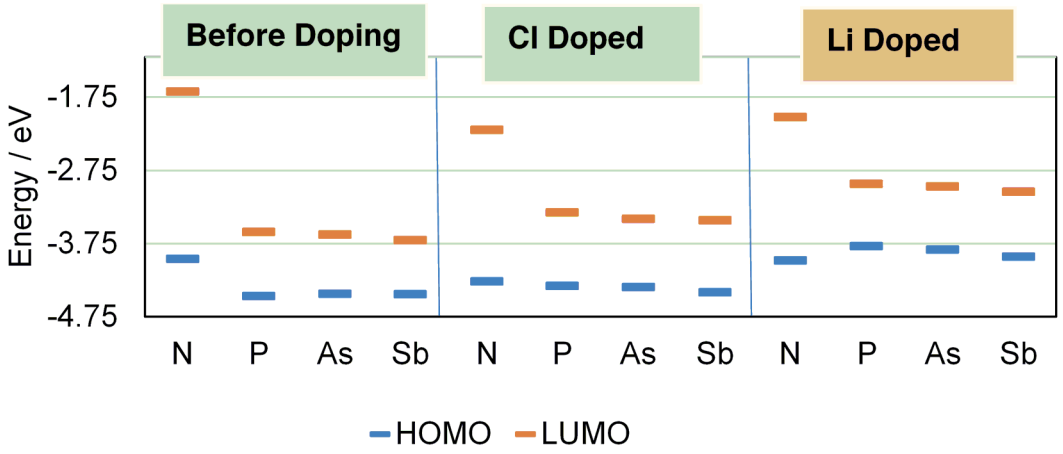

Figure 3.16: HOMO and LUMO levels of PPy and analogs before and after doping

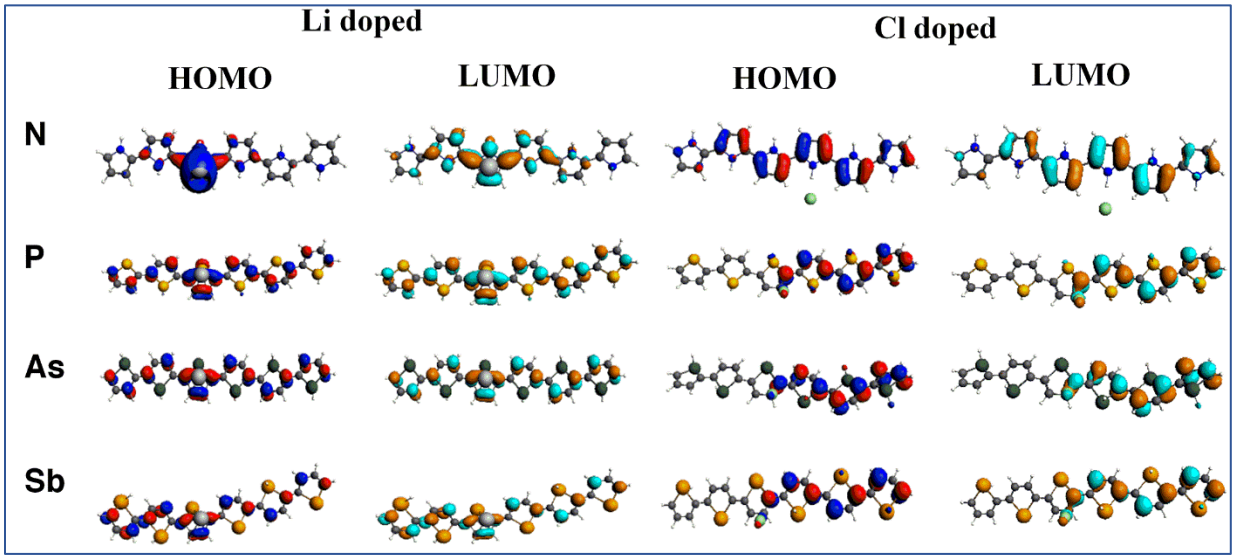

Figure 3.17: HOMO and LUMO of PPy and analogs after doping

3.3.2 Periodic calculations

As discussed earlier for PTh and analogs, in molecular calculations, the structure is free to move in all three directions while in periodic calculations it is fixed in one direction. As a result, systematic differences in geometry parameters and HOMO-LUMO gaps were observed when comparing periodic calculations with molecular calculations due to these reasons.

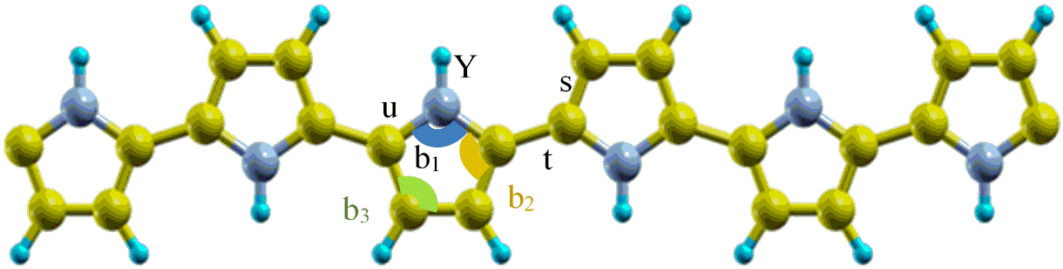

Figure 3.18: The optimized structure of periodic PPy : N was replaced by P, As, Se to get the analogs. The values correspond to bond lengths (s, t, u) and angles (b_1, b_2, b_3) are given in Table 3.12.

Figure 3.18 shows the optimized structure of PPy from the periodic calculations. The supercell contains 24 carbon (C) atoms, 6 nitrogen (N) atoms and 18 hydrogen (H) atoms. The N atom was replaced by P, As and Sb to get the corresponding analogs. The bond distances and angles are given in Table 3.12. Similar trends can be seen when comparing with the molecular calculations. For instance, an increase in C-Y bond distance and decrease in C-Y-C bond angle are found when the heteroatom Y is going from N to Sb. In the periodic calculations, the C-Y bond distance is going from 1.46 Å - 2.19 Å and the C-Y-C bond angle from 113.91º-80.47º when Y is going from N to Sb. The aromaticity is decreasing in the order of N>P>As>Sb. The decreased bridging bond length along with the series again proves increased quinoid resonance. The bridging bond or the bond between monomers is marked as 't' in Figure 3.18. According to Table 3.12, the

corresponding bond distance for t(C-C) is decreasing when going from N to Sb (1.61 Å to 1.37 Å).

Table 3.12: Bond lengths (in Å) and bond angles (in °) of PTh and analogs before doping with reference to figure 3.18-Periodic calculations.

Heteroatom (Y)	s(C=C)	t(C-C)	u(C-Y)	b1(C-Y-C)	b2(Y-C-C)	b3(C-C-C)
N	1.39	1.61	1.46	113.9	101.5	111.6
P	1.39	1.41	1.84	91.1	108.3	115.7
As	1.41	1.37	1.99	85.6	109.1	117.9
Sb	1.42	1.37	2.19	80.5	108.4	120.6

Table 3.13: Conduction band width (W_{CB}), valence band width (W_{VB}), HOMO-LUMO gap (E_{gap}) of PPy and analogs (in eV) form periodic calculations. Experimental band gap (E_{gap} Exp. - in eV) is also given for PPy.

Heteroatom	W_{CB}	W_{VB}	E_{gap}	E_{gap} Exp.[1]
N	0.23	0.27	2.05	2.85
P	0.56	0.59	0.21	
As	0.48	0.51	0.45	
Sb	0.43	0.45	0.58	

Periodic calculation results for the conduction bandwidth (W_{CB}), valence bandwidth (W_{VB}), and HOMO-LUMO gap (E_{gap}) of PPy and analogs are given in Table 3.13. Both W_{CB} and the W_{VB} are decreasing when going from P to Sb, showing that these materials become less favorable for doping when going form P to Sb.

PPy analogs have very narrow band gaps as already observed in the molecular calculations. The HOMO-LUMO gap of PPy is 2.05 eV, and, by replacing N with its higher analogs, a significant decrease in band gap is observed. Molecular calculations have again resulted in higher values for the HOMO-LUMO gap when compared to the periodic calculations due to the reasons discussed under PTh.

The resulting electronic band structures, before and after doping, are given in Figure 3.19. The corresponding energy gaps are given in Table 3.14 for Li and Cl doped polymers. It is clear from the band structure diagrams that all the polymers are having a direct band gap at the Γ point, similar to the PPy series discussed above. According to Figure 3.19, Li doping causes the band gap to shift below the Fermi level while Cl doping causes the band gap to shift above the Fermi level similar to the observations for PTh. These shifts are also summarized in Table 3.14. The Li dopant facilitates n-type doping by donating electron charge, hence the Fermi level moves up, whereas Cl dopant facilitates p-type doping by withdrawing electron charge, hence the Fermi level moves

down compared to the undoped state. With this shift in Fermi level, metallic conductivities can be expected from these doped polymers as we observed in the PTh series.

Figure 3.19: Electronic band structures of PPy and analogs before and after doping

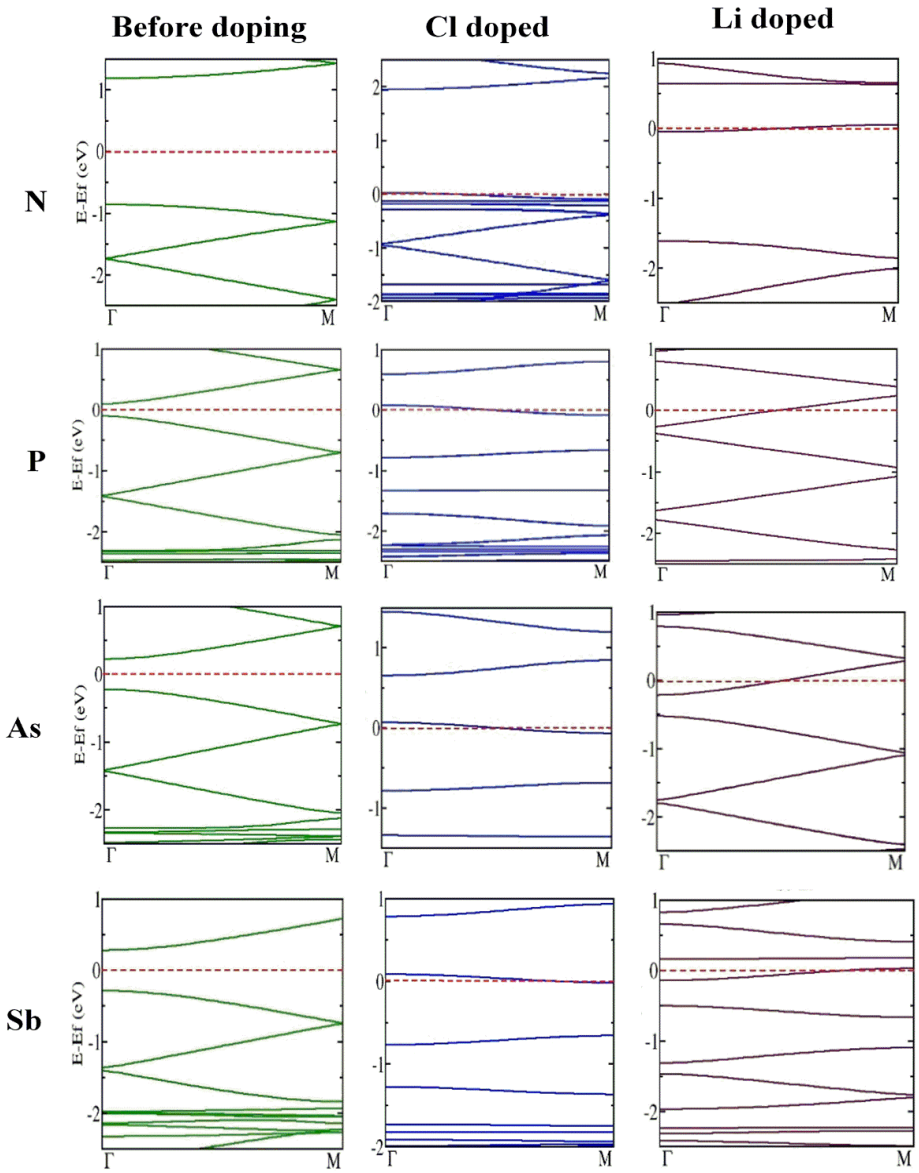

Table 3.14: Shift in Fermi level, Energy gap (E_{gap}) of PTh and analogs; after doping with Cl and Li (in eV) form periodic calculations

Heteroatom	Cl doped		Li doped	
	E_{gap}	Shift in Fermi level[a]	E_{gap}	Shift in Fermi level[a]
N	1.92	-1.05	1.55	1.17
P	0.51	-0.22	0.12	0.46
As	0.59	-0.16	0.31	0.56
Sb	0.69	-0.20	0.17	0.55

[a]Shift in Fermi level =Fermi level at doped state - Fermi level at undoped state

3.4 APPLICATIONS

A series of CPs namely, PTh, PPy and their higher period analogs have been investigated at the presence of Li and Cl atomic dopants. With doping, CP can go from insulator to semiconductor or conductor. With enhanced conductivities, CPs can have successful applications in biosensors, drug delivery and bioactuators. Easy synthesis, easy surface modification, good stability, the ability to support cell adhesion and growth of different cell types are some of the other properties which help CPs to stand out among any other candidate materials.[53]

In large capacity energy storage systems, organic redox flow batteries are one of the promising alternatives to lithium-ion and sodium-sulfur batteries. Nevertheless, low electrical conductivity, resulting in low current density and low power density, lowers the device performance. Oh et al.[12] presents increased cell potential with PTh in redox flow batteries, redox activity at (-2.0 V) and 0.5 V for n-type and p-type doping respectively. That is, this cell can be operated at 2.5 V cell potential. The cell has shown stable charge/discharge performance with high energy efficiency of about 60.9%. Because of the expected enhanced conductivities, doped PTh, PPy and their analogs studied here can be suitable candidate materials for organic redox flow batteries. Grid-level energy

storage, smart clothes, integrated-circuit smart cards, RFID tags and smart packaging are some of the applications that require battery performance. For these applications, currently available batteries reach their limitations. These battery applications require thin-film materials. Good conductivity, flexibility, low toxicity, rapid charging, excellent cycle life, easy synthesis are the other expected properties required of the materials. CPs are suitable candidates to fulfill all of these requirements.[54]

Widening of the solar energy absorption spectrum from ultraviolet to near IR region is one of the main research interests in the photovoltaic cell development. With a broad absorption spectrum, the photovoltaic cell guarantees high photocurrents, hence high efficiencies. Upon irradiation with sunlight, CPs show capability for light absorption and emission, charge generation and transport.[55] With low band gap CPs, we can expect solar energy absorption up to the near IR region. The open-circuit voltage (V_{OC}) of the photovoltaic cell is one of the parameters which determines the photovoltaic cell performance. The maximum V_{OC} one can achieve from an organic solar cell is the difference between the HOMO of the electron donor and the LUMO of electron acceptor. Low band gap CPs are usually used as donor materials.[55] When the CP acts as the donor, a low HOMO level is important to achieve higher V_{OC}.[6] Therefore, knowing about the levels of the HOMO and the LUMO are also important to develop promising materials.

In order to enhance solar energy absorption, multijunction organic photovoltaics is one of the options where different band gaps materials are combined. With the optimal combination of different band gap materials, multijunction organic photovoltaics can achieve efficiency higher than the single junction (band gap) solar cells.[56] In a single junction solar cell, photons that have energies below the band gap are not absorbed and photons that are having energies higher than the band gap are absorbed, but part of the energy is lost as heat. In a multijunction solar cell a high

band gap top material absorbs higher energy photons and lower energy photons which are passing through the top material are absorbed by the lower lying material having a slightly lower band gap. Thus, multijunction solar cells use two or more materials with different band gaps. The series of materials presented in this chapter which have a range of band gaps would also be useful when designing a highly efficient multijunction solar cell.

3.5 CONCLUSIONS

A theoretical study of doping of CPs was performed with DFT calculations using the GGA(PBE) functional. Two atomic dopants, namely Li and Cl, were used to facilitate n-type and p-type doping. The CPs PTh, PPy and their analogs (S replaced by O, Se, Te in PTh, and N replaced by P, As, Sb in PPy) were investigated. Structural and electronic changes upon doping were analyzed with molecular and periodic calculations. Slight variations in geometry parameters and band gaps were observed between periodic and molecular calculations. However, the observed trends are more or less the same, and the two types of calculations complement and augment each other. Successful doping was confirmed by observed structural changes in the CPs. Mulliken population analysis was used to evaluate the amount of charge gained or donated by the dopants. The band structure diagrams obtained from periodic calculations show upward or downward shifts in the Fermi level with Li and Cl, respectively. A decrease in HOMO-LUMO gaps was observed upon doping. This is particularly prominent in PTh and analogs. These new materials will be useful for various device applications.

References

(1) Salzner, U.; Lagowski, J. B.; Pickup, P. G.; Poirier, R. A. Comparison of Geometries and Electronic Structures of Polyacetylene, Polyborole, Polycyclopentadiene, Polypyrrole, Polyfuran, Polysilole, Polyphosphole, Polythiophene, Polyselenophene and Polytellurophene. *Synth. Met.* **1998**, *96* (3), 177–189.

(2) Kaloni, T. P.; Schreckenbach, G.; Freund, M. S. Band Gap Modulation in Polythiophene and Polypyrrole-Based Systems. *Sci. Rep.* **2016**, *6* (1), 36554.

(3) Zamoshchik, N.; Bendikov, M. Doped Conductive Polymers: Modeling of Polythiophene with Explicitly Used Counterions. *Adv. Funct. Mater.* **2008**, *18* (21), 3377–3385.

(4) Ullah, H.; Ayub, K.; Ullah, Z.; Hanif, M.; Nawaz, R.; Shah, A.-H. A.; Bilal, S. Theoretical Insight of Polypyrrole Ammonia Gas Sensor. *Synth. Met.* **2013**, *172* (Supplement C), 14–20.

(5) Mahrok, A. K.; Carrera, E. I.; Tilley, A. J.; Ye, S.; Seferos, D. S. Synthesis and Photophysical Properties of Platinum-Acetylide Copolymers with Thiophene, Selenophene and Tellurophene. *Chem. Commun.* **2015**, *51* (25), 5475–5478.

(6) Pander, P.; Motyka, R.; Zassowski, P.; Lapkowski, M.; Swist, A.; Data, P. Electrochromic Properties of Novel Selenophene and Tellurophene Derivatives Based on Carbazole and Triphenylamine Core. *J. Phys. Chem. C* **2017**, *121* (21), 11027–11036.

(7) Jo, W. J.; C. Borrelli, D.; Bulović, V.; Gleason, K. Photovoltaic Effect by Vapor-Printed Polyselenophene. *Org. Electron. Phys. Mater. Appl.* **2015**, *26*, 55–60.

(8) Mehmood, U.; Al-Ahmed, A.; Hussein, I. A. Review on Recent Advances in Polythiophene Based Photovoltaic Devices. *Renew. Sustain. Energy Rev.* **2016**, *57*, 550–561.

(9) Chen, Z.; Lemke, H.; Albert-Seifried, S.; Caironi, M.; Nielsen, M. M.; Heeney, M.; Zhang, W.; McCulloch, I.; Sirringhaus, H. High Mobility Ambipolar Charge Transport in Polyselenophene Conjugated Polymers. *Adv. Mater.* **2010**, *22* (21), 2371–2375.

(10) Charlebois, I.; Gravel, C.; Arrad, N.; Boissinot, M.; Bergeron, M. G.; Leclerc, M. Impact of DNA Sequence and Oligonucleotide Length on a Polythiophene-Based Fluorescent DNA Biosensor. *Macromol. Biosci.* **2013**, *13* (6), 717–722.

(11) Plante, M.-P.; Bérubé, È.; Bissonnette, L.; Bergeron, M. G.; Leclerc, M. Polythiophene Biosensor for Rapid Detection of Microbial Particles in Water. *ACS Appl. Mater. Interfaces* **2013**, *5* (11), 4544–4548.

(12) Oh, S. H.; Lee, C.-W.; Chun, D. H.; Jeon, J.-D.; Shim, J.; Shin, K. H.; Yang, J. H. A Metal-Free and All-Organic Redox Flow Battery with Polythiophene as the Electroactive Species. *J. Mater. Chem. A* **2014**, *2* (47), 19994–19998.

(13) Liu, L.; Tian, F.; Wang, X.; Yang, Z.; Zhou, M.; Wang, X. Porous Polythiophene as a Cathode Material for Lithium Batteries with High Capacity and Good Cycling Stability. *React. Funct. Polym.* **2012**, *72* (1), 45–49.

(14) Polythiophene-based materials for nonvolatile polymeric memory devices - Li - 2013 - Polymer Engineering & Science - Wiley Online Library http://onlinelibrary.wiley.com/doi/10.1002/pen.23800/full (accessed Jan 11, 2018).

(15) McConnell, R. M.; Godwin, W. E.; Baker, S. E.; Powell, K.; Baskett, M.; Morara, A. Polyfuran and Co-Polymers: A Chemical Synthesis. *Int. J. Polym. Mater. Polym. Biomater.* **2004**, *53* (8), 697–708.

(16) González-Tejera, M. J.; de la Blanca, E. S.; Carrillo, I. Polyfuran Conducting Polymers: Synthesis, Properties, and Applications. *Synth. Met.* **2008**, *158* (5), 165–189.

(17) Ninis, O.; Abarkan, M.; Bouachrine, M. Spectroscopic Analysis of Polyfuran and Theoretical Investigation of Electronic Properties of Oligofurans: Destined for the Solar Cell Applications. In *2014 International Renewable and Sustainable Energy Conference (IRSEC)*; 2014; pp 593–595.

(18) Ohsawa, T.; Kaneto, K.; Yoshino, K. Electrical and Optical Properties of Electrochemically Prepared Polyfuran. *Jpn. J. Appl. Phys.* **1984**, *23* (9A), L663.

(19) Sultana, I.; Rahman, Md. M.; Wang, J.; Wang, C.; Wallace, G. G.; Liu, H.-K. All-Polymer Battery System Based on Polypyrrole (PPy)/Para (Toluene Sulfonic Acid) (PTS) and Polypyrrole (PPy)/Indigo Carmine (IC) Free Standing Films. *Electrochimica Acta* **2012**, *83*, 209–215.

(20) Xin, P.; Jin, B.; Li, H.; Lang, X.; Yang, C.; Gao, W.; Zhu, Y.; Zhang, W.; Dou, S.; Jiang, Q. Facile Synthesis of Sulfur–Polypyrrole as Cathodes for Lithium–Sulfur Batteries. *ChemElectroChem* **2017**, *4* (1), 115–121.

(21) Bof Bufon, C. C.; Heinzel, T. Polypyrrole Thin-Film Field-Effect Transistor. *Appl. Phys. Lett.* **2006**, *89* (1), 012104.

(22) Jain, R.; Jadon, N.; Pawaiya, A. Polypyrrole Based next Generation Electrochemical Sensors and Biosensors: A Review. *TrAC Trends Anal. Chem.* **2017**, *97*, 363–373.

(23) Preethichandra, D. M. G.; Onoda, M. Functional Design of Electrochemical Biosensors Using Polypyrrole. *Electron. Commun. Jpn.* **2016**, *99* (7), 55–63.

(24) Hong, J.-Y.; Jeon, S. O.; Jang, J.; Song, K.; Kim, S. H. A Facile Route for the Preparation of Organic Bistable Memory Devices Based on Size-Controlled Conducting Polypyrrole Nanoparticles. *Org. Electron.* **2013**, *14* (3), 979–983.

(25) Ullah, H.; Shah, A.-H. A.; Bilal, S.; Ayub, K. Doping and Dedoping Processes of Polypyrrole: DFT Study with Hybrid Functionals. *J. Phys. Chem. C* **2014**, *118* (31), 17819–17830.

(26) Alemán, C.; Oliver, R.; Brillas, E.; Casanovas, J.; Estrany, F. A Combined Theoretical and Experimental Investigation about the Influence of the Dopant in the Anodic Electropolymerization of α-Tetrathiophene. *Chem. Phys.* **2006**, *323* (2), 407–412.

(27) Salzner, U. Theoretical Investigation of Excited States of Oligothiophenes and of Their Monocations. *J. Chem. Theory Comput.* **2007**, *3* (3), 1143–1157.

(28) Kaloni, T. P.; Schreckenbach, G.; Freund, M. S. Structural and Electronic Properties of Pristine and Doped Polythiophene: Periodic versus Molecular Calculations. *J. Phys. Chem. C* **2015**, *119* (8), 3979–3989.

(29) Zamoshchik, N.; Salzner, U.; Bendikov, M. Nature of Charge Carriers in Long Doped Oligothiophenes: The Effect of Counterions. *J. Phys. Chem. C* **2008**, *112* (22), 8408–8418.

(30) Dai, Y.; Blaisten-Barojas, E. Energetics, Structure, and Charge Distribution of Reduced and Oxidized n-Pyrrole Oligomers: A Density Functional Approach. *J. Chem. Phys.* **2008**, *129* (16), 164903.

(31) Dai, Y.; Chowdhury, S.; Blaisten-Barojas, E. Density Functional Theory Study of the Structure and Energetics of Negatively Charged Oligopyrroles. *Int. J. Quantum Chem.* **2011**, *111* (10), 2295–2305.

(32) Dai, Y.; Wei, C.; Blaisten-Barojas, E. Density Functional Theory Study of Neutral and Oxidized Thiophene Oligomers. *J. Chem. Phys.* **2013**, *139* (18), 184905.

(33) Prada, S.; Giordano, L.; Pacchioni, G. Li, Al, and Ni Substitutional Doping in MgO Ultrathin Films on Metals: Work Function Tuning via Charge Compensation. *J. Phys. Chem. C* **2012**, *116* (9), 5781–5786.

(34) Salzner, U. Electronic Structure of Conducting Organic Polymers: Insights from Time-Dependent Density Functional Theory: Electronic Structure of Conducting Organic Polymers. *Wiley Interdiscip. Rev. Comput. Mol. Sci.* **2014**, *4* (6), 601–622.

(35) Hernandez, V. Lattice Dynamics and Vibrational Spectra of Pristine and Doped Polyconjugated Polyfuran. *J. Chem. Phys.* **1993**, *98(2)*,769-783.

(36) Bak, B.; Christensen, D.; Hansen-Nygaard, L.; Rastrup-Andersen, J. The Structure of Thiophene. *J. Mol. Spectrosc.* **1961**, *7*, 58–63.

(37) Kupka, T.; Wrzalik, R.; Pasterna, G.; Pasterny, K. Theoretical DFT and Experimental Raman and NMR Studies on Thiophene, 3-Methylthiophene and Selenophene. *J. Mol. Struct.* **2002**, *616* (1–3), 17–32.

(38) *Advances in Heterocyclic Chemistry*; Academic Press, 1977.

(39) Alkan, F.; Salzner, U. Theoretical Investigation of Excited States of Oligothiophene Anions. *J. Phys. Chem. A* **2008**, *112* (27), 6053–6058.

(40) Okur, S.; Salzner, U. Theoretical Modeling of the Doping Process in Polypyrrole by Calculating UV/Vis Absorption Spectra of Neutral and Charged Oligomers. *J. Phys. Chem. A* **2009**, *113* (31), 9050–9050.

(41) Ramirez-Solis, A.; Kirtman, B.; Bernal-Jaquez, R.; Zicovich-Wilson, C. M. Periodic Density Functional Theory Studies of Li-Doped Polythiophene: Dependence of Electronic and Structural Properties on Dopant Concentration. *J. Chem. Phys.* **2009**, *130* (16), 164904.

(42) Heeney, M.; Zhang, W.; Crouch, D. J.; Chabinyc, M. L.; Gordeyev, S.; Hamilton, R.; Higgins, S. J.; McCulloch, I.; Skabara, P. J.; Sparrowe, D.; et al. Regioregular Poly(3-Hexyl)Selenophene: A Low Band Gap Organic Hole Transporting Polymer. *Chem. Commun.* **2007**, *0* (47), 5061–5063.

(43) Dai, G.; Chang, J.; Jing, L.; Chi, C. Diacenopentalene Dicarboximides as New N-Type Organic Semiconductors for Field-Effect Transistors. *J. Mater. Chem. C* **2016**, *4* (37), 8758–8764.

(44) Grenz, D. C.; Schmidt, M.; Kratzert, D.; Esser, B. Dibenzo[a,e]Pentalenes with Low-Lying LUMO Energy Levels as Potential n-Type Materials. *J. Org. Chem.* **2017**.

(45) Singh, V.; Bougher, T. L.; Weathers, A.; Cai, Y.; Bi, K.; Pettes, M. T.; McMenamin, S. A.; Lv, W.; Resler, D. P.; Gattuso, T. R.; et al. High Thermal Conductivity of Chain-Oriented Amorphous Polythiophene. *Nat. Nanotechnol.* **2014**, *9* (5), 384.

(46) Vessally, E. Aromatic Stability Energy Studies on Five-Membered Heterocyclic C4H4M(M = O, S, Se, Te, NH, PH, AsH and SbH): DFT Calculations. *J. Struct. Chem.* **2008**, *49* (6), 979–985.

(47) Horner, K. E.; Karadakov, P. B. Chemical Bonding and Aromaticity in Furan, Pyrrole, and Thiophene: A Magnetic Shielding Study. *J. Org. Chem.* **2013**, *78* (16), 8037–8043.

(48) Hutchison, G. R.; Zhao, Y.-J.; Delley, B.; Freeman, A. J.; Ratner, M. A.; Marks, T. J. Electronic Structure of Conducting Polymers: Limitations of Oligomer Extrapolation Approximations and Effects of Heteroatoms. *Phys. Rev. B* **2003**, *68* (3), 035204.

(49) Seo, D.-K.; Hoffmann, R. Direct and Indirect Band Gap Types in One-Dimensional Conjugated or Stacked Organic Materials. *Theor. Chem. Acc.* **1999**, *102* (1–6), 23–32.

(50) Perry, E. E.; Chiu, C.-Y.; Moudgil, K.; Schlitz, R. A.; Takacs, C. J.; O'Hara, K. A.; Labram, J. G.; Glaudell, A. M.; Sherman, J. B.; Barlow, S.; et al. High Conductivity in a Nonplanar N-Doped Ambipolar Semiconducting Polymer. *Chem. Mater.* **2017**, *29* (22), 9742–9750.

(51) Dissanayake, D. M. N. M.; Ashraf, A.; Dwyer, D.; Kisslinger, K.; Zhang, L.; Pang, Y.; Efstathiadis, H.; Eisaman, M. D. Spontaneous and Strong Multi-Layer Graphene n-Doping on Soda-Lime Glass and Its Application in Graphene-Semiconductor Junctions. *Sci. Rep.* **2016**, *6*, 21070.

(52) Nygaard, U.; Nielsen, J. T.; Kirchheiner, J.; Maltesen, G.; Rastrup-Andersen, J.; Sørensen, G. O. Microwave Spectra of Isotopic Pyrroles. Molecular Structure, Dipole Moment, and 14N Quadrupole Coupling Constants of Pyrrole. *J. Mol. Struct.* **1969**, *3* (6), 491–506.

(53) Kaur, G.; Adhikari, R.; Cass, P.; Bown, M.; Gunatillake, P. Electrically Conductive Polymers and Composites for Biomedical Applications. *RSC Adv.* **2015**, *5* (47), 37553–37567.

(54) Muench, S.; Wild, A.; Friebe, C.; Häupler, B.; Janoschka, T.; Schubert, U. S. Polymer-Based Organic Batteries. *Chem. Rev.* **2016**, *116* (16), 9438–9484.

(55) Xu, T.; Yu, L. How to Design Low Bandgap Polymers for Highly Efficient Organic Solar Cells. *Mater. Today* **2014**, *17* (1), 11–15.

(56) Xiao, X.; Lee, K.; Forrest, S. R. Scalability of Multi-Junction Organic Solar Cells for Large Area Organic Solar Modules. *Appl. Phys. Lett.* **2015**, *106* (21), 213301.

Chapter 4 : RESULTS AND DISCUSSION - PROJECT II

Tunability of HOMO- LUMO Levels and Band Gaps in Polythiophene Based Conducting Polymers by Introducing Peripheral Groups

4.1 INTRODUCTION

4.1.1 Research objective

The objective of this research is to study the tunability of the band gap and HOMO-LUMO energy levels of polythiophene-based conducting polymers by introducing different peripheral groups. This study also results in new candidate materials for potential applications.

4.1.2 Introduction

Polythiophene (PTh) is one of the most widely studied conjugated polymer.[1] PTh is having many applications such as in solar cells, thin-film transistors,[2] bio-sensors,[3,4] batteries,[5,6] and memory devices[7] Many reports can be found about tunning of the HOMO-LUMO gap and energy levels of PTh. [1] Sulfur (S) is the heteroatom in PTh and the LUMO is having a considerable contribution from the heteroatom.[8] As discussed in chapter 3, the HOMO level remains essentially constant when changing the heteroatom. On the other hand, one can tune the LUMO level just by replacing the heteroatom with different atoms like Se or Te.[8] The HOMO and LUMO levels also depend on the degree of electron delocalization in the polymer.[9] Addition of electron-withdrawing groups to a molecule results in LUMO and HOMO lowering.[9–12] If a molecule is acting as a donor in a solar cell, a low HOMO is necessary to obtain high voltage from the solar cell but intense LUMO lowering of the same molecule destroys the capability of transferring electrons to the acceptor. Meanwhile, the addition of electron-donating groups results in increased HOMO and LUMO

levels.[11,12] When a molecule is acting as a donor in a solar cell, increased HOMO level gives low voltage in the solar cell.[13]

The geometry of the polymeric material is also important. The random nature of conformations and packing results in difficulties for controlling the bulk material performance. The polymer poly-3-hexylthiophene (P3HT) is one example which forms quasi-crystalline aggregates in thin films. These aggregates are having π- π stacked P3HT chains and successful applications in photovoltaics are reported.[14–16] In the P3HT monomer, the peripheral H atom attached to the 3rd carbon is replaced by a hexyl group. The ability to form π- π stacked chains favors interchain exciton coupling.[17] Poly(3-dodecylthiophene) (P3DDT) is another example for substituted PTh which has dodecyl groups attached.[18] Single-walled carbon nanotubes (SWCNTs) are popular as they can be used successfully in electronic and optoelectronic devices. During the synthesis of SWCNTs, a mixture of metallic and semiconducting nanotubes is generated which need refining. They also have a wide range of band gaps and diameters. Sorting and separation of these SWCNT can be done by polymer wrapping. The tight wrapping of the polymer to the curved nanotube surface is important.[19–21] π- π interactions of conjugated polymers favor polymer wrapping. The polymer aligns along the SWCNT's surface with a preferred angle due to the strong van der Waals interactions between the conjugated π-bonds in both conjugated polymers and SWCNT. Electron-rich polymers selectively disperse semiconducting SWCNT while electron-poor polymers favor metallic SWCNT over semiconducting SWCNT. The electron-poor polymers disperse a mixture of metallic and semiconducting SWCNT. The dispersion fractions are controlled by the electron density of the polymer and by decreasing the electron density of the polymer, a higher fraction of metallic SWCNT can be dispersed. [22,23] Substituted polythiophene is one of the polymers used for the polymer wrapping and poly-3-alkylthiophenes are popular. [19,21] Helical polymers are also of

research interest. They are having applications in molecular recognition, as a scaffold, and in chiral sensing. [24] Sterically hindered side groups force the polymer into a helical conformation. McLeod et. al. report torsional angle and HOMO-LUMO gap changes in P3HT. Experimental studies show that annealing reduces the HOMO-LUMO gap. The annealing process helps to generate a flat molecule. [25] In other words, the relative flatness of the polymer backbone is strongly correlated to the HOMO-LUMO gap. Planarization of the backbone is observed in poly(3-(2,5-dioctylphenyl)thiophene) (PDOPT) with bulky side groups. A redshift of its electronic transition is also observed indicating planarization has reduced the HOMO-LUMO gap.[26]

In the present study tuning of the HOMO-LUMO gap of PTh and of the HOMO and LUMO levels separately was done by introducing different electron-donating and electron-withdrawing peripheral groups. Then the heteroatom, S, was replaced by Se, and also molecules containing alternating S and Se heteroatoms were studied with electron-donating and electron-withdrawing peripheral groups.

PTh models having six repeating units (hexamers) were considered for the theoretical calculations. Oligomers having 6 thiophene monomers are reasonably representing the polymer PTh. [27] As electron-donating groups $-CH_3$, $-OCH_3$ and $-N(CH_3)_2$ were used, and as electron-withdrawing groups -CHO, $-COOCH_3$, -CN and $-NO_2$ were used. Five different structures were considered by attaching substituent groups at different positions (Figure 4.1). Substitution groups, $-OCH_3$, $-N(CH_3)_2$ and -CHO, $-COOCH_3$ were used with S replaced by Se in PTh (polyselenophene) and S-Se alternating heteroatoms containing molecule.

In the monomer 3-alkylthiophene, the peripheral H atom attached to the 3rd carbon is replaced by an alkyl group. According to the experimental results, in 3-alkylthiophene, Head-Tail-Head-Tail (HT-HT) is the most prominent orientation. [28] Two 3-alkylthiophene monomers are coupled

between 2 and 5 positions to make the dimer HT-HT. As a starting point, this experimental structure was considered. The structure 5 (figure 4.1) is showing the oligomer having HT-HT coupling. The other structures under consideration were designed by removing either several electron-donating or several electron-withdrawing groups from structure 5.

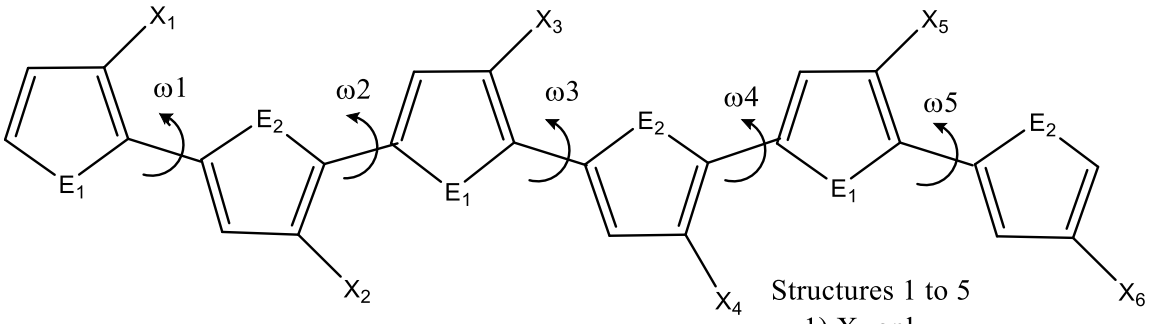

E_1 and E_2 = S,S / Se,Se / S,Se

Structures 1 to 5
1) X_6 only
2) X_1 and X_6
3) X_2 and X_4
4) X_2, X_4 and X_6
5) X_1 to X_6

Figure 4.1: Schematic diagram of the molecules in this study. "E" represents the heteroatom, "X" represents the positions where electron-donating or withdrawing groups are attached and ω is the dihedral angle (torsion angle) considering two heteroatoms in adjacent monomeric units. Five different structures were considered as given under 1 – 5.

4.2 RESULTS AND DISCUSSION

The effect of different electron-donating and electron-withdrawing substituents on the geometry and electronic properties were compared with the properties of the bare molecule. Figure 4.2 is showing the optimized structures of PTh and -OCH_3 substituted PTh. Oligomers containing six monomers were used for the calculations. Therefore PTh contains 6 sulfur atoms and the molecule is named as 6S. When the S atom is replaced by the Se, it is named as 6Se and the structure having

alternating heteroatoms is named as 3S3Se. The HOMO-LUMO levels and band gaps are given in tables 4.1 and 4.2. Dihedral angle along the polymer chain (as marked in figure 4.1) is given in table 4.3/4.4.

Five different structures were considered by changing the number and the position of substituents attached (Figure 4.1). The 1st structure is having one attachment, the 2nd and 3rd are having two attachments, the 4th one is having three and the 5th one is having six groups attached. If the attached group is an electron-donating group, the 1st structure is less electron-rich and 5th structure is the most electron-rich structure.

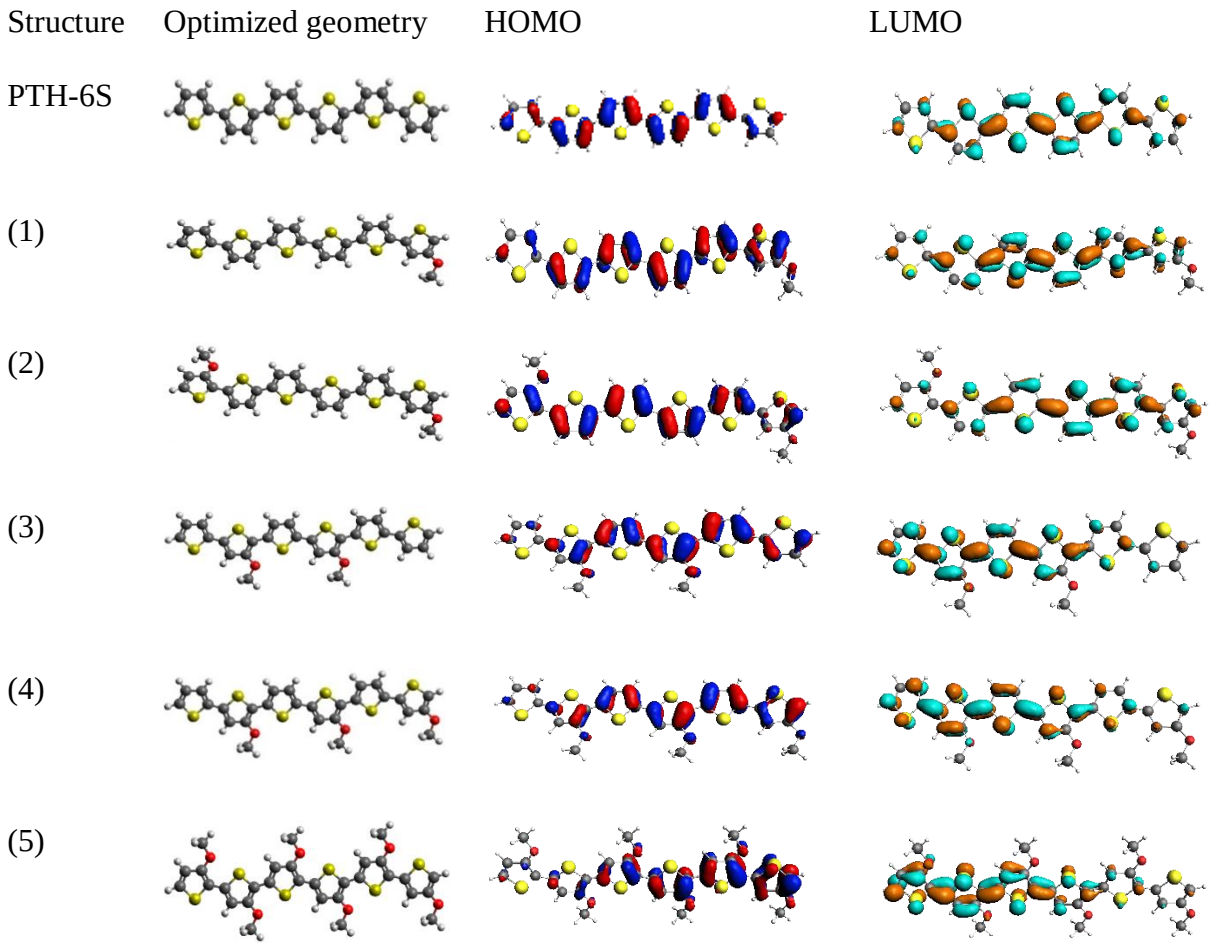

Figure 4.2: Optimized structures, HOMO and LUMO of PTh and PTh with -OCH_3 groups attached

Table 4.1: The HOMO-LUMO levels and band gaps (in eV) for polymers with electron-donating groups. See figure 4.1 for the nomenclature of structures 1–5.

	$-OCH_3$			$-N(CH_3)_2$			$-CH_3$		
Structure	HOMO	LUMO	band gap	HOMO	LUMO	band gap	HOMO	LUMO	band gap
E_1, E_2 = S, S (PTh)									
6S	-4.57	-3.02	1.55	-4.57	-3.02	1.55	-4.57	-3.02	1.55
1	-4.57	-3.01	1.56	-4.52	-2.97	1.55	-4.55	-3.03	1.52
2	-4.42	-2.87	1.55	-4.42	-2.82	1.60	-4.55	-2.93	1.62
3	-4.33	-2.91	1.42	-4.32	-2.87	1.45	-4.48	-2.96	1.52
4	-4.32	-2.91	1.41	-4.31	-2.84	1.47	-4.46	-2.93	1.53
5	-3.86	-2.69	1.17	-3.87	-2.63	1.24	-4.02	-2.84	1.18
E_1, E_2 = Se, Se									
6Se	-4.57	-3.16	1.41	-4.57	-3.16	1.41			
1	-4.50	-3.22	1.28	-4.44	-3.17	1.26			
2	-4.34	-3.08	1.26	-4.36	-3.03	1.33			
3	-4.30	-3.08	1.22	-4.29	-3.03	1.26			
4	-4.26	-3.08	1.18	-4.23	-3.03	1.20			
5	-3.82	-2.86	0.96	-4.03	-2.84	1.19			
E_1, E_2 = S, Se									
3S3Se	-4.58	-3.12	1.46	-4.58	-3.12	1.46			
1	-4.57	-3.11	1.46	-4.48	-3.05	1.43			
2	-4.39	-2.99	1.40	-4.40	-2.92	1.49			
3	-4.32	-3.00	1.32	-4.36	-2.93	1.43			
4	-4.23	-3.00	1.23	-4.28	-2.95	1.33			
5	-3.85	-2.79	1.06	-3.98	-2.73	1.25			

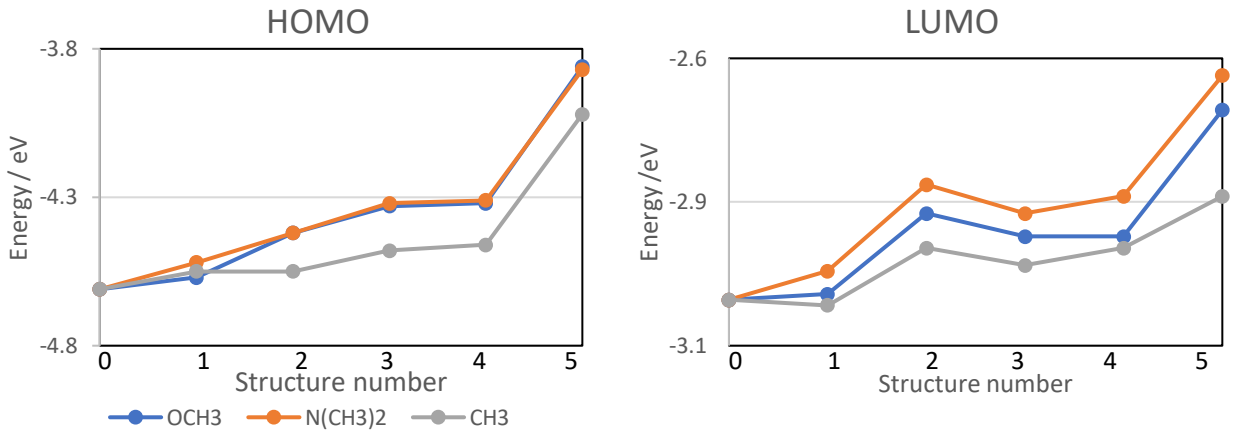

(a) **(b)**

Figure 4.3: a) HOMO b) LUMO of PTh with different electron-donating substituents. Structure number is given as figure 4.1. Structure 0 represents PTh

Both HOMO and LUMO are delocalized over the polymer chain (Figure 4.2). The LUMO is having a considerable contribution from the heteroatom when comparing with the HOMO. When we observed the absolute values of the HOMO level of PTh (Tables 4.1 and 4.2), it remains essentially constant at -4.6 eV when the heteroatom is changed from S to Se (6S to 6Se) and even in the 3S3Se structure. On the other hand, the LUMO level is changing from -3.02 to -3.12 and to -3.19 for 6S, 3S3Se and 6Se respectively. Previous reports also show that, in PTh, the HOMO level does not have significant contributions from the heteroatom S.[8,29,30] The lower ionization potential of Se compared to the S in PTh moves the LUMO level down, and this results in a decreased band gap when going from S to Se.

After replacing the peripheral hydrogens with different electron-donating and electron-withdrawing groups, both HOMO and LUMO levels showed changes (Table 4.1 and Table 4.2). Figure 4.2 is also showing that the attached groups are having a certain contribution to the HOMO

and LUMO. With electron-donating groups both HOMO and LUMO levels are increasing and with electron-withdrawing groups both HOMO and LUMO levels are decreasing in energy. The electron-donating power of substituted groups are in the order of $-N(CH_3)_2 > -OCH_3 > -CH_3$. [31] Figure 4.3 clearly follows this trend. The increase in both HOMO and LUMO levels when $-N(CH_3)_2$ is attached is the highest with compared to $-OCH_3$ and $-CH_3$. The strong electron-withdrawing groups $-NO_2$ and -CN decrease both HOMO and LUMO levels compared to the less electron-withdrawing -CHO and $-COOCH_3$ (Figure 4.4).[32] $-NO_2$ is showing the most prominent effect. This change is very small when the oligomer is having only one substituent group attached. However, it is clearly visible when 5 groups are attached. As both HOMO and LUMO levels are changing, the change in the HOMO-LUMO gap is not that uniform. The structures containing 6Se and 3S3Se are showing similar trends in changes of HOMO and LUMO levels. The HOMO and LUMO values of 3S3Se containing structures are exactly within the values of 6S and 6Se as expected.

Table 4.2: The HOMO-LUMO levels and band gaps (in eV) for polymers with electron-withdrawing groups. See figure 4.1 for the nomenclature of structures 1–5.

	-CHO			-$COOCH_3$			-CN			-NO_2		
Structure	HOMO	LUMO	band gap	HOMO	LUMO	band gap	HOMO	LUMO	band gap	HOMO	LUMO	band gap
E_1, E_2 = S, S (PTh)												
6S	-4.57	-3.02	1.55	-4.57	-3.02	1.55	-4.57	-3.02	1.55	-4.57	-3.02	1.55
1	-4.75	-3.22	1.53	-4.73	-3.19	1.54	-4.81	-3.27	1.54	-4.82	-3.54	1.28
2	-4.98	-3.42	1.56	-4.80	-3.16	1.64	-4.98	-3.46	1.52	-5.06	-3.74	1.32
3	-5.14	-3.46	1.68	-5.05	-3.26	1.79	-5.10	-3.54	1.56	-5.20	-3.78	1.42
4	-5.27	-3.61	1.66	-5.24	-3.31	1.93	-5.30	-3.73	1.57	-5.46	-3.99	1.47
5	-5.89	-4.05	1.84	-5.36	-3.27	2.09	-5.86	-4.30	1.56	-6.18	-4.52	1.66
E_1, E_2 = Se, Se												
6Se	-4.57	-3.16	1.41	-4.57	-3.16	1.41						
1	-4.70	-3.39	1.31	-4.70	-3.38	1.32						
2	-5.00	-3.47	1.53	-4.70	-3.45	1.45						
3	-5.00	-3.75	1.25	-4.81	-3.49	1.32						
4	-5.11	-3.88	1.23	-4.92	-3.57	1.35						
5	-5.81	-4.17	1.64	-5.36	-3.27	2.09						
E_1, E_2 = S, Se												
3S3Se	-4.58	-3.12	1.46	-4.58	-3.12	1.46						

1	-4.73	-3.30	1.43	-4.79	-3.24	1.55	
2	-4.94	-3.49	1.45	-4.75	-3.23	1.52	
3	-5.09	-3.52	1.57	-5.03	-3.29	1.74	
4	-5.22	-3.65	1.57	-5.14	-3.35	1.79	
5	-5.85	-4.07	1.77	-5.38	-3.47	1.91	

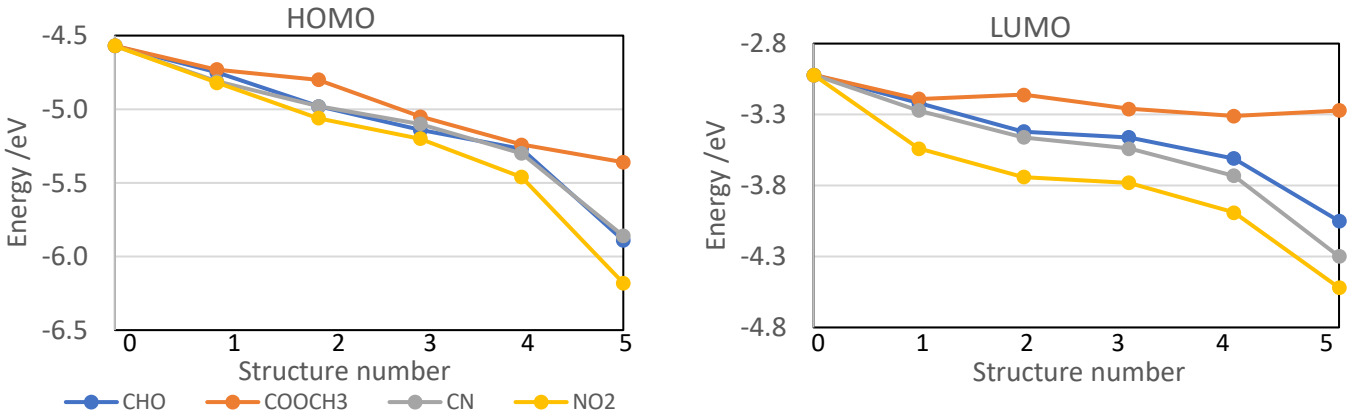

(a) **(b)**

Figure 4.4: a) HOMO b) LUMO of PTh with different electron-withdrawing substituents. Structure number is given as figure 4.1. The structure 0 represents PTh

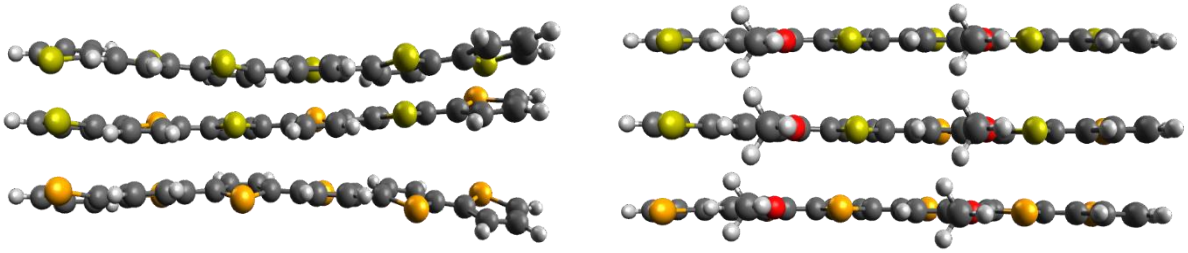

(a) **(b)**

Figure 4.5: Optimized structures of oligomers (6S, 3S3Se, 6Se) a) before attaching different peripheral groups; b) with two -OCH_3 attached (structure 3)

Structural changes are also observed in the substituted structures. The peripheral groups control the backbone conformation. The torsional angle, ω, is the dihedral angle considering two heteroatoms in adjacent monomeric units (Figure 4.1) and the values are summarized in tables 4.3 and 4.4. Figure 4.5 shows the optimized structures of 6S, 6Se, 3S3Se oligomers without and with

two -OCH_3 groups attached. A recent study based on polythiophene geometry and number of monomers shows that the polythiophene stays flat when it is having a fewer number of monomers and it becomes curved when the number of monomers increases. [33] In the oligomers of the present study, the dihedral angle (ω) is in the range of 165-175, 164-170, 165-172º in 6S, 6Se, 3S3Se oligomers, respectively, and after the substitution of two -OCH_3, it is nearly 180º Figure 4.5. The substituted groups have made the oligomer flat. A flat structure is also observed when the oligomer is having six -OCH_3 groups attached. The 2 lone pairs of -OCH_3 can increase the conjugation and hence promote a flat structure. On the other hand, -CH_3 is having the least electron-donating power and the structure containing 6 -CH_3 (structure 5) groups is showing planarization compared to the other structures containing -CH_3.

According to the results of chapter 3, the bond length between heteroatom and carbon increases when going from S to Se. The C-S bond length is 1.75 Å while the C-Se bond length is 1.90 Å. With this lengthening of the bond, a decrease in angles is also observed; the C-S-C angle is 92.3º and the C-Se-S angle is 87.7º. The periodic calculations clearly show a decrease in bridging bond length (the bond between two monomers) when the heteroatom is changing from S to Se in PTh. It is 1.46 Å for PTh, and when Se is present it is 1.42 Å. The decreased bridging bond length proves increased quinoid resonance when going from S to Se.[34] Planarization of the molecule (dihedral angle close to 180º) is observed in 6Se, with the attachment of two -$N(CH_3)_2$. This may be a combined effect of increased resonance in 6Se compared to the PTh and the electron-donation by the donor group -$N(CH_3)_2$. The dihedral angle when two -$N(CH_3)_2$ are attached in PTh does not have the value of 180º When six -$N(CH_3)_2$ are attached (structure 5), planarization is not observed as in structure 5 of -OCH_3. Steric effects may determine the structure in these cases as -$N(CH_3)_2$ contains 2 relatively bulky CH_3 groups. The planarization of the molecule resulting from the

combined effect of increased resonance in 6Se compared to the PTh and the electron-donation by the attached groups is also clear in all the other 6Se structures having -OCH_3. Overall the dihedral angle is closer to 180º compared to PTh or 3S3Se based structures. With the attachment of electron-withdrawing groups this planarization is not prominent.

Most of the dihedral angles are showing deviations from 180º. Electron-withdrawing groups disturb the conjugation in the backbone. The bridging bond lengths of the -CHO, -$COOCH_3$, -$N(CH_3)_2$ and -OCH_3 containing structures 5 of PTh are 1.45, 1.45, 1.44, 1.43 Å respectively. The decreased bridging bond length when going from electron-withdrawing groups to the electron-donating groups proves increased quinoid resonance.[34] The 6Se structure 5 with the same attachments show bridging bond lengths as 1.44, 1.44, 1.42, 1.42 Å respectively.

Table 4.3: Dihedral angles (º) along the polymer chain (see figure 4.1) for polymers with electron-donating groups

	-CH_3									
Structure	ω1	ω2	ω3	ω4	ω5					
E_1, E_2 = S, S (PTh)										
6S	168.9	165.1	168.5	165.9	175.2					
1	174.7	175.3	168.9	172.9	178.9					
2	172.9	161.3	162.1	161.8	171.3					
3	163.6	168.5	168.3	173.7	176.0					
4	178.4	174.5	172.7	174.7	175.0					
5	179.5	173.3	179.9	178.7	178.8					
	-OCH_3					-$N(CH_3)_2$				
Structure	ω1	ω2	ω3	ω4	ω5	ω1	ω2	ω3	ω4	ω5
E_1, E_2 = S, S (PTh)										
6S	168.9	165.1	168.5	165.9	175.2	168.9	165.1	168.5	165.9	175.2

1	173.2	162.5	165.6	162.8	172.3	163.7	168.7	175.1	162.4	157.2
2	177.5	162.0	170.5	166.9	159.9	165.9	156.6	166.3	156.5	157.8
3	179.0	179.7	179.6	179.2	179.7	168.7	167.4	166.9	163.7	161.9
4	177.4	177.7	175.4	179.6	178.2	167.6	169.7	170.3	179.9	155.4
5	179.6	179.5	179.9	179.9	179.3	164.1	149.8	164.9	173.3	164.6
E_1, E_2 = Se, Se										
6Se	170.5	163.7	166.2	164.0	170.3	170.5	163.7	166.2	164.0	170.3
1	180.0	179.4	179.6	178.7	179.8	167.9	165.7	172.4	168.4	167.1
2	178.8	175.1	172.4	177.4	172.2	179.2	179.3	179.1	179.4	179.8
3	176.3	179.1	178.2	179.8	177.7	179.8	179.0	179.0	179.5	178.6
4	179.2	178.3	168.4	177.9	165.8	178.6	179.0	169.4	172.5	162.8
5	179.2	179.3	179.1	179.4	179.8	177.9	174.0	171.9	179.3	174.8
E_1, E_2 = S, Se										
3S3Se	165.0	172.3	169.5	170.1	167.9	165.0	172.3	169.5	170.1	167.9
1	168.5	167.4	165.8	162.5	161.1	169.0	167.0	176.7	164.7	161.4
2	180.0	166.7	171.7	169.0	165.6	171.5	161.1	163.9	159.9	161.9
3	179.7	179.4	179.7	179.5	179.8	166.8	164.8	159.1	168.5	158.9
4	176.3	180.0	174.7	178.4	166.5	172.9	173.8	176.5	174.5	171.8
5	179.5	177.1	179.0	177.6	179.8	170.4	159.5	176.0	164.3	159.4

Table 4.4: Dihedral angles (º) along the polymer chain (see figure 4.1) for polymers with electron-withdrawing groups

	-CN					-NO_2				
Structure	ω1	ω2	ω3	ω4	ω5	ω1	ω2	ω3	ω4	ω5
E_1, E_2 = S, S (PTh)										
6S	168.9	165.1	168.5	165.9	175.2	168.9	165.1	168.5	165.9	175.2
1	172.4	167.4	167.4	170.3	169.4	179.4	169.8	173.3	172.9	170.4
2	178.1	171.5	167.8	170.0	169.5	179.0	174.6	173.6	174.8	169.1

3	173.4	166.4	172.6	172.1	173.6	165.8	158.8	169.8	163.7	176.1
4	166.1	167.6	171.3	168.9	168.1	164.9	166.3	164.1	164.3	173.6
5	177.6	176.0	174.4	179.6	175.6	164.8	157.8	156.4	155.3	149.3
	-CHO					-$COOCH_3$				
Structure	ω1	ω2	ω3	ω4	ω5	ω1	ω2	ω3	ω4	ω5
E_1, E_2 = S, S (PTh)										
6S	168.9	165.1	168.5	165.9	175.2	168.9	165.1	168.5	165.9	175.2
1	178.5	170.0	169.1	175.6	167.5	178.6	165.8	166.2	158.3	172.5
2	145.9	172.4	164.3	175.5	170.1	143.8	152.8	166.9	157.8	158.2
3	179.6	140.7	174.9	148.1	163.3	159.7	142.6	154.4	140.5	170.2
4	173.9	145.6	161.6	144.9	167.7	159.8	136.7	163.6	135.4	156.3
5	138.2	146.4	141.9	145.1	142.4	142.1	124.9	132.6	146.7	155.8
E_1, E_2 = Se, Se										
6Se	170.5	163.7	166.2	164.0	170.3	170.5	163.7	166.2	164.0	170.3
1	169.0	171.0	170.8	176.8	174.9	165.5	164.3	165.9	165.0	157.1
2	136.8	149.1	169.5	153.7	162.3	148.6	153.8	173.2	161.9	170.0
3	165.8	143.1	170.2	145.1	165.9	166.0	141.3	153.9	139.1	157.9
4	167.6	139.2	165.1	142.1	165.4	169.7	140.7	155.6	137.9	159.2
5	140.3	138.9	148.5	148.0	139.0	149.6	26.6	121.3	148.4	151.7
E_1, E_2 = S, Se										
3S3Se	165.0	172.3	169.5	170.1	167.9	165.0	172.3	169.5	170.1	167.9
1	169.9	178.8	176.2	165.2	170.7	165.2	156.8	161.4	158.0	158.6
2	142.4	177.6	172.6	172.9	179.8	148.8	152.2	169.8	153.1	160.2
3	164.5	145.8	160.2	145.8	162.6	157.5	140.2	152.0	138.8	157.1
4	165.6	143.8	168.3	143.3	164.5	171.6	137.4	161.8	129.1	146.1
5	133.5	143.8	140.01	148.2	138.7	144.1	34.4	128.8	143.2	144.9

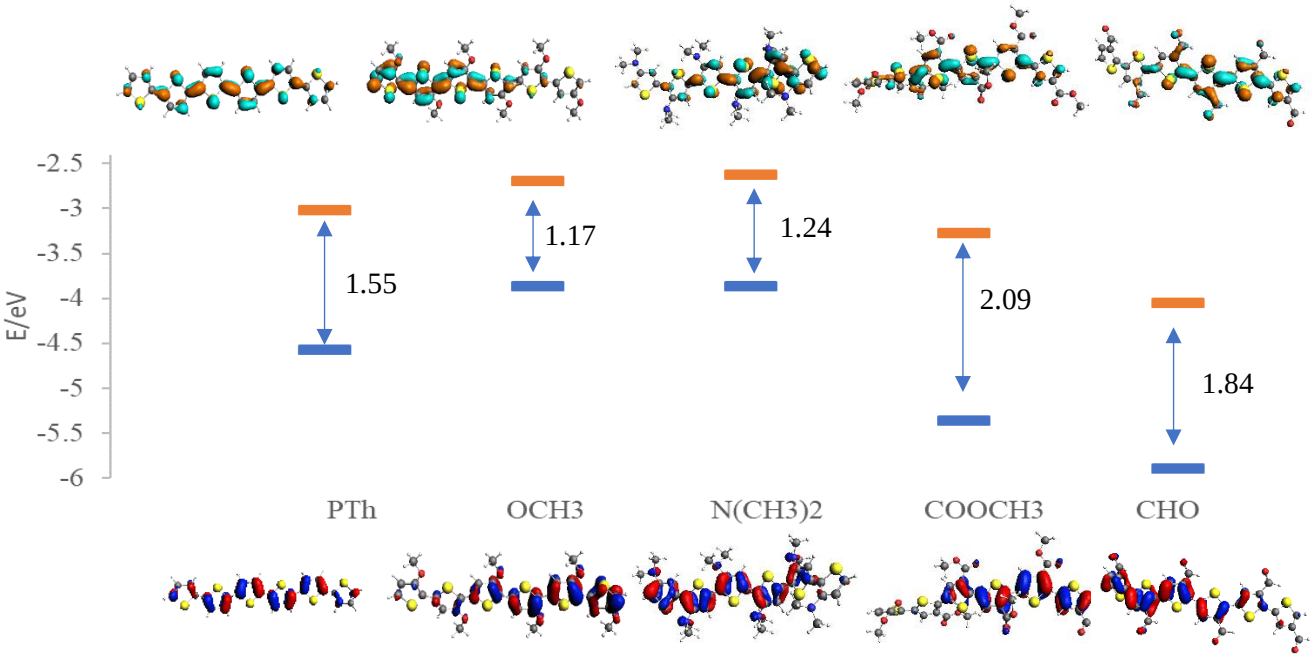

Figure 4.6: HOMO-LUMO gap (in eV) of PTh and structure 5 (see figure 4.1) of PTh with different groups attached

Figure 4.6 is showing the HOMO and LUMO of PTh (structure 5), substituted with different electron-donating and electron-withdrawing substituents. It has been proven that planarization reduces the band gap. [25,26] The PTh attached with -OCH_3 is having dihedral angles in the range 179.3 -179.9º. The other structures are showing dihedral angles in the ranges of 149.8-173.3º, 124.9-155.8º, 138.2-146.4º for -$N(CH_3)_2$, -$COOCH_3$, -CHO respectively. Among these 4 different molecules, the lowest band gap is obtained by the mostly planarized molecule, that is the molecule having 6 -OCH_3 attached. When we compare the -$N(CH_3)_2$ and -OCH_3 containing 6S, 6Se and 3S3Se structures, more planarized structures were obtained with the attachments of -OCH_3 compared to -$N(CH_3)_2$ attached structures (Table 4.3). Further, the HOMO-LUMO gap of -OCH_3 containing structures are small compare to -$N(CH_3)_2$ attached structures except in structure 1 (Table 4.1). Structure 1 is having only one attachment and it is having less effect on the structure.

4.3 CONCLUSIONS

The tuning of the HOMO-LUMO gap of PTh was achieved by replacing the peripheral hydrogen in PTh with different electron-donating and electron-withdrawing groups. As electron-donating groups -CH_3, -OCH_3 and -$N(CH_3)_2$ were used, and as electron-withdrawing groups -CHO, -$COOCH_3$, -CN and -NO_2 were used. Further, several substituents, specifically -OCH_3, -$N(CH_3)_2$ and -CHO, -$COOCH_3$ were used with S replaced by Se in PTh (polyselenophene) and molecules containing alternating heteroatoms S-Se. Different structures were considered by attaching different numbers of electron-donating and electron-withdrawing groups at different places in the oligomers having 6 monomers.

With the modification of the chemical structure, electronic and structural changes were observed. The addition of electron-donating groups results in increased HOMO and LUMO levels and the addition of electron-withdrawing groups results in decreased HOMO and LUMO levels. The values observed for the HOMO-LUMO gap were somewhat less uniform. Planarization of the molecule was observed with electron-donating groups. The location of the attached group is also important in planarizing the molecule. Electron-withdrawing groups disturb the conjugation in the backbone. More reduced band gaps were observed for the planarized molecules. By changing the heteroatom from S to Se more planarized structures were observed. The structures containing both S and Se as heteroatoms were having intermediate properties. These results can be useful when designing novel polymeric materials for solar cells as well as SWCNT refining. The HOMO-LUMO gap and levels are important in solar cells. In SWCNT refining, the geometry of the polymer and the electron density of the polymer are important.

References

(1) Kaloni, T. P.; Giesbrecht, P. K.; Schreckenbach, G.; Freund, M. S. Polythiophene: From Fundamental Perspectives to Applications. *Chem. Mater.* **2017**, *29* (24), 10248–10283.

(2) Chen, Z.; Lemke, H.; Albert-Seifried, S.; Caironi, M.; Nielsen, M. M.; Heeney, M.; Zhang, W.; McCulloch, I.; Sirringhaus, H. High Mobility Ambipolar Charge Transport in Polyselenophene Conjugated Polymers. *Adv. Mater.* **2010**, *22* (21), 2371–2375.

(3) Charlebois, I.; Gravel, C.; Arrad, N.; Boissinot, M.; Bergeron, M. G.; Leclerc, M. Impact of DNA Sequence and Oligonucleotide Length on a Polythiophene-Based Fluorescent DNA Biosensor. *Macromol. Biosci.* **2013**, *13* (6), 717–722.

(4) Plante, M.-P.; Bérubé, È.; Bissonnette, L.; Bergeron, M. G.; Leclerc, M. Polythiophene Biosensor for Rapid Detection of Microbial Particles in Water. *ACS Appl. Mater. Interfaces* **2013**, *5* (11), 4544–4548.

(5) Oh, S. H.; Lee, C.-W.; Chun, D. H.; Jeon, J.-D.; Shim, J.; Shin, K. H.; Yang, J. H. A Metal-Free and All-Organic Redox Flow Battery with Polythiophene as the Electroactive Species. *J. Mater. Chem. A* **2014**, *2* (47), 19994–19998.

(6) Liu, L.; Tian, F.; Wang, X.; Yang, Z.; Zhou, M.; Wang, X. Porous Polythiophene as a Cathode Material for Lithium Batteries with High Capacity and Good Cycling Stability. *React. Funct. Polym.* **2012**, *72* (1), 45–49.

(7) Kumar, M. R.; Rahman, G. M. A.; Thomson, D. J.; Freund, M. S. Controlling Volatility in Solid-State, Redox-Based Memory Devices Using Heterojunction Barriers to Ion Transport. *Chem. Commun.* **2012**, *48* (75), 9409–9411.

(8) Kaloni, T. P.; Schreckenbach, G.; Freund, M. S. Band Gap Modulation in Polythiophene and Polypyrrole-Based Systems. *Sci. Rep.* **2016**, *6* (1), 36554.

(9) Kim, B.-G.; Ma, X.; Chen, C.; Ie, Y.; Coir, E. W.; Hashemi, H.; Aso, Y.; Green, P. F.; Kieffer, J.; Kim, J. Energy Level Modulation of HOMO, LUMO, and Band-Gap in Conjugated Polymers for Organic Photovoltaic Applications. *Adv. Funct. Mater.* **2013**, *23* (4), 439–445.

(10) Casey, A.; Dimitrov, S. D.; Shakya-Tuladhar, P.; Fei, Z.; Nguyen, M.; Han, Y.; Anthopoulos, T. D.; Durrant, J. R.; Heeney, M. Effect of Systematically Tuning Conjugated Donor Polymer Lowest Unoccupied Molecular Orbital Levels via Cyano Substitution on Organic Photovoltaic Device Performance. *Chem. Mater.* **2016**, *28* (14), 5110–5120.

(11) Nagahora, N.; Yahata, S.; Goto, S.; Shioji, K.; Okuma, K. 2,5-Diaryltellurophenes: Effect of Electron-Donating and Electron-Withdrawing Groups on Their Optoelectronic Properties. *J. Org. Chem.* **2018**, *83* (4), 1969–1975.

(12) Sutradhar, T.; Misra, A. Role of Electron-Donating and Electron-Withdrawing Groups in Tuning the Optoelectronic Properties of Difluoroboron–Napthyridine Analogues. *J. Phys. Chem. A* **2018**, *122* (16), 4111–4120.

(13) Elumalai, N. K.; Uddin, A. Open Circuit Voltage of Organic Solar Cells: An in-Depth Review. *Energy Environ. Sci.* **2016**, *9* (2), 391–410.

(14) Xu, B.; Sai-Anand, G.; Gopalan, A.-I.; Qiao, Q.; Kang, S.-W. Improving Photovoltaic Properties of P3HT:IC60BA through the Incorporation of Small Molecules. *Polymers* **2018**, *10* (2), 121.

(15) Kiymaz, D.; Yagmurcukardes, M.; Tomak, A.; Şahin, H.; Senger, R. T.; Peeters, F. M.; Zareie, H. M.; Zafer, C. Controlled Growth Mechanism of Poly (3-Hexylthiophene) Nanowires. *Nanotechnology* **2016**, *27* (45), 455604.

(16) Niles, E. T.; Roehling, J. D.; Yamagata, H.; Wise, A. J.; Spano, F. C.; Moulé, A. J.; Grey, J. K. J-Aggregate Behavior in Poly-3-Hexylthiophene Nanofibers. *J. Phys. Chem. Lett.* **2012**, *3* (2), 259–263.

(17) Brown, P. J.; Thomas, D. S.; Köhler, A.; Wilson, J. S.; Kim, J.-S.; Ramsdale, C. M.; Sirringhaus, H.; Friend, R. H. Effect of Interchain Interactions on the Absorption and Emission of Poly(3-Hexylthiophene). *Phys. Rev. B* **2003**, *67* (6), 064203.

(18) Wu, H.; Higaki, Y.; Nojima, S.; Takahara, A. Orientation and Crystallization of Regioregular Poly(3-Dodecylthiophene) in Alumina Nanopores. *Soft Matter* **2017**, *13* (26), 4661–4666.

(19) Wang, H.; Koleilat, G. I.; Liu, P.; Jiménez-Osés, G.; Lai, Y.-C.; Vosgueritchian, M.; Fang, Y.; Park, S.; Houk, K. N.; Bao, Z. High-Yield Sorting of Small-Diameter Carbon Nanotubes for Solar Cells and Transistors. *ACS Nano* **2014**, *8* (3), 2609–2617.

(20) Gomulya, W.; Gao, J.; Loi, M. A. Conjugated Polymer-Wrapped Carbon Nanotubes: Physical Properties and Device Applications. *Eur. Phys. J. B* **2013**, *86* (10), 404.

(21) Wan Chik, M.; Hussain, Z.; Zulkefeli, M.; Tripathy, M.; Kumar, S.; Majeed, A.; Byrappa, K. Polymer-Wrapped Single-Walled Carbon Nanotubes: A Transformation toward Better Applications in Healthcare. *Drug Deliv. Transl. Res.* **2018**, *9*.

(22) Varghese, N.; Ghosh, A.; Voggu, R.; Ghosh, S.; Rao, C. N. R. Selectivity in the Interaction of Electron Donor and Acceptor Molecules with Graphene and Single-Walled Carbon Nanotubes. *J. Phys. Chem. C* **2009**, *113* (39), 16855–16859.

(23) Fong, D.; Adronov, A. Recent Developments in the Selective Dispersion of Single-Walled Carbon Nanotubes Using Conjugated Polymers. *Chem. Sci.* **2017**, *8* (11), 7292–7305.

(24) Leysen, P.; Teyssandier, J.; De Feyter, S.; Koeckelberghs, G. Controlled Synthesis of a Helical Conjugated Polythiophene. *Macromolecules* **2018**, *51* (9), 3504–3514.

(25) McLeod, J. A.; Pitman, A. L.; Kurmaev, E. Z.; Finkelstein, L. D.; Zhidkov, I. S.; Savva, A.; Moewes, A. Linking the HOMO-LUMO Gap to Torsional Disorder in P3HT/PCBM Blends. *J. Chem. Phys.* **2015**, *143* (22), 224704.

(26) Raithel, D.; Simine, L.; Pickel, S.; Schötz, K.; Panzer, F.; Baderschneider, S.; Schiefer, D.; Lohwasser, R.; Köhler, J.; Thelakkat, M.; et al. Direct Observation of Backbone Planarization via Side-Chain Alignment in Single Bulky-Substituted Polythiophenes. *Proc. Natl. Acad. Sci.* **2018**, *115* (11), 2699–2704.

(27) Kaloni, T. P.; Schreckenbach, G.; Freund, M. S. Structural and Electronic Properties of Pristine and Doped Polythiophene: Periodic versus Molecular Calculations. *J. Phys. Chem. C* **2015**, *119* (8), 3979–3989.

(28) Oliveira, M. A. de; Almeida, W. B. de; Santos, H. F. dos. Structure and Electronic Properties of Alkylthiophenes Coupled by Head-to-Tail and Head-to-Head Regioselectivity. *J. Braz. Chem. Soc.* **2004**, *15* (6), 832–838.

(29) Ramirez-Solis, A.; Kirtman, B.; Bernal-Jaquez, R.; Zicovich-Wilson, C. M. Periodic Density Functional Theory Studies of Li-Doped Polythiophene: Dependence of Electronic and Structural Properties on Dopant Concentration. *J. Chem. Phys.* **2009**, *130* (16), 164904.

(30) Heeney, M.; Zhang, W.; Crouch, D. J.; Chabinyc, M. L.; Gordeyev, S.; Hamilton, R.; Higgins, S. J.; McCulloch, I.; Skabara, P. J.; Sparrowe, D.; et al. Regioregular Poly(3-Hexyl)Selenophene: A Low Band Gap Organic Hole Transporting Polymer. *Chem. Commun.* **2007**, *0* (47), 5061–5063.

(31) Zhang, X.; Yang, J.; Lu, M.; Gong, X. Theoretical Studies on the Stability of Phenylpentazole and Its Substituted Derivatives of –OH, –OCH_3, –OC_2H_5 and –$N(CH_3)_2$. *RSC Adv* **2014**, *4* (99), 56095–56101.

(32) Sharber, S. A.; Baral, R. N.; Frausto, F.; Haas, T. E.; Müller, P.; Thomas III, S. W. Substituent Effects That Control Conjugated Oligomer Conformation through Non-Covalent Interactions. *J. Am. Chem. Soc.* **2017**, *139* (14), 5164–5174.

(33) Dai, Y.; Wei, C.; Blaisten-Barojas, E. Density Functional Theory Study of Neutral and Oxidized Thiophene Oligomers. *J. Chem. Phys.* **2013**, *139* (18), 184905.

(34) Vessally, E. Aromatic Stability Energy Studies on Five-Membered Heterocyclic C4H4M(M = O, S, Se, Te, NH, PH, AsH and SbH): DFT Calculations. *J. Struct. Chem.* **2008**, *49* (6), 979–985.

Chapter 5 : CONCLUSIONS AND OUTLOOK

5.1 CONCLUSIONS

This thesis presents a computational investigation of the tunability of HOMO-LUMO levels and band gaps in conducting polymers. Theoretical calculations were done with DFT using the GGA(PBE) functional.

Chapter 3 discusses the changes in HOMO-LUMO levels and band gap by doping of conducting polymers. PTh, PPy and their analogs (S is replaced by O, Se, Te in PTh and N is replaced by P, As, Sb in PPy) were used as the CPs under this study. To facilitate the n-type and p-type doping, two atomic dopants namely Li and Cl were used. Structural and electronic changes upon doping were analyzed with molecular and periodic calculations. A decrease in HOMO-LUMO gaps was observed after doping and it was prominent in PTh and analogs. The band structure diagrams obtained from periodic calculations show upward or downward shifts in the Fermi level with Li and Cl, respectively. With this shift in Fermi level, metallic conductivities can be expected from these doped polymers. Possible applications of these polymers are discussed in chapter 3.

Chapter 4 discusses the changes in HOMO-LUMO levels and band gap of PTh based polymers by their modifications through substituents. The tuning of the HOMO-LUMO gap was done by replacing the peripheral hydrogen in PTh by different electron-donating and electron-withdrawing groups. Further, substitution groups were used with S replaced by Se in PTh (polyselenophene) and S-Se alternating heteroatoms containing molecules. Different structures were considered by attaching a different number of electron-donating and electron-withdrawing groups at different places in the oligomers having 6 monomers. The addition of electron-donating groups results in increased HOMO and LUMO levels and the addition of electron-withdrawing groups results in decreased HOMO and LUMO levels. The values observed for the HOMO-LUMO gap were

somewhat less uniform. Planarization of the molecule was observed with electron-donating groups. Electron withdrawing groups disturb the conjugation in the backbone. More reduced band gaps were observed with the planarized molecules. By changing the heteroatom from S to Se more planarized structures were observed. The structures containing both S and Se as heteroatoms were having intermediate properties.

The HOMO – LUMO gap and levels are unique properties of a molecule which can be used to make predictions about capabilities of the molecule. As presented in this thesis, doping and modifications through substituents can be used successfully to tune the HOMO – LUMO gap and levels of CPs. In PTh and PPy based polymers, the HOMO level remains essentially constant when changing the heteroatom. One can tune the LUMO level just by replacing the heteroatom with different atoms. Doping or peripheral substituents change both HOMO and LUMO levels. Changes in HOMO and LUMO levels finally change the band gap. Changes in HOMO – LUMO gap and levels of PTh and PPy based polymer series are presented here and these results can be useful when designing novel polymeric materials for various applications.

5.2 OUTLOOK

The following are possible directions for continuing the work in this thesis.

1. Modification of structural and electronic properties of oligothiophenes through substituents are presented in chapter 4. This study can be applied to all the polymers presented in chapter 3. That is PTh, PPy and their analogs (S is replaced by O, Te in PTh and N is replaced by P, As, Sb in PPy).

2. Oligomers having different combinations of heteroatoms can also be studied with doping (as in chapter 3) as well as peripheral substituents (as in chapter 4).

3. For the study in chapter 4, other sets of electron-donating and electron-withdrawing groups can be incorporated.

4. Geometry and electron density of the polymer is important in SWCNT refining. For this application, the polymer should align along the SWCNT's surface. Electron-rich polymers selectively disperse semiconducting SWCNT while electron-poor polymers favor metallic SWCNT over semiconducting SWCNT. The electron-poor polymers disperse a mixture of metallic and semiconducting SWCNT. Molecular-dynamic simulations can be carried out to study the wrapping carefully.[1,2] The polymer-wrapped SWCNTs with good solubility in water can have applications in biological environments.[3] SWCNTs are hydrophobic like other nanotubes. Polymers which are suitable to increase the solubility in water should have hydrophobic and hydrophilic sections. The hydrophobic backbone of the polymer keeps contact with the nanotube and hydrophilic groups attached to the polymer can be exposed to water. Therefore, geometry and wrapping of polymers designed with different functional groups are important. For instance, Poly(3-dodecylthiophene) is more hydrophobic than Poly(3-methylthiophene).[4] These polymers can be carefully modified by attaching different hydrophilic groups. A larger set of polymers would provide different options to an experimentalist.

5. All the calculations in this study have used GGA (PBE) functional. To see the trends, this functional is good enough and it is having good computational speed. However, it contains unphysical Coulombic self-repulsion which is leading to a systematic underestimation of band gaps.[5] One could perform the same calculations with a different functional (hybrid) to get band gaps which can be more quantitatively correct, and hence realistic in comparison to the experimental situation.

References

(1) Caddeo, C.; Melis, C.; Colombo, L.; Mattoni, A. Understanding the Helical Wrapping of Poly(3-Hexylthiophene) on Carbon Nanotubes. *J. Phys. Chem. C* **2010**, *114* (49), 21109–21113.

(2) Von Bargen, C. D.; MacDermaid, C. M.; Lee, O.-S.; Deria, P.; Therien, M. J.; Saven, J. G. Origins of the Helical Wrapping of Phenyleneethynylene Polymers about Single-Walled Carbon Nanotubes. *J. Phys. Chem. B* **2013**, *117* (42), 12953–12965.

(3) Wan Chik, M.; Hussain, Z.; Zulkefeli, M.; Tripathy, M.; Kumar, S.; Majeed, A.; Byrappa, K. Polymer-Wrapped Single-Walled Carbon Nanotubes: A Transformation toward Better Applications in Healthcare. *Drug Deliv. Transl. Res.* **2018**, *9*.

(4) Li, D.-F.; Wang, H.-J.; Fu, J.-X.; Wang, W.; Jia, X.-S.; Wang, J.-Y. Preparation of a Hydrophobic Polythiophene Film to Improve Protein Adsorption and Proliferation of PC 12 Cells. *J. Phys. Chem. B* **2008**, *112* (51), 16290–16299.

(5) Crowley, J. M.; Tahir-Kheli, J.; Goddard, W. A. Resolution of the Band Gap Prediction Problem for Materials Design. *J. Phys. Chem. Lett.* **2016**, *7* (7), 1198–1203.